A Power System Protection Scheme Combining Impedance Measurement and Travelling Waves: Software and Hardware Implementation

by

Vajira Pathirana

A dissertation submitted to the Faculty of Graduate Studies in partial fulfillment of the requirements for the degree of

Doctor of Philosophy

The Department of Electrical and Computer Engineering

The University of Manitoba

Winnipeg, Manitoba, Canada

© April 2004

THE UNIVERSITY OF MANITOBA

FACULTY OF GRADUATE STUDIES

*****

COPYRIGHT PERMISSION

A Power System Protection Scheme Combining Impedance Measurement and Travelling Waves: Software and Hardware Implementation

BY

Vajira Pathirana

A Thesis/Practicum submitted to the Faculty of Graduate Studies of The University of Manitoba in partial fulfillment of the requirement of the degree

Of

DOCTOR OF PHILOSOPHY

Vajira Pathirana © 2004

Permission has been granted to the Library of the University of Manitoba to lend or sell copies of this thesis/practicum, to the National Library of Canada to microfilm this thesis and to lend or sell copies of the film, and to University Microfilms Inc. to publish an abstract of this thesis/practicum.

This reproduction or copy of this thesis has been made available by authority of the copyright owner solely for the purpose of private study and research, and may only be reproduced and copied as permitted by copyright laws or with express written authorization from the copyright owner.

To my loving parents

Acknowledgements

I would like to express my sincere thanks to Prof.P.G. McLaren for his continuous advice, guidance and encouragement throughout the course of this work. I consider myself privileged to have had the opportunity to work under his guidance. I greatly appreciate the advice and assistance received from Dr.Udaya Annakkage to complete my research. I am also grateful to Mr.Adrian Castro of Manitoba Hydro for his advice and guidance. I must also thank the technical staff at the Department of Electrical and Computer Engineering, especially Mr.Erwin Dirks and Mr.Alan McKay for their valuable support.

I wish to thank Dr.Rohitha Jayasinghe and Dr.Dharshana Muthumuni of Manitoba HVDC Research Center, Mr.Tom Hendrick of Texas Instruments Inc., Mr.Steve Zachman and Mr.Bill Pitman of Hyperception Inc., and Mr.Hugh Pollitt-Smith of Canadian Microelectronics Corporation for their technical assistance. The financial support received from Manitoba Hydro, the Faculty of Graduate Studies at the University of Manitoba and the National Science and Engineering Research Council is greatly appreciated. I must also express my gratitude to the staff of the Center for Advanced Power Systems and National High Magnetic Fields Laboratory at the Florida State University, FL for their financial support and providing facilities to carry out part of my research.

I would like to thank all my friends at the Power Tower and the staff of the Department of Electrical and Computer Engineering for their continuous encouragement and for making my years at the University of Manitoba a pleasant experience.

This acknowledgement will not be complete without thanking my family. I extend my heartfelt gratitude to my parents. They were always understanding and encouraged me during my hard times. I would like to also thank my brothers and my sister for all the love and support.

Vajira Pathirana

April 2004

Summary

For the stability of the electrical network, it is important to clear faults on high voltage transmission lines quickly with the aid of a high-speed protection system. The conventional method of fault detection is mainly based on impedance measurement techniques. Under fault conditions the measured impedance is proportional to the distance to the fault from the relay location. To calculate the impedance, the fundamental frequency components of the voltage and current signals have to be extracted. The filtering involved in this process has an inherent delay. Any attempt to increase fault detection speed can affect the accuracy of the distance estimation and hence the reliability of the protection scheme.

Fault generated transients or travelling wave signals provide the very first information about a possible disturbance on the line and hence can be used to detect faults very quickly. Ultra-high-speed distance protection schemes based on fault initiated travelling waves measure the distance to the fault using the time taken for a wave to travel from the relaying point to the fault and back. However, travelling wave based protection schemes have reliability issues and have not been well accepted by relay engineers despite their fast fault detection capabilities.

In this thesis, a hybrid protection scheme is proposed which uses positive features of both travelling wave algorithm and impedance measurement technique in a single relay. The travelling wave information is used to achieve fast fault detection speeds while the impedance measurement is used to improve the reliability of the overall protection scheme. The thesis also investigates the possibility of accelerating the zone 2 protection of an impedance relay depending on the travelling wave information. The proposed algorithm has been verified through simulations of a practical three phase power system. The relaying functions have been tested using a laboratory prototype implemented on a Texas Instruments digital signal processor. The results indicate that the fault detection speed is improved while maintaining a high reliability level.

List of Principal Symbols

V_{pk}, I_{pk}	Peak voltage and current signals
V_p, I_p	Phase voltage and current signals
ω	Angular frequency
R, L, C	Resistance, inductance and capacitance per unit length
$[V_p], [I_p]$	Phase voltage and current matrices
$[V_{abc}], [I_{abc}]$	Three phase voltage and current matrices
$[V_{012}], [I_{012}]$	Symmetrical component matrices of the three phase voltage and current
$[\Delta V], [\Delta I]$	Phase voltage and current deviation matrices
$[Z_p], [Y_p]$	Phase impedance and admittance matrices
$[V^{(m)}], [I^{(m)}]$	Modal voltage and current matrices
$[\Delta V^{(m)}], [\Delta I^{(m)}]$	Modal voltage and current deviation matrices
$[S], [Q]$	Modal transformation matrices
$[Z_0]$	Characteristic impedance matrix of the line
$[Z^{(m)}]$	Modal characteristic impedance matrix of the line
f_1, f_2	Backward and forward travelling waves
S_1, S_2	Backward and forward relaying signals
a	Velocity of propagation
X_f	Distance from the relay location to the fault
R_f	Fault resistance
R_x	Autocorrelation of signal x
$\Phi_{S_2S_1}$	Crosscorrelation between S1 and S2
$\rho_{S_2S_1}$	Correlation coefficient between S1 and S2
Γ	Travel time of the transmission line
ϕ	Fault inception angle

Table of Contents

1 General Introduction 1
- 1.1 Introduction . . . 1
- 1.2 Transmission Line Protection . . . 2
- 1.3 Motivation Behind the Research . . . 5
- 1.4 Main Objectives of the Research . . . 6
- 1.5 Thesis Overview . . . 7

2 Transmission Line Protection Algorithms 9
- 2.1 Introduction . . . 9
- 2.2 Early Developments . . . 10
- 2.3 Digital Distance Relay Algorithms . . . 12
- 2.4 Algorithms Based on Transient Signals . . . 15
  - 2.4.1 Protection Based on Incremental Signals . . . 16
  - 2.4.2 Travelling Wave Relaying Algorithms . . . 20
- 2.5 Other Recent Developments . . . 28

3 Theoretical Aspects 37
- 3.1 Introduction . . . 37
- 3.2 Theory of Travelling Wave Protection . . . 38
  - 3.2.1 Transient Waves . . . 38
  - 3.2.2 Basic Principles Developed on a Single Phase Model . . . 38
  - 3.2.3 Three Phase Systems . . . 48
  - 3.2.4 Fault Direction . . . 51
  - 3.2.5 Determination of Fault Location . . . 52
  - 3.2.6 Correlation Techniques . . . 53
- 3.3 Theory of Impedance Measurement Algorithm . . . 57
  - 3.3.1 Background . . . 57
  - 3.3.2 Impedance Relay Implementation . . . 58
  - 3.3.3 Impedance Zone . . . 60
- 3.4 Combined Algorithm . . . 61
  - 3.4.1 Concept . . . 61
  - 3.4.2 Key Issues . . . 62
  - 3.4.3 Decision Process . . . 64
  - 3.4.4 Design Considerations . . . 67
- 3.5 Operating Principle of the Hybrid Algorithm . . . 70
  - 3.5.1 Algorithm One . . . 71
  - 3.5.2 Algorithm Two . . . 73

4 Simulation Studies 77
- 4.1 Introduction . . . 77
- 4.2 System Configuration . . . 78
- 4.3 Protection Simulation . . . 80
  - 4.3.1 Travelling Wave Algorithm . . . 81

4.3.2 Impedance Measurement Algorithm 84
4.3.3 Combining the Algorithms 86
4.4 Simulation Cases 86
4.5 Accelerating Zone 2 Protection 90

5 Laboratory Prototype 98
5.1 Introduction 98
5.2 Design Considerations 99
5.2.1 System Requirements 99
5.2.2 Relay Test Setup 102
5.3 Choice of Hardware and Software 102
5.4 Spectrum Board Configuration 103
5.4.1 Spectrum Dakar F5 Carrier Board 103
5.4.2 Spectrum DL3-A1 104
5.4.3 Limitations of Dakar Configuration 105
5.5 Texas Instruments C6x Configuration 106
5.5.1 C6711 DSK 106
5.5.2 Programming the DSK 108
5.5.3 Choice of Analog to Digital Converters for C6711 DSK 110
5.6 THS1206EVM Analog to Digital Converter 111
5.7 TLV2548EVM Analog to Digital Converter 114
5.8 ADS8364EVM Analog to Digital Converter 123
5.9 Hybrid Algorithm Implementation 129
5.10 Test Results 130

6 Conclusions and Recommendations 135

Appendices

A Transmission Line Theory 139

B Three Phase Transmission Lines 146

C Signal Processing Techniques 155

D Impedance Measurement of Transmission Lines 161

E Line Configuration and Parameters 167

F Hardware Information 169

Acronyms 175

References 178

List of Figures

2.1 Development of protection relay 10
2.2 Directional determination of RALDA relay 18
2.3 Fault trajectory and operating principle of Vitins' algorithm 19

3.1 Principle of superposition applied to a faulted network 40
3.2 Bewley lattice diagram of wavefronts generated by a fault 41
3.3 The propagation and reflection of wavefronts in a forward fault 43
3.4 Wave propagation for a reverse fault 46
3.5 Mho and quadrilateral characteristic of impedance relay 60
3.6 Block diagram of a digital impedance relay 61
3.7 Block diagram of the hybrid relay 69
3.8 Flowchart for algorithm 1 72
3.9 Flowchart for algorithm 2 76

4.1 Network diagram for 500 kV system 79
4.2 Line transposing intervals of the 500kV line 79
4.3 The 500kV three phase power system used for simulations 80
4.4 The fault transients generated by a three phase to ground fault: $x_{RF} = 325km$ 82
4.5 The relaying signal for a three phase fault: $x_{RF} = 325km$ 84
4.6 The impedance loci for the three phase fault: $x_{RF} = 325km$ 85
4.7 The trip signals issued for the three phase fault: $x_{RF} = 325km$ 87
4.8 The relaying signal for a phase B to ground fault: $x_{RF} = 270km, \phi = 60^0$. 88
4.9 The relaying signal for a phase C to ground fault: $x_{RF} = 195km, \phi = 3^0$ . . 89
4.10 The relaying signal for a phase A to ground fault: $x_{RF} = 220km, \phi = 154^0$. 90
4.11 The relaying signal for a close-up B to ground fault: $x_{RF} = 25km, \phi = 90^0$. 91
4.12 The relaying signal for three phase to ground fault: $x_{RF} = 525km$ 92
4.13 The impedance loci for three phase to ground fault: $x_{RF} = 525km$ 92
4.14 The 500kV line with two relays connected by a communication channel . . 94
4.15 The fault transients generated by three phase to ground fault: $x_{RF} = 500km$ 94
4.16 The impedance loci for three phase fault: $x_{RF} = 525km$, (a) R_1 (b) R_2 . . . 95
4.17 Relaying signals of the three phase to ground fault: $x_{RF} = 500km$ 97

5.1 A typical digital relay configuration 99
5.2 Laboratory test setup of a digital relay 102
5.3 Functional block diagram of the C6711 106
5.4 CCS development flow 109
5.5 THS1206 block diagram 112
5.6 Connecting THS1206 to the C6711 DSK 113
5.7 TLV2548 functional block diagram 115
5.8 Connection between TLV2548EVM and C6711DSK 116
5.9 Interfacing the TLV2548 to the McBSP 118
5.10 Connecting the ADS8364EVM to the DSK 125
5.11 Interfacing the ADS8364 to the C6711 DSK 126
5.12 Part of the graphical user interface arrangement 131

5.13 The setup used for testing the hybrid relay 132
5.14 The waveforms and trip signals obtained from RTP for a three phase fault . 133

A.1 The distributed parameter model of a transmission line (a) a section of unit length(b) the transmission line 140
A.2 The distributed parameter model for a lossy line 144

B.1 Representation of a three phase transmission line with an earth return . . . 146
B.2 Equivalent circuit of unit length of a 3-phase transmission line 147

E.1 Tower configuration 167

F.1 The McBSP block diagram 170
F.2 The McBSP clock and frame generation circuitry 172
F.3 The McBSP sample rate generator 172
F.4 The C6711 timers 173

List of Tables

2.1 Phase selection scheme 20
2.2 Phase-to-phase-to-ground fault identification 20

4.1 Simulation Results I 93
4.2 Simulation Results II 96

5.1 TLV2548 command set 121
5.2 TLV2548 configuration register bit definitions 122
5.3 ADS8364EVM address map 124
5.4 ADS8364 data input/command 128
5.5 Test Results 134

F.1 McBSP registers 171
F.2 Timer registers 174

Chapter 1

General Introduction

1.1 Introduction

The growing demand for power and high transmission efficiencies has prompted construction of extra high voltage (EHV) transmission lines. These high voltage lines have become the backbone of the bulk power transmission over long distances. The complexity of the power network and the low stability margins at which they now operate have dramatically increased the occurrence of catastrophic failures in electric power systems [1]. On the other hand, the hardship and economic penalties associated with such events have become more important since the society relies heavily on the availability of quality power supply. Although complete immunity from such catastrophic failures is not easy to achieve, new developments in the transmission line protection show promising signs that cascading system outages can be minimized and mitigated. The greatest danger to a healthy power system is instability resulting from faults that are not cleared quickly. High speed fault isolation is required to ensure that the power system will not run into transient stability problems and also to reduce the damage due to electrodynamic and thermal stresses on the equipment. The stability of the power system can be greatly improved by reducing the fault clearance time, especially of those faults in EHV lines.

The capital investment involved in generation, transmission and distribution of electrical

power is so high that proper precautions have to be taken to ensure that the equipment not only operates at high efficiency, but are also protected from possible faults. Protection relays are designed to quickly detect possible disturbances and isolate the faulted system from the rest of the network. The faster the fault is cleared, the smaller the disturbance the fault will inflict on the system. A protective relay is required to satisfy four basic functional characteristics - reliability, selectivity, speed and sensitivity. Reliability of a protective relay is a basic requirement. The protective relay has to be dependable, but secure: the relay must always operate for a fault within its zone of protection, but should not operate otherwise. The relay must operate when it is required and should not operate unnecessarily. Selectivity is the basic requirement of the relay in which it should be possible to select which part of the system is faulty and which is not and should isolate the faulty part of the system from the healthy one. Fault detection speed of a relay is an important feature. The shorter the time for which a fault is allowed to exist, the less damage the fault will inflict on the system. The speed and reliability in protective relays have always been a compromise. The faster the fault detection is, the less reliable the overall scheme becomes, especially for faults close to the relay operating boundary. Finally, a relay should be sufficiently sensitive so that it operates reliably when required under the actual conditions in the system which produce the least tendency for operation.

1.2 Transmission Line Protection

The distance relays, the fundamental component of almost all EHV transmission line protection, operate on the impedance measured at the relay location. In a digital distance relay, the impedance seen at the relay is calculated from the fundamental frequency (50/60Hz) component of the voltage and current signals. When a fault occurs, the sudden changes in the steady state values of voltage and current signals generate high frequency transient signals. The high frequency components in fault waveforms present undesirable effects to most distance protection algorithms based on the power frequency component. In a distance

relay based on impedance measurement, the accuracy of the impedance estimation depends on how accurately the fundamental components are extracted or, in other words, how well the unwanted signal components are eliminated. The processes of sampling and extracting the fundamental component involve filtering the signals, which inherently incorporates a delay. Since impedance is a phasor quantity, it takes time to change from a load condition (pre-fault) value to a fault condition (post-fault) value. This directly affects the fault detection time, and hence the total fault clearing time. For an impedance relay, the accuracy of the impedance estimate may go down with the increase in the speed at which that estimate is obtained [2]. The error caused by non-fundamental frequency signals depends on the operating speed since the operating speed depends on the sampling window used to extract the fundamental frequency components. On the other hand, the reach setting of an impedance relay is determined by the error of its impedance estimate and hence an impedance relay with a particular reach setting cannot operate at arbitrarily high speeds [3]. For instance, a relay using a one cycle sampling window could be set with a reach setting of 80% of the line to assure dependable operation in the presence of noise. With a half cycle window, the calculation error is high and the relay would be set to see only 60% of the line. In adaptive impedance relay schemes, digital relays can accommodate the errors caused by the transients by dynamically adjusting the sample window. However there is always a compromise between the operating speed and the relay reach [3]. In essence, for faults towards the reach of the relay, an impedance relay will have a longer operating time than that for a close-up fault.

The inherent delay in filters makes it difficult to improve the speed of an impedance relay any further. A directional teleprotection scheme in which the relays at the opposite ends of the transmission line are connected through a communication channel could achieve fast fault clearance time for line end faults. However, the reliability of such a scheme will depend on the reliability of the communication channel. An alternative approach is to use non-power frequency components in the fault signals, particularly travelling wave

components. When a fault occurs on a transmission line, the sudden discharge of line charges at the fault location generates transient waves. Immediately after the fault, the *distortions* caused by these transient waves can be observed superimposed on the steady state voltage and current waveforms. In long EHV lines, these high frequency oscillations in voltage and current waveforms become significant. These transient signals (travelling waves) subsequently propagate along the transmission line at a velocity close to the speed of light and reflect at discontinuities [4]. The repeated reflection of these transient wavefronts cause the voltage and current signals to change from the pre-fault steady state values to the post-fault values. These wavefronts contain valuable information about the fault type, location of the fault and fault inception angle. The sign, magnitude and timing between the various wavefronts arriving at the line end contain information from which the fault location can be calculated within a few milliseconds of the fault initiation.

The travelling wave based protection schemes demonstrate fast fault detection times since the wavefronts carry the very first information about a possible disturbance in the system. Many suggestions for utilizing high frequency transient signals to achieve ultra high speed fault detection were suggested in the late 70's and early 80's. The method suggested by Crossley and McLaren [5] showed a way to find the distance to the fault with a reasonable accuracy which allowed the relay to be selective. This algorithm uses a correlation technique to recognize the initial reflected wavefront returning from the fault. The distance to the fault is proportional to the time delay between the first wavefront detected at the relay location and the associated reflected wavefront from the fault.

However, protection schemes based on travelling waves had to face reliability issues. Such schemes have failed to detect faults under certain conditions [6, 7]. Two main concerns have been identified:

1. When a fault occurs close to the relaying point (close-up fault), the repeated reflection of wavefronts between the fault and the discontinuity behind the relay will create very high frequency transients. The closer the fault is to the relay, the more prominent

will be the high frequency components in the transient signals. Without high fidelity transducers that will not degrade the wavefront information and a processor capable of handling fast computations, a travelling wave protection scheme will find it difficult to distinguish between the arrival of consecutive wavefronts. Although current transformers (CT) are capable of reproducing an acceptable replica of the current signals [8], capacitor coupled voltage transformers (CCVT) have a relatively low bandwidth [9, 10]. Unless an alternate method such as an optical voltage transducer (OVT) is available to measure the voltage signals, most travelling wave schemes might fail to detect close-up faults.

2. On the rare occasion when a phase to ground fault occurs near zero voltage level (small fault inception angle), the fault generated transient waves will not contain any steep wavefronts. The wavefronts are not distinct and difficult to isolate for measurement purposes. A travelling wave protection scheme may fail detecting such a fault.

1.3 Motivation Behind the Research

The reliability of the relay algorithm is a major factor concerning the selection of a protection scheme. The fast fault detection capability of travelling wave relay schemes may be tarnished by their inability to detect faults under all possible conditions. Although impedance measurement technique might take a full 60Hz cycle to detect a fault near the reach point, the operating time can become comparatively low for close-up faults [2]. Hence there is less requirement for a travelling wave type measurement in order to speed up the relay trip time. Where there is a need for speed up is towards the reach point of the impedance measuring technique. In this thesis, a new method was investigated to combine the information contained in the fault-generated wavefronts with the impedance measurement at the relay location in a single relay to develop a reliable, but high-speed protection algorithm. If the fault is too close to be detected by the travelling wave scheme, the impedance relay

acts as a fast backup. In addition, the measured impedance will fall within the protective zone for faults with zero inception angles, thus enhancing the reliability of the combined scheme.

The motivation behind cascading the travelling wave information and impedance measurement in a hybrid scheme was to design a reliable and high-speed protection scheme. The algorithms operate in parallel and need high speed processing. Modern digital signal processors (DSP) and analog to digital converters (ADC) can handle various measurements and extensive calculations involved in such complex algorithms [11]. The hybrid relay requires an inter-trip signal for faults which occur on the line outside the maximum length of the zone 1 protection zone. The maximum protection length depends on the accuracy of the distance estimate. The accuracy hence depends on the resolution of the measuring transducers and the processing power of the DSP.

1.4 Main Objectives of the Research

The main objectives of this research were:

1. Recognizing the problem areas associated with the existing transmission line protection schemes;
2. Introducing a solution to those problems through a hybrid algorithm;
3. Developing the mathematical basis for the hybrid algorithm;
4. Simulating the proposed method to verify its operation;
5. Identifying the hardware and software limitations in a real-time implementation of the algorithms;
6. Evaluating the protection response of the hybrid scheme by building and testing a laboratory prototype.

The thesis investigates how the hybrid algorithm can overcome the limitations of both travelling wave and impedance measurement schemes. Two hybrid algorithms have been developed to analyze the possible improvements that can be achieved through the proposed protection scheme.

1. Algorithm 1 analyzes how the hybrid scheme operates as the primary protection of a power network.

2. Algorithm 2 analyzes how the travelling wave information and the zone 2 protection of the impedance relay can be combined to achieve fast fault detection.

1.5 Thesis Overview

The thesis progressively discusses the approach employed to achieve the above targets. This chapter gives a general introduction to the thesis.

Chapter 2 gives an overview of the history of protection schemes associated with transmission line protection. More emphasis is placed on the digital distance relays of the last three decades. The chapter then reviews the ultra high speed line protection relaying algorithms. Algorithms with different protection philosophies are discussed. These algorithms are mainly based on travelling wave theory but the principle of operation may be different. This chapter also discusses other recent developments in transmission line protection schemes.

The theoretical aspects behind the relaying scheme are described in chapter 3. The chapter reviews the theory associated with the travelling wave protection and impedance measurement of a transmission network. The basic theory of travelling wave protection was developed for a single phase lossless line and was then extended to a three phase system. The incremental phase voltage and current signals which contain transient information were decomposed into their respective independent modes using modal analysis theory. The concept and key issues behind the hybrid algorithm are explained next. This involves

a discussion about the problem areas associated with both travelling wave and impedance protection schemes. The last section of the chapter explains the operating principle behind the hybrid relay and discusses the two main algorithms.

In chapter 4 the simulation results are outlined. The PSCAD electromagnetic transient program [12] was used for the simulations. A three phase power system was modelled with PSCAD to generate the voltage and current signals under fault conditions. Different library modules were created in PSCAD for each block component of the hybrid algorithm. Different fault scenarios were investigated to identify the limitations and advantages of the new scheme. The fault type, fault inception angle, the fault distance and fault resistance were all considered in simulations to decide on the relay threshold settings. Comparisons were made between the proposed hybrid algorithm and the existing distance protection schemes.

Chapter 5 details the hardware and software implementation of the proposed hybrid distance protection scheme. The real time implementation of the algorithm required high performance hardware due to the high sampling rates associated with the travelling wave relay and the implementation of the two algorithms in parallel. However, to keep the cost of the final product low, the hardware already available in the lab and inexpensive off-the-shelf evaluation hardware were used. Because of this decision, the hardware implementation became a lengthy process, but the cost of the final product was kept low. This chapter briefly introduces the different hardware arrangements we tried and the reasons why some of them could not be used.

Finally, in chapter 6 conclusions are drawn. Few suggestions suggestions are given for future work covering the points which still need further research in order to increase the relay speed and accuracy.

The appendices introduce the mathematical derivations and details about different theories used in the main chapters of the thesis. References are made to the appendices wherever required. At the end of the appendices is a list of the acronyms used throughout the thesis.

Chapter 2

Transmission Line Protection Algorithms

2.1 Introduction

Transmission line protection began more than ten decades ago with over-current protection and since then has developed into a large industry. The majority of protection principles were developed within the first few decades after the over-current principle was introduced. These principles are still applied in protection schemes today, although the technology used has changed substantially as summarized in Fig.2.1. The introduction of computers and digital technology has been an important milestone in the history of power system protection. Digital relays have mostly replaced the pre-existing electromechanical and static relays and introduced new relaying principles which were not feasible before. The advancements in communication technology and new protocols that allow direct relay-to-relay communication have lead the way to intelligent electronic devices (IED).

This chapter examines the developments in transmission line protection. More emphasis is placed on the digital relays. The early digital distance protective relay algorithms based on power frequency signals are discussed first. Only noteworthy developments until the

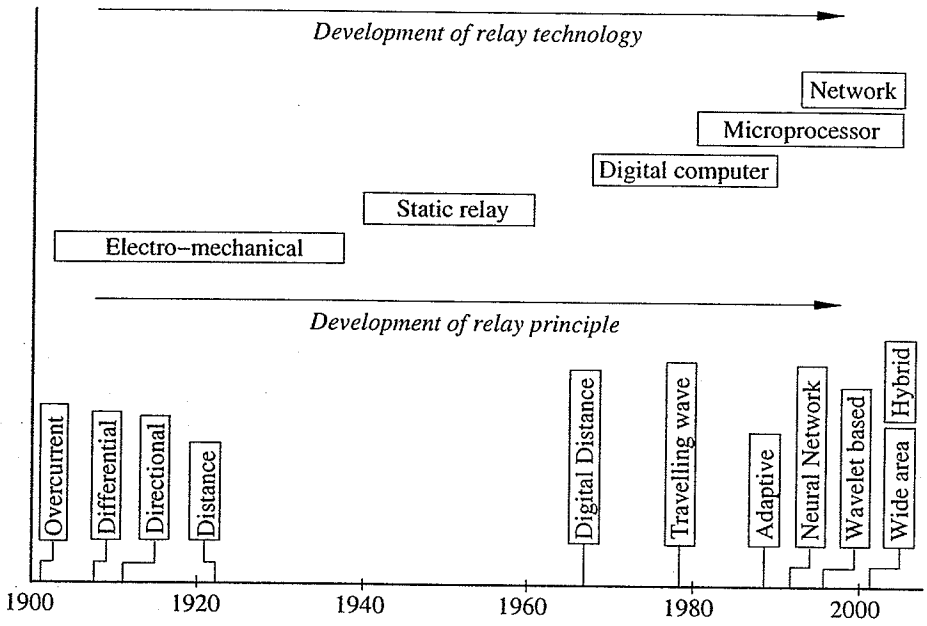

Figure 2.1: Development of protection relay

early 1980's are considered here since later developments were mainly based on the concepts instigated during this period. The discussion then concentrates on non-power system frequency methods, especially protection schemes based on travelling waves. For the completion of the review, some of the later developments such as adaptive schemes, methods based on artificial intelligence and wavelet algorithms are discussed at the end.

2.2 Early Developments

The earliest relays to be used in transmission line protection were all *electromechanical.* The very first relays were based on the over-current principle which was introduced around 1902. The inverse time-current relationship was suitable for time graded over-current discrimination systems. These early devices not only had to detect fault conditions, but also had to generate sufficient torque to trip the *breaker* on which the system was fixed. The latter requirement placed very severe restrictions on the sensitivity of these devices. Due to the inherent long operating times, they could not be used in networks where fast fault clearance was needed. The over-current principle was followed by differential protection schemes after

1905. These systems compared the line currents at opposite ends of the transmission line and used a communication link to transmit required information between the ends. The concept of directional discrimination of faults was introduced around 1909. The pilot wires were used as a means of conveying information from one end of a protected feeder to the other and a system was proposed to use the pilot wires to convey an interlock signal from end to end. The application of a restraining force proportional to the system voltage to an over-current induction disc type relay produced a time of operation roughly proportional to the distance to the fault from the relaying point. The distance relay indicated a measure of the impedance of the line at the relay point. The development of distance relays in the form of impedance relays started with this concept in 1923. All of the relays developed until 1940's were electromechanical relays. These electromechanical distance relays later achieved very high precision in the form of *induction cup mho relays.* The mho relay gave a closed characteristic of the fault impedance locus and therefore allowed discrimination against faults in other phases. Mho relays were therefore mainly incorporated as starting units in the majority of distance relaying schemes. The mho characteristic is still widely applied in distance relays [13].

The early 1940's showed the way into the development of relays using electronic devices. These relays are known as *static relays.* The first static relays were designed using thermionic valves. But all such relays had a disadvantage with respect to the electromagnetic relays due to the relatively short life of thermionic valves. The advent of the transistor led the way to the development of different distance protection schemes. Using transistor circuits several new protection concepts were developed during this period: phase comparator, block spike comparator, and block average comparator to name a few.

The concept of *sampling and holding* the voltage and current signals, and the development of *digital computers*, led to *digital* (numerical) protection schemes [14]. Although there was a lot of resistance to the adoption of computers for relaying functions by the relay engineers, the relay technology has gone through rapid development since the digital com-

putation was introduced in late 1960's. Numerical impedance calculation methods allowed digital techniques to be used in transmission line protection. Microprocessors started replacing the digital computers by early 1980's, but the concept of digital computing has stayed the same. Today, extra high voltage transmission lines are protected with very reliable, secure digital distance relays and they have virtually replaced all previous electromechanical relays.

2.3 Digital Distance Relay Algorithms

Using digital technologies in protective relays started in the late 60's with the rapid development of digital computers. Digital techniques demonstrated added flexibility in design as well as improved performance and reliability. In digital distance protective relays, the apparent impedance at the relay location is calculated from the sampled voltage and current signals. The impedance seen by the relay is proportional to the distance between the fault and the relaying point. The digital estimation is fairly accurate when both voltage and current signals are pure 60Hz sinusoids. However, in the presence of transients, the accuracy can be affected. To remove the effects of transients, the signals must be low pass filtered before sampling.

Rockerfeller [15] showed the possibility of utilizing a digital computer for protection applications. He proposed a complete group of programmes for the protection of equipment both internal (transformers, busbars) and external (transmission lines) to the substation. He introduced a new concept of protecting transmission lines as part of the function of a master digital computer. Logic operations were assigned to detect a fault, locate it and initiate the opening of the appropriate circuit breaker. He mentioned that there was no reason to stop the application of a digital computer to perform the complete substation protective relaying functions.

Mann and Morrison [16, 17] proposed a method of calculating the line impedance by a predictive calculation of peak voltage and peak current. The impedance was calculated by

dividing the peak voltage by the peak current. If the voltage and current signals were given by $V_{pk}\sin\omega t$ and $I_{pk}\sin(\omega t+\phi)$ respectively, a digital computer sampling sinusoidal waves determined the peak as follows:

$$v^{'} = \omega V_{pk}\cos\omega t \tag{2.1}$$

$$V_{pk}^2 = v^2 + \left[\frac{v^{'}}{\omega}\right]^2 \tag{2.2}$$

$$\phi = \tan^{-1}\left[\frac{\omega i}{i^{'}}\right] - \tan^{-1}\left[\frac{\omega v}{v^{'}}\right] \tag{2.3}$$

where v, i are the instantaneous voltage and current samples and $v^{'}, i^{'}$ are their derivatives. ω is the angular frequency of the sinusoidal waveforms. The phase angle, ϕ was calculated from the phase angle difference between voltage and current phasors. The transients generated due to a fault can include an exponentially decaying component (dc offset) in addition to the high frequency signals. Such exponentially decaying components on the current and voltage signals can cause difficulties in the application of the above algorithm.

Gilcrest et al [18] suggested a method to reduce the effects of dc offset transients and subnormal frequency components. The method suggested by Mann and Morrison [16] was modified to use the first and second differences, rather than the sample values and the first differences. Hence the peak and phase values were given by

$$V_{pk}^2 = v^{'2} + \left[\frac{v^{''}}{\omega}\right]^2 \tag{2.4}$$

$$\phi = \tan^{-1}\left[\frac{\omega i^{'}}{i^{''}}\right] - \tan^{-1}\left[\frac{\omega v^{'}}{v^{''}}\right] \tag{2.5}$$

where $v^{''}$ and $i^{''}$ are the second derivative of the voltage and current signals.

Ranjbar and Cory [19] used an equation of the form

$$v = Ri_x + L\frac{di_y}{dt} \tag{2.6}$$

to find fault conditions. i_x and i_y were made out of combinations of phase currents. R and L were the resistance and inductance of the transmission line. Integrating the above equation over time instants t_1 to t_2 and again over t_3 to t_4, the following equations were obtained.

$$\int_{t_1}^{t_2} v dt = R\int_{t_1}^{t_2} i_x dt + L(i_{y2} - i_{y1}) \tag{2.7}$$

$$\int_{t_3}^{t_4} v dt = R\int_{t_3}^{t_4} i_x dt + L(i_{y4} - i_{y3}) \tag{2.8}$$

From the above integration, the values of R and L were calculated. This method improved the accuracy of the resistance and inductance calculation to the fault. The integration also filtered out the low order harmonics.

Gilbert and Shovlin [20] proposed an algorithm which calculated the apparent resistance and reactance to the fault using voltage and current samples. The algorithm used three consecutive data samples of voltage and current signals taken at known time intervals. The apparent resistance to the fault (R_f) and the apparent reactance to the fault (X_f) calculated using the three consecutive data samples are given by

$$R_f = \frac{2v_{n-1}i_{n-1} - v_n i_{n-2} - v_{n-2} i_n}{2(i_{n-1}^2 - i_{n-2} i_n)} \tag{2.9}$$

$$X_f = \frac{v_{n-1}i_n - v_n i_{n-1}}{i_{n-1}^2 - i_{n-2} i_n} \sin(\delta) \tag{2.10}$$

where δ is the angle equivalent to the time interval between the samples. The calculated value of the apparent resistance was independent of sampling rate and therefore was not affected by the system frequency. However, the apparent reactance to the fault was sensitive to the changes in system frequency.

Miki et al [21] explained how the reliability of a digital distance protection scheme can be improved through redundancy of hardware. In their implementation, they suggested an integral filter to suppress the higher harmonics. They investigated the operating character-

istics of a mho relay and a reactance relay using a microcomputer.

Most of these algorithms really didn't consider the presence of transients in the measured signals. McLaren and Redfern [22] were among many others who recognized the presence of transients in the waveforms. They suggested using Fourier Series based processing to extract the fundamental voltage and current components. The extracted fundamental components were used to calculate the apparent impedance. The filter characteristics showed that the Fourier series method gave a considerable rejection of non-fundamental components.

Different techniques were proposed during this time and later to extract the fundamental frequency information to estimate the impedance of the transmission line. These algorithms focused on filtering decaying exponential component and some harmonics and then determining the fundamental voltage and current phasors. The use of least square filters [23], Kalman filters [24], Fourier transform based filters [22], and correlation based methods [25] suggested different methods of estimating the line impedance. Digital distance relays have come a long way from these early developments. The modern relays use either Discrete Fourier Transform (DFT) or Fast Fourier Transform (FFT) based methods to extract the fundamental frequency components. One cycle DFT or FFT is capable of extracting the fundamental frequency components accurately while eliminating the higher order harmonics. All modern distance relays are developed using high speed digital signal processors.

2.4 Algorithms Based on Transient Signals

The algorithms discussed in the previous section use filters to attenuate the high frequency signals generated by the fault transients. The presence of transients influences the accuracy of the impedance estimate. The filtering process involved an inherent delay and could not be eliminated from the algorithms. The attempts to increase the speed of the impedance relays showed that making the relay faster affected the accuracy of the impedance measurement [2]. The need to improve the fault clearance times motivated several researchers to consider

high frequency transient signals for relaying purposes. Different protection techniques based on non-power frequency signals have been investigated with the developments in the digital technology. In particular the use of *incremental signals* for directional comparison and *travelling-wave* techniques for distance measurement gained wide acceptance. The relays developed using both these principles have the advantages of fast response, directionality, and immunity to power swings and CT saturation. In this section, the transient based relaying concepts are discussed. Transient based protection can be broadly categorized into protection based on incremental signals and protection based on travelling waves.

2.4.1 Protection Based on Incremental Signals

A fault on a transmission line can cause the post-fault voltage and current at the relay location to deviate from the steady state pre-fault voltage and current signals. This can be shown as

$$\tilde{v}(t) = v(t) + \Delta v(t) \tag{2.11}$$

$$\tilde{i}(t) = i(t) + \Delta i(t) \tag{2.12}$$

where v, i are the pre-fault measurements and $\tilde{v}, \tilde{i}$ are the measured fault quantities. Δv and Δi denote the fault generated voltage and current deviations from the pre-fault steady state signals. The incremental signals are obtained by subtracting the pre-fault steady state signals from the fault measured signals. The most commonly used method to derive the incremental components is using the measured signals taken exactly one cycle before as the instantaneous estimate of the steady state signal. A low pass filter is used to get rid of undesired noise in the estimate. Another approach is to use high pass filters to suppress the steady state signals so that only the transient signals will be present in the relaying signals. Under normal steady state conditions, the incremental quantities are zero except for the presence of noise. These incremental signals have been used in ultra-high-speed

(UHS) protection schemes.

In the RALDA relay [26], high speed fault detection and discrimination were achieved using incremental components generated due to a fault. The decisions were taken by observing the direction of travelling wave phenomena on the line after the occurrence of a fault. The concept was based on the fact that a fault initiates a voltage wave travelling along a transmission line in the positive direction which is accompanied by a companion current travelling wave of the same sign and a similar voltage wave travelling in the negative direction is accompanied by a current wave of opposite sign. A comparison between the polarities of the initial voltage and current deviations was used to determine the direction to the fault. The polarity comparison was done at the opposite ends of the line by exchanging the information through a communication channel. For an internal fault, the polarities were different at both ends, while for an external fault the polarities were different only at one end. The Fig.2.2[1] shows the actual sign of the observed deviations for different fault scenarios.

Vitins [27] proposed a method in which the fault direction was determined based on the fault trajectory of the scaled current deviation against the voltage deviation. The simple power system shown on Fig.2.3(a) is used to explain the concept. The deviation signals Δv and Δi measured at the relay location p were given by

$$\Delta v(t) = -\frac{X_s}{X_s + X_f} E \cos(\omega t + \gamma) \tag{2.13}$$

$$\Delta i(t) = -\frac{1}{X_s + X_f} E[\sin(\omega t + \gamma) - \sin\gamma] \tag{2.14}$$

where E is the rated peak voltage and γ is the fault inception angle. The current deviation contains a constant dc-offset, the magnitude of which depends on γ. The occurrence of a fault was represented by a fault trajectory on the $R.\Delta i$ - Δv plane as shown in Fig.2.3(b). Here R is the replica impedance(equal to the line surge impedance). The figure shows the

[1]Obtained from [26]

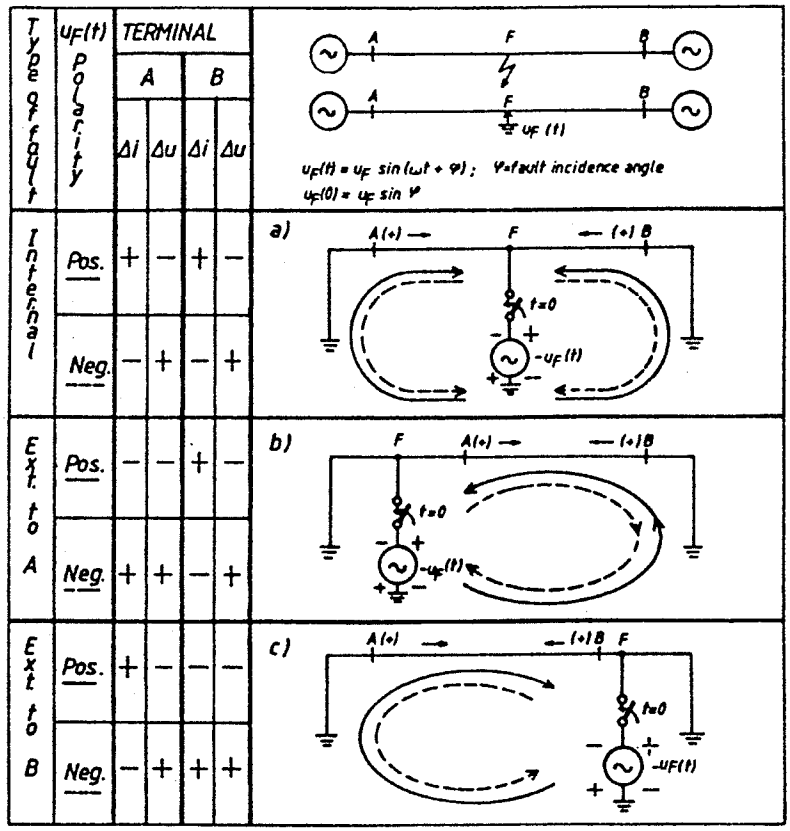

Figure 2.2: Directional determination of RALDA relay

boundaries suggested by the author for forward and reverse faults. An initial excursion into the first or third quadrant showed a reverse fault while an initial excursion into the second or fourth quadrant indicated a forward fault. By exchanging the directional information at the opposite ends of the line using a communication channel, the correct location of the fault was detected.

Very recently, Thomas et al [28] developed a phase selection algorithm based on superimposed voltage and current components initiated by faults. The output of the phase selection algorithm can be used for single pole tripping schemes. The phase selection criteria is based on a set of parameters (S) deduced by the incremental signals. Table 2.1 shows the phase selection scheme used and Table 2.2 shows the method used to identify phase-to-phase-to-ground faults.

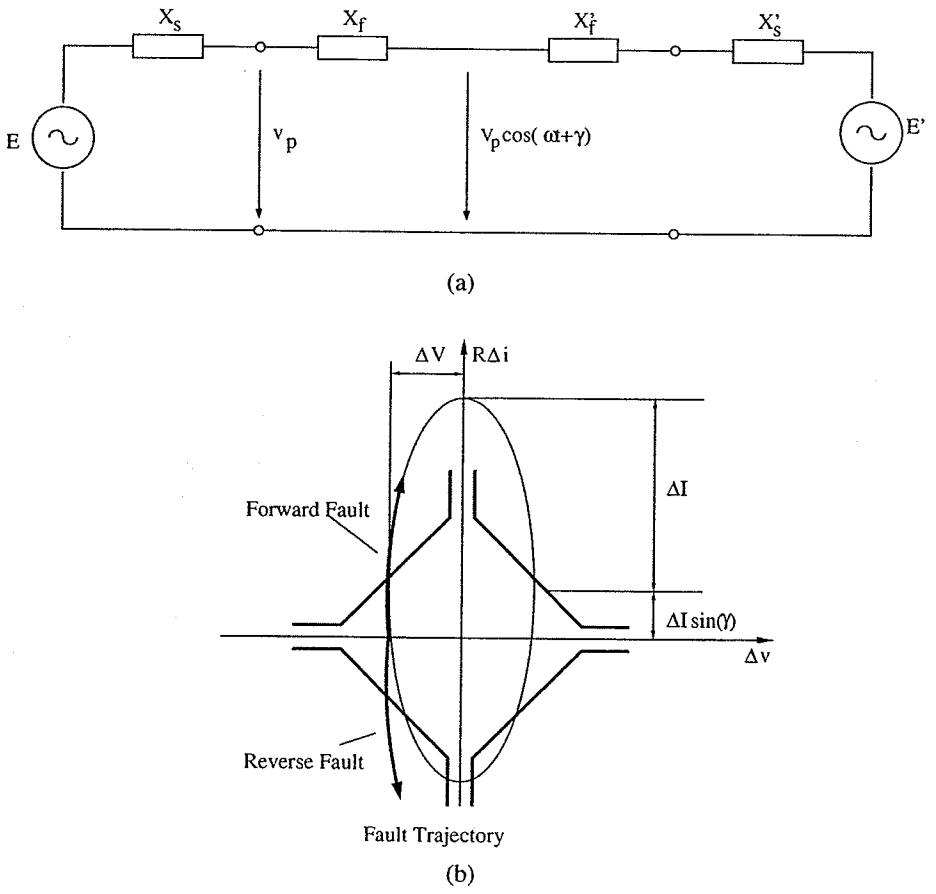

Figure 2.3: Fault trajectory and operating principle of Vitins' algorithm

The aerial phase voltages, V_p^{α} are given by

$$V_p^{\alpha} = V_p - V_0 \tag{2.15}$$

where V_p is the voltage of phase p and V_0 is the calculated ground mode voltage. The threshold δ was set at 0.1 p.u. voltage. The test must be true for half a cycle of the power frequency signals. The authors claimed that the proposed phase selection method is faster than the traditional methods and valid over a broad frequency band.

Parameter label	Definition of the parameter	Selection test for this parameter	Indicated fault type if test is true
S_1	$V_a^\alpha - V_b^\alpha$	$S_1 < \delta$	phase c-to-ground
S_2	$V_c^\alpha - V_a^\alpha$	$S_2 < \delta$	phase b-to-ground
S_3	$V_b^\alpha - V_c^\alpha$	$S_3 < \delta$	phase a-to-ground
S_4	V_c^α	$S_4 < \delta$	phase a-to-phase b
S_5	V_b^α	$S_5 < \delta$	phase a-to-phase c
S_6	V_a^α	$S_6 < \delta$	phase b-to-phase c
S_7	$1/3(V_a + V_b + V_c)$	$S_7 < \delta$ only	symmetric three phase

Table 2.1: Phase selection scheme

Selection test	Fault type
$S_4/S_7 < 2Z_1/Z_0$	phase a-to-phase b-to-ground
$S_5/S_7 < 2Z_1/Z_0$	phase a-to-phase c-to-ground
$S_6/S_7 < 2Z_1/Z_0$	phase b-to-phase c-to-ground

Table 2.2: Phase-to-phase-to-ground fault identification

2.4.2 Travelling Wave Relaying Algorithms

In a distributed parameter model of a transmission line, the relationship between voltage v, current i, time t and distance x is fully described by the telegraph equation (see Appendix A). The solution to the telegraph equation can be expressed in terms of backward f_1 and forward f_2 travelling waves as

$$v(x,t) = f_1(x-at) - f_2(x+at) \tag{2.16}$$

$$i(x,t) = \frac{1}{Z_c}[f_1(x-at) + f_2(x+at)] \tag{2.17}$$

where Z_c is the characteristic impedance of the line and a is the surge velocity. The backward and forward travelling waves can be expressed in terms of incremental voltage Δv and incremental current Δi signals by

$$S_1(t) = 2f_1(t) = \Delta v(t) + Z_c \Delta i(t) \tag{2.18}$$

$$S_2(t) = 2f_2(t) = \Delta v(t) - Z_c \Delta i(t) \tag{2.19}$$

where S_1 is the backward wave relaying signal and S_2 is the forward wave relaying signal. The travelling wave protection schemes described in this section use the relaying signals S_1 and S_2. A detailed discussion of travelling wave theory will be presented in section 3.2.

In 1978, Dommel and Michels [29] presented a directional discriminant travelling wave function which showed a value zero for a backward fault and a known constant for faults in the forward direction. The discriminant function, DF is given by

$$DF = [\Delta v + Z_c \Delta i]^2 + \frac{1}{\omega^2}\left[\frac{d}{dt}\Delta v + Z_c \frac{d}{dt}\Delta i\right]^2 \tag{2.20}$$

$$= S_1^2 + \frac{1}{\omega^2}\left[\frac{d}{dt}S_1\right]^2 \tag{2.21}$$

where ω is the fundamental angular frequency. The function DF is independent of the fault inception angle and line termination. For a reverse fault, $DF = 0$ for a time equal to twice the travel time of the protected line. For a forward fault, the value of DF theoretically stays constant ($DF = 8V_{rms}^2$) from the time the first wavefront is sensed to the time its reflection arrives back from the fault location for an internal fault and from the opposite end for an external fault. The directional comparison was done by exchanging the information via a carrier communication channel.

In 1980, Johns [30] proposed a directional comparison scheme based on the travelling wave information. The sequence in which the forward and backward travelling wave signals exceed a certain threshold was analyzed at both ends of the transmission line and this information was shared through a communication channel. For a fault in the backward direction, and a time duration equal to twice the travel time of the protected line, $S_2 > 0$ and $S_1 = 0$. For a forward fault, the signals S_1 and S_2 satisfies the condition $S_2 \leq S_1$.

In 1983, Crossley and McLaren [5] proposed a distance protection scheme based on travelling wave theory. The authors used a cross-correlation function to recognize the initial wavefront reflected from the fault. The fault direction was determined by the sequence in which S_1 and S_2 exceed a predetermined threshold. For a detected forward fault, a section

of the relaying signal S_2 representing the forward travelling wavefront was stored and cross-correlated with subsequent sections of relaying signal S_1. To obtain a better correlation of S_1 and S_2, the mean values of the relaying signals were removed before calculating the cross-correlation function. The cross-correlation between the mean removed signals S_1 and S_2 is given by

$$\Phi_{S_1S_2}(m\Delta t) = \frac{1}{N}\sum_{k=1}^{N}[S_2(k\Delta t) - \overline{S_2}].[S_1(k\Delta t + m\Delta t) - \overline{S_1}] \tag{2.22}$$

where $\overline{S_1}$ and $\overline{S_2}$ are the mean values of the signals S_1 and S_2 respectively. The cross-correlation function shows a maximum value when the section S_1 is similar to the stored section S_2. The time delay to reach this maximum corresponds to twice the distance between the measuring point and the fault location.

Rajendra and McLaren [31, 32] extended the techniques proposed in [5] to the protection of teed circuits. The authors described several new travelling wave techniques to analyze the faults on teed circuits. They suggested a polarity change criterion that enabled the local end relay to distinguish between a fault on the local branch and that of a fault on one of the tee branches by sensing the polarity changes in the first and second backward travelling wave in S_1. The polarity criterion was based on the fact that a fault on the local branch will result in opposite changes in signal S_1 whereas a fault on an adjacent branch will result in identical signal changes. The authors also suggested a method based on autocorrelation function to classify faults between local and remote branches of a teed circuit. In this method, the output section corresponding to the maximum of the cross-correlation function is autocorrelated with sections of the entire cross-correlation function output. By doing so, it was possible to determine the successive peaks of the cross-correlation output. It was observed that the ratio of the time delays between successive peaks in the autocorrelation output is approximately unity for a fault on the local branch whereas a low ratio is obtained for an external fault or a remote branch.

In 1986, Mansour and Swift [33] presented a multi-microprocessor based faulted phase selection and fault classification relay. An algorithm based on two discriminant functions derived from the forward and backward travelling waves and their differentiations was used to identify faulted phases. A table based on the transformation matrix used to decouple the phase signals into their respective modal signals was proposed to identify different fault scenarios. The backward and forward discriminant functions D_B and D_F respectively for mode (k) were defined as

$$D_B = \left[S_1^{(k)}\right]^2 + \frac{1}{\omega^2}\left[\frac{d}{dt}S_1^{(k)}\right]^2 \tag{2.23}$$

$$D_F = \left[S_2^{(k)}\right]^2 + \frac{1}{\omega^2}\left[\frac{d}{dt}S_2^{(k)}\right]^2 \tag{2.24}$$

Here, the surge impedance Z_c in (2.19) was replaced with the surge impedance associated with mode (k) for each mode. The authors presented fault classification truth tables for modal components found using Clarke, Wedepohl and Karrenbauer transformations.

Shehab-Eldin and McLaren [34] identified several problem areas associated with travelling wave protection and suggested new techniques to improve the distance protection scheme proposed by Crossley [5]. In Crossley's method, a reference signal representing the first wavefront which leaves the relay location is stored and then a corresponding reflected wavefront is found through correlation. The duration of this stored section is inversely proportional to the wave transit time. The authors found that by using a fixed storage duration, the protection scheme may not be able to detect either faults close to the relay (if the duration is long) or faults close to the remote bus bar (if the duration is short). They suggested an improved method in which the final output is obtained by simple addition of short and long window correlation outputs to form a composite correlation output. The next improvement was suggested for close-up faults. For close-up faults, the travel time is small and the relay may not be able to distinguish between the consecutive wavefronts. The authors found that for close-up faults, the cross-correlation output is unidirectional and has

a very high value in magnitude. This situation was identified by comparing the average value or the root mean square (RMS) value of the cross-correlation function instead of the peak magnitude. The RMS value, d was evaluated over a time period equal to twice the travel time, τ of the protected line length. The value of d is given by

$$d = \sqrt{\frac{1}{2\tau}\int_0^{2\tau} (\phi_{S_1,S_2})^2} \tag{2.25}$$

If d shows a value high and unidirectional, the disturbance is identified as a close-up fault. When a fault occurs with an inception angle near or equal to zero, the relaying signals become very small in magnitude and have a slow rate of rise. The authors described a method to determine the inception angle, θ for single line to ground faults and suggested a compensation method of relaying signal magnitudes. This modification did not affect the cross-correlation shape, but increased the magnitude. The relaying signals were modified as

$$S_{1m} = S_1[1 + |\cos\theta|] \tag{2.26}$$

$$S_{2m} = S_2[1 + |\cos\theta|] \tag{2.27}$$

Christopoulos et al [35] proposed a method based on travelling waves to calculate the distance to the fault. Initially, the magnitudes of the first voltage and current waves to arrive at the relay location after a fault were measured. From the voltage and current, apparent fault resistance was calculated. The magnitudes of subsequent voltage increments and the time duration elapsed since the arrival of the first wave were then determined. For each of the subsequent increments, the values were processed to find the apparent fault resistance. When two values of fault resistance agreed, the elapsed time gave the distance to the fault. This system could not detect faults with small inception angles. In addition, the reflection coefficients of the busbar where the relay was located and the remote end

busbar were assumed to be constant, which may not be true in a real system.

In a separate publication, Christopoulos et al [36] discussed the limitations in their previous approach [35] and suggested several improvements. To systematically decide the arrival of travelling waves at the relay location, the authors developed a method based on cross-correlation algorithm used by Crossley and McLaren [5]. The values of the cross-correlation output were used to estimate the reflection coefficient at the fault location, and hence the fault resistance. The fault resistance estimate was used to determine whether the surge reflected from the fault point rather than from some other discontinuity on the transmission line. The authors have also suggested methods to offset the errors caused by varying reflection coefficients at the relay busbar.

A method for fault location on transmission lines using the maximum likelihood estimate of the arrival times of reflected travelling waves was presented by Ancell and Pahalawatte [37]. The reflected travelling waves were expressed in terms of a set of incident waves which were termed the basis signals s_i. A model of the measured fault transient $\hat{y}(k)$ was given in the form

$$\hat{y}(k) = \sum_{i=1}^{I} s_i(k - \tau_i)a_i \qquad k = 1, \cdots, N \tag{2.28}$$

where k is the sample index, $s_i(k)$ is the basis signal, a_i is the associated reflection coefficient, τ_i is the arrival time of the i^{th} signal, I is the expected number of signals, and N is the number of samples. Then (2.28) can be written in the matrix form

$$\hat{y} = S(\tau)a \tag{2.29}$$

where

$$\hat{y} = [y(1), y(2), \cdots, y(N)]^T \tag{2.30}$$

$$S(\tau) = [s_1(\tau_1), s_2(\tau_2), \cdots, s_I(\tau_I)] \tag{2.31}$$

$$s_i(\tau_i) = [s_i(1-\tau_i), s_i(2-\tau_i), \cdots, s_i(N-\tau_i)]^T \tag{2.32}$$

$$a = [a_1, a_2, \cdots, a_I]^T \tag{2.33}$$

$$\tau = [\tau_1, \tau_2, \cdots, \tau_I]^T \tag{2.34}$$

The maximum likelihood parameter method determines a set of parameters $\hat{a}_{ML}$ and $\hat{\tau}_{ML}$. The maximum likelihood estimate of $\hat{a}$ is given by

$$\hat{a}_{ML} = [S(\hat{\tau})^T V^{-1} S(\hat{\tau})]^{-1} S(\hat{\tau})^T V^{-1} y \tag{2.35}$$

The maximum likelihood estimate of $\hat{\tau}_{ML}$ is the $\hat{\tau}$ which maximizes the function

$$J(\hat{\tau}) = y^T V^{-1} S(\hat{\tau}) [S(\hat{\tau})^T V^{-1} S(\hat{\tau})]^{-1} S(\hat{\tau})^T V^{-1} y - y^T V^{-1} y \tag{2.36}$$

Now, by estimating τ, the fault distance can be found. The authors claim that the maximum likelihood method performs better than the correlation method, especially when the faults have small inception angles. However, this method requires much more computational time than the correlation method and hence is difficult to implement as a real-time application.

After 1995, many different algorithms based on travelling wave signals could be found in the literature, especially using wavelet transform, artificial intelligence methods and most recently using high frequency current transients [38]. Some of them are described in section 2.5. Only two other interesting developments are discussed in this section.

Liang et al [39] proposed a pattern recognition technique for travelling wave protection. The method suggested ways to eliminate problems associated with the standard correlation

method suggested in [5]. First, instead of using the correlation method to identify the reflecting wavefronts, the authors suggested a pattern recognition technique based on *nearest neighbor method.* Then they suggested a composite function which is based on both correlation function and the nearest neighbor method to improve the performance. The nearest neighbor method states that the pattern of an input vector is determined by the nearest space distance between this vector and some reference vectors. The algorithm successively measures the space distance between the stored section of the first forward travelling wave, S_2 and the section of backward travelling wave, S_1. When a surge with the same shape as the reference signal arrives, the output of the space distance will give the minimum value. Before calculating the space distance, the mean values are removed and the signals are normalized.

$$\hat{S_1}(k) = \frac{|S_1(k) - \overline{S_1}|}{\max(S_1)} \tag{2.37}$$

$$\hat{S_2}(k) = \frac{|S_2(k) - \overline{S_2}|}{\max(S_2)} \tag{2.38}$$

Then the city block distance or Manhattan distance, d_M of the two signals is calculated by

$$d_M(k) = \sum_{k=1}^{N} |\hat{S_1}(k) - \hat{S_2}(k)| \tag{2.39}$$

The composite function, $\phi_c(k)$ is a combination of $d_M(k)$ and the correlation function $\phi(k)$.

$$\phi_c(k) = \frac{\phi(k)}{d_M(k) + C_1} \tag{2.40}$$

where the constant C_1 avoids overflowing when the measured distance is zero. The maximum $\phi_c(k)$ can be used to estimate the fault distance. The composite function improves accuracy of the distance calculation.

In another paper [40], the same authors proposed an adaptive travelling wave protection algorithm using two correlation functions. This adaptive method allows the protection

scheme to identify high impedance faults, which a travelling wave protection relay based on standard correlation algorithm may fail to detect. According to the algorithm, for low resistance faults, the fault distance is estimated from the standard correlation function, while for high resistance faults, an auxiliary correlation function is utilized. An adaptive strategy guarantees that the signal with most prominent feature is taken as the template to find the correlation, which improves the accuracy and the reliability of the algorithm.

2.5 Other Recent Developments

Power system protection had traditionally relied on the measurement of power frequency component. Digital technology did allow some new techniques to be investigated. The directional comparison schemes, travelling wave algorithms, and other transient based techniques have become popular as ultra-high-speed protection methods. The adaptive protection schemes have been well accepted due to the improved stability they provide. Methods that depend on *artificial intelligence* (AI) and *wavelet transforms* have shown improved performance. This section very briefly discusses such recent developments.

Adaptive Protection

Adaptive protection is not a new concept. Time-delay overcurrent relays adapt their operating time to fault current magnitude. Directional relays adapt to the direction of fault current. These, however, are permanent characteristics of a relay or relay system and are included as part of the original design or installation to perform a given function. The concept of adaptive relaying is based on the fact that many relay settings are dependent upon assumed conditions on the power system. With complex interconnected power networks today, it is difficult to assume some of these conditions. To facilitate all possible scenarios the protection scheme may have to handle, the actual protection settings in use are often not optimal for any particular system state. If the relay needs to operate with an optimal setting for a given condition of the power network, then the setting has to adapt itself to

the real-time system states as the system conditions change. Phadke and Horowitz [41] mentioned, "In every phase of the development of a system's protection, a balance must be struck between economy and performance, dependability and security, complexity and simplicity, speed and accuracy, credible vs conceivable. The objective of providing adaptive relay settings is to minimize compromises and allow relays to respond to actual system conditions."

Rockefeller et al showed how the concepts of adaptive relaying can be introduced on the existing power system [42]. They showed the situations where adaptive relaying can be used and their advantages:

- Adaptive system impedance model (permits calculation of fault-distribution): Improved relaying reliability and possible avoidance of future line construction;
- Adaptive sequential instantaneous tripping (detection of far-end breaker openings): Faster back-up protection and possible elimination of the need for a second pilot scheme;
- Adaptive multi-terminal relay coverage (accounts for changes in infeed ratios): Improved zone 1 and zone 2 settings;
- Adaptive zone 1 ground distance (accounts for large apparent impedance in fault resistance): Greater sensitivity to high resistance ground faults;
- Adaptive response to defective relaying equipment: Minimizes need for second pilot scheme and need to take affected line out of service;
- Adaptive reclosing: Faster restoration following incorrect trips, reduced number of unsuccessful reclosures, reduced shaft fatiguing;
- Variable breaker-failure timing (detects failure to interrupt): Improves back-up timing margins and eliminates unneeded tripping of back-up breakers;

- Adaptive last-resort islanding (system splitting to isolate generators with manageable load levels): Improved probability of maintaining units in service to facilitate load restoration;
- Adaptive internal logic monitoring: Improved relaying reliability;
- Relay setting coordination checks (checks coverage and selectivity): Coordination optimized, starting from existing power system conditions and minimizes operating constraints.

They showed how the adaptive techniques can be implemented using the slow speed responses of a SCADA system, in contrast to the high-speed channels used in pilot relaying between interconnected transmission line terminals.

Horowitz et al presented an analysis of adaptive relaying concepts during the same time [43]. They defined the adaptive concept as "Adaptive protection is a protection philosophy which permits and seeks to make adjustments to protection functions in order to make them more attuned to prevailing power system conditions". In their paper, they had investigated the adaptive techniques applied to multi-terminal transmission line protection, relay settings and automatic circuit breaker reclosing control. They showed how the adaptive relay settings can be used in situations such as pre-fault load effect, cold load pickup, source impedance ratio, line charging and system asymmetries.

Protection Based on Artificial Intelligence

Artificial neural networks operate on the assumptions drawn on the behavior of biological neural networks. An artificial neural network (ANN), or commonly known as artificial intelligence (AI) provides a viable alternative to modelling nonlinear systems where it is difficult to obtain a deterministic model to represent the system behavior. ANNs have advantages as well as disadvantages: the implementation of the ANN does not require complete understanding about the system behavior and hence can be used in extremely

complex situations. However, training and testing of ANNs can take a long time and the accuracy of the network depends on the size and the accuracy of the test set. The solutions based on ANNs use different methods to increase performance in terms of speed of operation and efficiency. ANNs have been used in various industries and have proved to be a vital tool in applications related to power systems. One of the areas of power systems engineering that gained more attention with use of ANNs is distance protection. A lot of applications of ANNs can be found in relay literature, but we will only consider three applications for this discussion.

Sidhu et al [44] presented an ANN based approach to determine the direction to the fault. The directional discrimination was achieved through a multi-layer feed-forward neural network. The paper discusses important issues related to the implementation of the ANN: preparation of suitable training data, selection of a suitable ANN structure, training of the ANN, and evaluation of the trained network using test patterns. The data for training was obtained by simulating the power system on EMTDC. During the selection process of ANN structure, number of layers, transfer function, number of neurons and number of inputs and outputs had to be chosen appropriately to identify all fault conditions.

Coury and Jorge [45] showed how the magnitudes of the three phase voltage and current phasors can be utilized in an ANN based protection relay to achieve fast and precise operation under different fault conditions and changes in the network. The neural network they used was based on the backpropagation algorithm. The backpropagation algorithm works by adjusting the weights which are connected in successive layers of multi-layer perceptrons. The ANN based approach made it possible to extend the zone 1 reach of distance relays, hence improving the security.

Venkatesan and Balamurugan [46] developed a real-time fault detector for the distance protection application based on artificial neural networks. The paper describes their approach to data analysis, feature extraction, software design and simulation, quantization, performance analysis, hardware design and implementation of the ANN based relay. For

the software design an ANN simulator has been developed using the C++ programming language instead of using the commercially available simulators. The hardware implementation has been done using a single chip with both the preprocessors and the neural processor on the same chip. The relay could detect faults in the transmission line within one third of a power cycle from the inception of fault.

Wavelet Transform Methods

In recent years, researchers have developed powerful wavelet techniques for the multiscale representation and analysis of signals. These new methods differ from the traditional Fourier techniques. The Wavelet Transform (WT) is of interest for the analysis of non-stationary signals. It provides an alternative to the classical Short-Time Fourier Transform (STFT) or Gabor transform. In contrast to the STFT, which uses a single analysis window, the WT uses short windows at high frequencies and long windows at low frequencies. Wavelets localize the information in the time-frequency plane; in particular, they are capable of trading one type of resolution for another, which makes them especially suitable for the analysis of non-stationary signals [47].

The wavelet transform is an operation that transforms a function by integrating it with modified versions of some kernel function [48]. The kernel function is called the mother wavelet, and the modifications are translations and compressions of the mother wavelet. For a function to be a mother wavelet, it must be *admissible*. A function $g \in L^2(R)$ is admissible if

$$c_g \equiv \int_{-\infty}^{\infty} \frac{|G(\omega)|^2}{|\omega|} d\omega < \infty \tag{2.41}$$

where $G(\omega)$ is the Fourier transform of $g(t)$, $L^2(R)$ is the set of all square integrable or finite energy signals, and R denotes the real numbers. The constant c_g is the *admissibility constant* of the function $g(t)$, and the requirement that it is finite allows for inversion of the wavelet transform. Any admissible function can be a mother wavelet. For a given function

$g(t)$, the *mother wavelet* of the transform is assumed to be admissible. Wavelet transform can be in analog domain (Continuous Wavelet Transform, CWT) or digital domain (Discrete Wavelet Transform, DWT). The mother wavelets can be orthogonal or non-orthogonal. In much of the wavelet transform literature, dyadic orthogonal mother wavelets are chosen as the mother wavelet.

The CWT of a function $f(t)$ with respect to the wavelet function $\psi(t)$ is given by

$$W_\psi f(a,b) = \frac{1}{\sqrt{a}} \int_{-\infty}^{\infty} f(t)\psi^*[\frac{t-b}{a}]dt \tag{2.42}$$

where a and b are the scaling (dilation) and translation (time shift) constants respectively.

The DWT as applied to sampled waveform $f(k)$ is given by

$$W_\psi f(m,n) = \frac{1}{\sqrt{a_0^m}} \sum_k \psi^*[\frac{n-ka_0^m}{a_0^m}] \tag{2.43}$$

where the parameters a and b in (2.42) are replaced by a_0^m and ka_0^m, k and m being integer variables.

One important area of application where wavelet transform has been found to be relevant is power engineering. Lee et al [49] did a literature survey to find application of wavelets in power systems. They found that wavelet transform can be readily applied to power disturbance detection and localization, power disturbance data compression and storage, power disturbance identification and classification, power devices protection and power disturbance network/system analysis. Robertson et al [50] showed how wavelet transform can be used to identify the transients on the power system. In this section, we will discuss few applications of wavelet transform in transmission line protection schemes.

Magnago and Abur showed how the high frequency travelling waves can be identified with the aid of wavelet transform and how that information can be used to estimate the distance to the fault [51]. Two different approaches to estimate the fault location have been attempted. In one method, fault transients at the two ends of the transmission line are

identified through synchronized recording of transient signals. The recordings are synchronized using a GPS method. Time difference between the arrival of the wavefronts at the two ends are used to estimate the distance. In the second method only the measurements at one end are used for the protection. The arrival of the consecutive wavefronts are used to estimate the distance to the fault. Different algorithms are used in the case of grounded or ungrounded faults.

Shang et al [52] used wavelet transform to develop a high-speed protection algorithm for transmission line protection. The wavelet modulus maxima (WMM) was used as a criterion to detect fault conditions (the absolute local maximum values of the wavelet transform of the signal are called wavelet modulus maxima). The WMM must satisfy the condition given by

$$|W_{max}x(t)| \leq ks^{\alpha} \tag{2.44}$$

Here, $W_{max}x(t)$ is the WMM of signal $x(t)$, k is a constant, s is scale and α is the Lipschitz exponent. The polarity of the WMM associated with consecutive wavefronts is used for the fault identification. Using this method, it is possible to identify special situations such as switching onto unloaded lines and onto faulted lines.

Yibin et al [53] proposed a way to use wavelet transform to extract the fundamental frequency components of the three phase signals and use the fundamental components to calculate the fault location. The wavelet method has been compared with the results obtained by using the standard Fourier transform methods.

Wai and Yibin [54] investigated a method to use wavelets for high impedance fault identification. They describe how high impedance faults and capacitor bank switching can be classified using wavelet analysis filter banks. The filter banks are implemented as cascaded quadrature mirror filters. The high impedance faults are modelled in an improved method to yield better simulation results. The wavelet transform of the transient signals showed different characteristics under high impedance faults and capacitor switching.

Wide Area Protection

In the early days, the primary function of protective relays was to simply protect the power system components. However, with the advent of the microprocessor relays, it became obvious that microprocessor relays can provide both protection and measurement functions. The ability of new microprocessor relays to communicate with each other and the availability of broadband communication links allowed them to share information that could be used for supervisory, control and protection purposes. Because of the advancing technology of protective relays and their communication capabilities, the new relays are called Intelligent Electronic Devices (IED) [55]. The high-speed communication links allowed relays to quickly update their status to each other or to a central control station. This technology advancements and the time synchronizing capability of GPS are used in the new wide area backup protection algorithms. Wide area backup protection schemes are considered a possible solution for preventing blackout situations. We will briefly discuss two methods used in wide area protection.

Serizawa et al [56] proposed a wide area current differential backup protection scheme. The current differential scheme provides a higher selectivity than the conventional backup protection employing distance relays. The proposed system configuration utilized ATM transmission networks and time synchronous systems. For the current differential protection scheme, the current measurements of each busbar and transmission lines and transformers connected to that bus bar are considered. For the backup protection of long transmission lines GPS synchronized current measurements were taken at the ends of the line.

Tan et al [57] proposed a wide area backup protection scheme that could prevent cascading outages in power systems. The backup protection scheme prevents cascaded tripping in two ways: 1) It determines the precise location of a fault so that only the circuit breakers necessary to isolate the fault are tripped and 2) It avoids unnecessary trips, due to hidden failure or overloading, by blocking the trip signals of conventional backup protection relays. To prevent cascading trips, a wide area backup protection expert system (BPES) is used.

BPES is a wide area communication network based protection system designed to protect a region of the network by providing selective and secure backups. The BPES operates in two modes: normal and emergency mode. During normal operation, the BPES monitors the open/closed states of circuit breakers and the operational response of conventional protection relays on the network. It changes to the emergency mode when a fault is detected and decides the best way to isolate the fault if the main protection has failed. The BPES may block a conventional backup protection relay if necessary. The paper extensively discusses the implementation details, the possible fault scenarios, and how the BPES can be used for preventive control of wide area blackouts.

Chapter 3

Theoretical Aspects

3.1 Introduction

The hybrid relay utilizes both travelling wave information derived from the high frequency transient signals and the impedance calculated from the fundamental components of the voltage and current signals. Before understanding how the hybrid relay works, it is important to have an idea about basic principles behind the travelling wave protection as well as impedance measurement scheme. In this chapter, we introduce theory behind these algorithms. The theory associated with the travelling wave protection will be discussed first. In order to simplify the explanation, a single phase lossless line will be used to introduce the theory. This explanation will then be extended to a three phase system. The travelling wave theory will be followed by an introduction to the impedance algorithm. Finally, we will discuss how the two algorithms are combined and the operating principle of the hybrid algorithm.

3.2 Theory of Travelling Wave Protection

3.2.1 Transient Waves

Faults which occur on a high voltage transmission line at an instant of a non-zero voltage will cause the pre-fault line charge to rapidly discharge. This can generate heavy surges on the transmission line which will propagate as waves. These waves will travel close to the speed of light along both directions of the transmission line from the fault point and reflect at discontinuities along the line, including the fault point itself. The repeated reflection of these surges or waves produces decaying high frequency voltage and current transients. Each wave is a composite of frequencies, ranging from a few kilohertz to several megahertz, having a fast rising front and a slower decaying tail [58]. These composite waves have a characteristic impedance that will depend on the line parameters. The waves continue to exist until they are damped out and a new power system equilibrium is reached. In an extra high voltage (EHV) transmission line, where the line length and the system capacitance are large, these transients become significant, specially with small resistance in the faulted network. These transient signals, which will be identified as travelling waves, can be utilized to detect faults in power transmission lines.

3.2.2 Basic Principles Developed on a Single Phase Model

The principles developed will be for lossless single-phase transmission lines. The lossy case has to be considered separately. However on EHV transmission lines, the effects of resistance in the fault loop is minimal and may be neglected in the derivations.

Principle of Superposition

The faulted network can be described using the *principle of superposition* as shown in Fig.3.1. The voltage and current signals are measured at the relay location R. Consider a line to ground fault at point F in Fig.3.1(a). The inception of a fault in the power system will

cause the post-fault voltage v_R and current i_R at the relay location R to deviate from the steady state pre-fault voltage v'_R and current i'_R. The deviation signals or the incremental components can be considered to be generated by switching on a fictitious voltage source at the fault point with a voltage equal in magnitude and opposite in sign to the pre-fault voltage at the fault point, and with all other sources suppressed.

The superposition of the pre-fault signals in Fig.3.1(b) and the deviation signals in Fig.3.1(c) produce the post-fault signals. We then have

$$v_R(t) = v'_R(t) + \Delta v_R(t) \tag{3.1}$$

$$i_R(t) = i'_R(t) + \Delta i_R(t) \tag{3.2}$$

where $\Delta v_R(t)$ and $\Delta i_R(t)$ are the fault generated voltage and current deviations from the steady state pre-fault values at the relay location respectively. The deviation signals $\Delta v_R(t)$ and $\Delta i_R(t)$ are readily obtained from the measured post-fault voltage v_R and current i_R signals by subtracting the sinusoidal pre-fault steady state voltage v'_R and current i'_R components. These superimposed quantities are used in the travelling wave relaying algorithms, as used by others in the past [5],[26]-[36].

The voltage deviation Δv_R will depend on the amplitude of the voltage at the fault location at the instant of the fault, impedance values of the sources and line and the fault resistance. The magnitude of the initial voltage deviation is maximal for faults occurring at the moment of a voltage maximum, while it is zero for faults occurring during a voltage zero. The current deviation Δi_R contains an exponentially decaying component commonly known as a constant dc-offset, the magnitude of which depends on the fault inception angle. The exponential component is maximal for faults incepted at a voltage zero and zero for faults occurring at a voltage maximum. The resistance in the fault loop will cause the offset in the current signal to decay. These resistances will further reduce the magnitude of both voltage and current deviations.

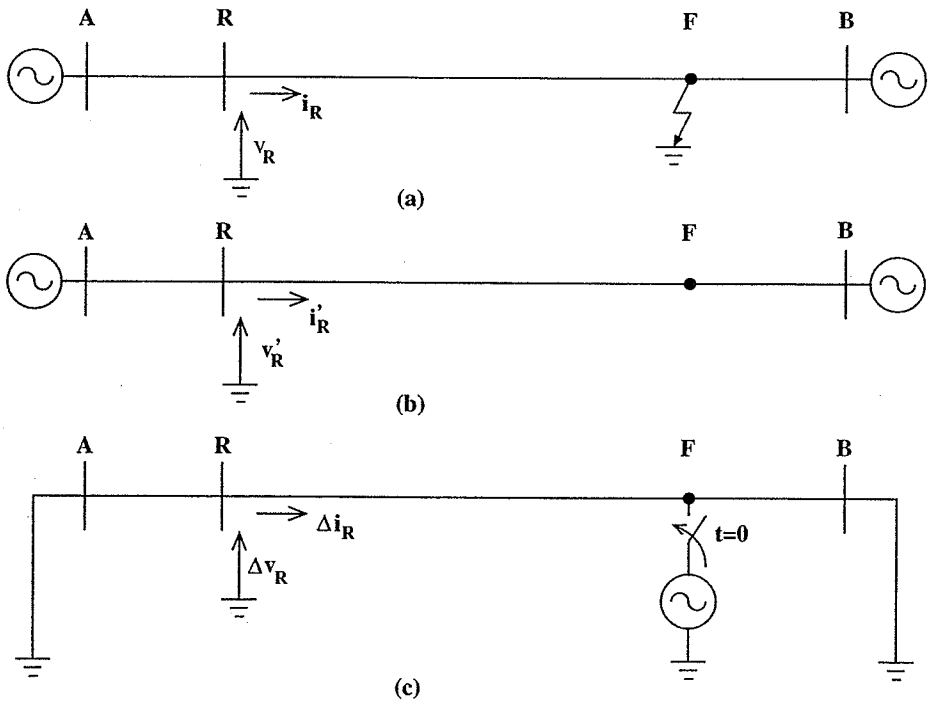

Figure 3.1: Principle of superposition applied to a faulted network

Travelling Waves

To illustrate the travelling wave phenomena, the Bewley Lattice diagram [4] can be used. Fig.3.2 shows the Bewley diagram of a single phase power system. The transmission lines connect two sources at busbars A and B to the middle busbar R. The voltage and current signals are measured at the busbar R. For a relay which protects line RB located at busbar R, the forward direction is considered as RB and the reverse direction is RA. When a line to ground fault in forward direction occurs at point F as shown, the fault generated wavefronts will travel along both directions of the line from the fault location.

The wavefronts which travel from the fault location F towards the measuring point R under a forward fault are known as backward travelling waves. These wavefronts will travel past R and reflect at busbar A. The reflected waves will then travel back towards the fault location F. The wavefronts which travel towards the forward direction from the relay location R are known as forward travelling waves. When these waves reach F, part of it

will reflect from the fault point F while the remaining part propagates towards the busbar B. These two components are known as reflected and transmitted waves, respectively.

The magnitude of the reflected and transmitted wavefronts will depend on the fault impedance and the impedance of the transmission line. The reflected wave components will travel back towards R again. The wavefronts which travel towards the busbar B from the fault location F will reflect from busbar B and reach F again. Part of them will be transmitted towards R and the other part will be reflected back towards busbar B. The wavefronts will continue to propagate and reflect in this manner until they are damped out.

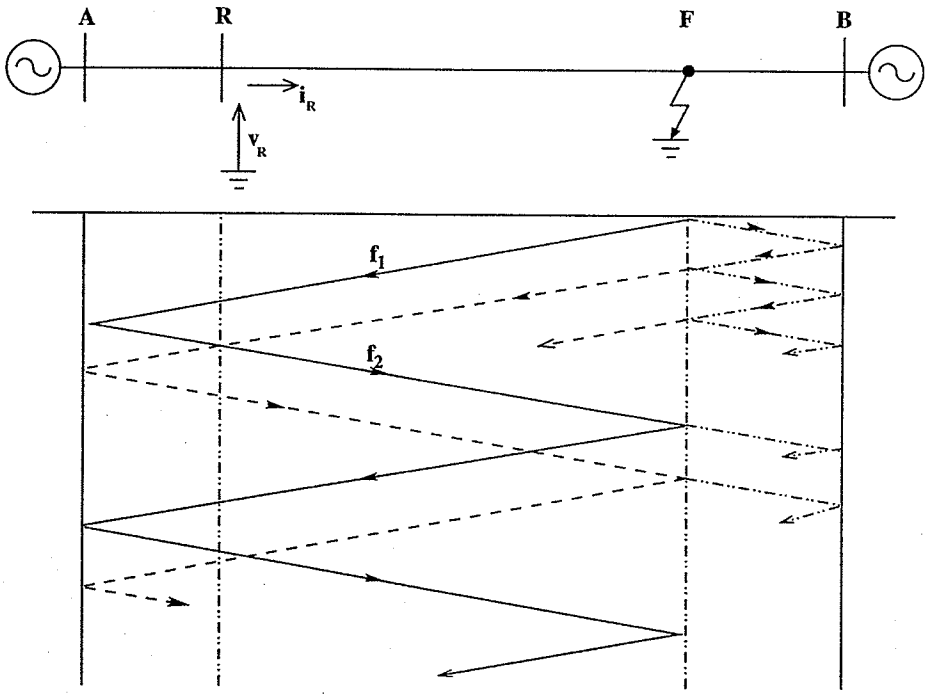

Figure 3.2: Bewley lattice diagram of wavefronts generated by a fault

The voltage and current signals on a transmission line can be considered to be a summation of a backward travelling wave F_1 and a forward travelling wave F_2 (see Appendix A). These waves propagate with a constant amplitude at a velocity slightly less than the speed of light. The amplitude and the shape of these waves may change in a lossy line. The

general solution of the wave equation is given by

$$v(x,t) = F_1(x-at) - F_2(x+at) \tag{3.3}$$

$$i(x,t) = \frac{1}{Z_c}[F_1(x-at) + F_2(x+at)] \tag{3.4}$$

where Z_c is the surge impedance of the line and 'a' is the propagation velocity of the waves in the line.

If only the incremental components are considered as in 3.1 and 3.2, the fault generated voltage and current deviations can be expressed as

$$\Delta v(x,t) = f_1(x-at) - f_2(x+at) \tag{3.5}$$

$$\Delta i(x,t) = \frac{1}{Z_c}[f_1(x-at) + f_2(x+at)] \tag{3.6}$$

where f_1 and f_2 are the backward and forward travelling waves calculated from the incremental components of the voltage and current signals. Hence from (3.5) and (3.6), it can be shown that

$$\Delta v(x,t) + Z_c.\Delta i(x,t) = 2.f_1(x-at) = S_1 \tag{3.7}$$

$$\Delta v(x,t) - Z_c.\Delta i(x,t) = -2.f_2(x+at) = S_2 \tag{3.8}$$

The signals S_1 and S_2 represent the backward and forward travelling waves and will be used as the backward and forward relaying signals in the travelling wave algorithm.

Forward Fault

Fig.3.3 shows the propagation and reflection of waves generated due to a forward fault on a transmission line. The wavefronts reflect at the fault point F, and the busbars A and B. The voltage and current signals are measured at busbar R. In order to derive the mathematical equations, the measured signals are considered to be the incremental

components as described in (3.3) and (3.4).

The first backward travelling wave f_1 reaches R at τ_1 seconds after the instant of fault inception and will reach busbar A at time τ. The wave f_1 reflects from busbar A and travels towards the fault location passing R at time τ_2. When the forward travelling wave f_2 reaches F at time 2τ, part of it will reflect from F while the remaining part propagates towards the busbar B. The part of the travelling wave f_2 that reflected from F (shown as f_{1r}) will reach the busbar R at time τ_3 and reflect from busbar A at time 3τ.

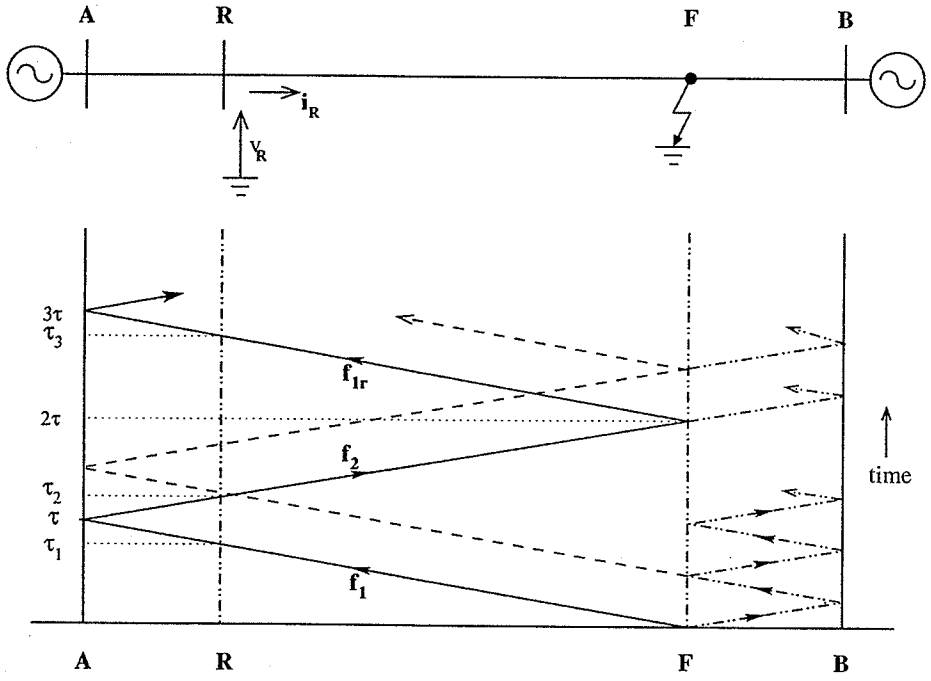

Figure 3.3: The propagation and reflection of wavefronts in a forward fault

As already mentioned, a fault can be described as introducing a voltage source equal in magnitude and opposite in sign at the fault point, at the time of the fault. If the pre-fault steady state voltage is given by $V_p \sin(\omega t + \phi)$, the voltage deviation Δv_F due to the fault is then

$$\Delta v_F(t) = -v_F^{\prime}(t) = -V_p \sin(\omega t + \phi) \tag{3.9}$$

where, $v_F^{\prime}$ is the pre-fault steady state voltage at point F. The voltage waveform is assumed

to be sinusoidal with a peak value $V_p = \sqrt{2}V_{rms}$.

If the fault occurs at time t, considering the wave propagation times shown in Fig.3.3, the voltage and current deviations seen at the relay point R can be combined to obtain the following relationships:

$$\Delta v_F(t) + Z_c.\Delta i_{RF}(t) = \Delta v_R(t+\tau_1) + Z_c.\Delta i_R(t+\tau_1) \quad (3.10)$$

$$\Delta v_F(t) - Z_c.\Delta i_{RF}(t) = \Delta v_R(t+\tau_1) - Z_c.\Delta i_R(t+\tau_1) \quad (3.11)$$

where Δi_{RF} is the deviation in current with current measurement taken as positive in the direction from relay point R to fault location F. τ_1 represents the travel time for the waves from F to R.

But at time τ_1, the forward travelling wave f_2 is equal to zero at the relaying point. Hence from (3.8) and (3.11)

$$\Delta v_R(t+\tau_1) - Z_c.\Delta i_R(t+\tau_1) = 0 \quad (3.12)$$

The condition in (3.9) combined with (3.12) yields

$$\Delta i_{RF}(t) = \frac{\Delta v_F(t)}{Z_c} = \frac{-V_p \sin(\omega t + \phi)}{Z_c}$$

Using the above results, (3.10) can be solved to give

$$\Delta v_R(t+\tau_1) + Z_c.\Delta i_R(t+\tau_1) = -2V_p \sin(\omega t + \phi) \quad (3.13)$$

By introducing a time shift, from (3.7) we thus obtain

$$f_1(t+\tau_1) = -2V_p \sin(\omega t + \phi)$$

$$f_1(t) = -2V_p \sin(\omega t - \omega\tau_1 + \phi) \quad (3.14)$$

for $\tau_1 < t < 2\tau + \tau_1$. The backward travelling wave f_1 is initially independent of the terminal conditions. If τ_1 is small compared to the period of the 60Hz signal, for a lossless line, it is possible to approximate f_1 of (3.14) to have a constant value of

$$f_1(t) \simeq -2V_p \sin(\phi) \tag{3.15}$$

for the time period $\tau_1 < t < 2\tau + \tau_1$.

When the backward travelling wave arrives at the line terminal, the wavefront will reflect and travel towards the fault again. This reflected wave will have a reduced amplitude compared to that of the incoming wave depending on the terminal conditions. The reflected wave will be of the "form"

$$f_2 = \xi f_1 \tag{3.16}$$

for $\tau_2 < t < 2\tau + \tau_2$ where ξ is the reflection coefficient of the termination. Hence from (3.15), the forward wave front of f_2 will have the "shape"

$$f_2(t) \simeq \xi 2V_p \sin(\phi) \tag{3.17}$$

The shape of this reflected waveform will mainly depend on the terminal characteristics. For example on a lossless line with surge impedance Z_c, if an incoming wave of the shape given in (3.15) reflects from a source consisting of a pure inductance L_s,

$$f_2(t) = V_p \sin(\phi) \left[1 - 2e^{-(\frac{t-\tau_2}{L_s}).Z_c}\right] \tag{3.18}$$

for $\tau_2 < t < 2\tau + \tau_2$. The high frequency steep signal will be reflected immediately and the low frequency signals will reflect with an exponential decay.

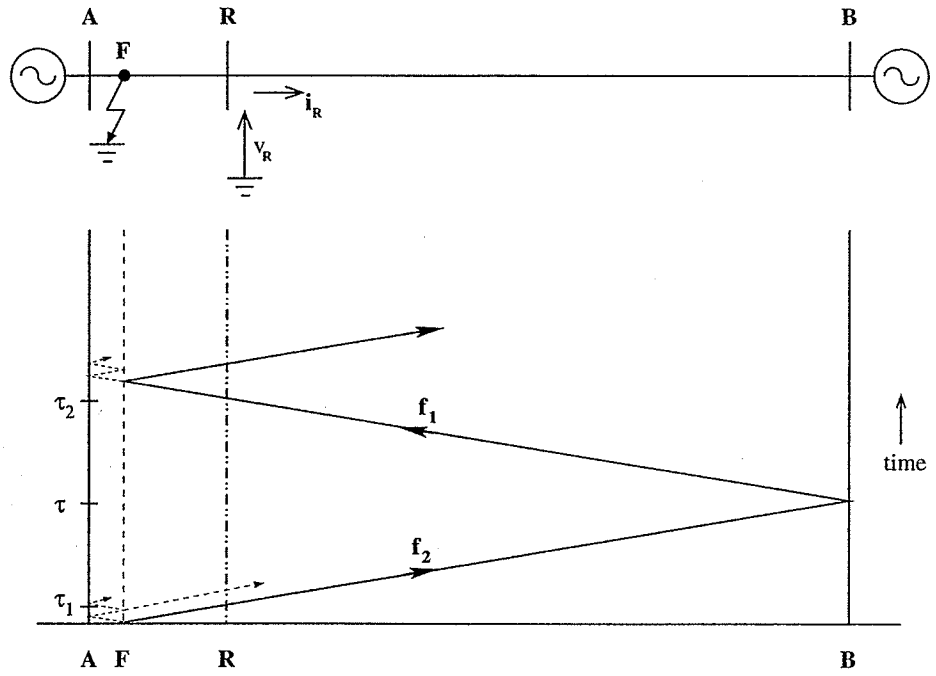

Figure 3.4: Wave propagation for a reverse fault

Reverse Fault

For a reverse fault with respect to the relaying point R, as in Fig.3.4, the relay first sees the forward travelling wave f_2. The travelling waves will propagate past R along the line and reflect at the remote busbar B. The first forward wavefront f_2 reaches R at time τ_1. This will reach busbar B at time τ. The wavefront f_2 will reflect from busbar B and travel towards the relay location R at time τ_2.

If the pre-fault steady state voltage is given by $V_p \sin(\omega t + \phi)$, the voltage deviation Δv_F due to the fault then is

$$\Delta v_F(t) = -V_p \sin(\omega t + \phi) \tag{3.19}$$

If the fault occurs at time t, considering the wave propagation times shown in Fig.3.4,

the voltage and current deviations seen at the relay point R can be combined to obtain

$$\Delta v_F(t) + Z_c.\Delta i_{RF}(t) = \Delta v_R(t+\tau_1) + Z_c.\Delta i_R(t+\tau_1) \quad (3.20)$$

$$\Delta v_F(t) - Z_c.\Delta i_{RF}(t) = \Delta v_R(t+\tau_1) - Z_c.\Delta i_R(t+\tau_1) \quad (3.21)$$

where Δi_{RF} is the deviation in current with current measurement taken as positive in the direction RB. τ_1 represents the travel time for the waves from F to R.

However, initially the backward travelling wave f_1 is equal to zero at the relaying point. Hence from (3.7) and (3.20)

$$\Delta v_R(t+\tau_1) + Z_c.\Delta i_R(t+\tau_1) = 0 \quad (3.22)$$

The condition in (3.19) combined with (3.22) yields

$$\Delta i_{RF}(t) = -\frac{\Delta v_F(t)}{Z_c} = \frac{V_p \sin(\omega t + \phi)}{Z_c} \quad (3.23)$$

Using the above results, (3.21) can be solved to give

$$\Delta v_R(t+\tau_1) - Z_c.\Delta i_R(t+\tau_1) = -2V_p \sin(\omega t + \phi) \quad (3.24)$$

By introducing a time shift, from (3.8) we thus obtain

$$f_2(t) = -2V_p \sin(\omega t - \omega\tau_1 + \phi) \quad (3.25)$$

for $\tau_1 < t < 2\tau + \tau_1$. The forward travelling wave f_2 is initially independent of the terminal conditions. If τ_1 is small compared to the period of the 60Hz signal, it is possible to approximate f_2 of (3.25) for the period $\tau_1 < t < 2\tau + \tau_1$ with

$$f_2(t) \simeq -2V_p \sin(\phi) \quad (3.26)$$

3.2.3 Three Phase Systems

Background

On a three phase transmission system, when a fault occurs on one conductor, transient currents will be induced in the healthy conductors due to the mutual coupling between them. The mutual elements of the surge impedance matrix allow the travelling waves to couple across the phases. The waves induced on sound phases from the faulted phase travel between the two ends of the line and subsequently interact with the waves on the faulted phase [59]. This could distort the waves on all three phases. Due to the coupling effect, the set of equations describing the propagation of waves on each phase become interdependent. According to the theory of natural modes [60], using modal transformation a three-phase coupled line can be decomposed into three independent modes of propagation or three single-phase lines (see Appendix B). The travelling wave theory applied for a single phase circuit can be readily applied to the independent modes separately to analyze the faults and hence to analyze a three phase system.

Modal Transformation

In developing the travelling wave theory for the single-phase system, the line was assumed to be ideal (no-loss). In a lossless line, the current and voltage waves are subject to the same attenuation and have the same velocity at all the frequencies. Attenuation and distortion are due to resistive elements and the effect of frequency dependent elements in the network. The frequency dependent, nonuniform distribution of the ground currents due to the earth conductivity has to be considered when dealing with an actual system. Appendix A discusses the formulation of travelling wave signals for a lossy line and Appendix B deals with the voltage current relationship in a three phase system and how the three phase system can be transformed into three independent single phase systems or modes.

The relationship between the three phase signals and modal components for voltage and current signals is given by

$$\begin{aligned} [v(t)] &= [S][v^{(m)}(t)] \\ [i(t)] &= [Q][i^{(m)}(t)] \end{aligned} \tag{3.27}$$

where $[S]$ and $[Q]$ are the voltage and current modal transformation matrices respectively. $[v^{(m)}(t)]$ and $[i^{(m)}(t)]$ are the modal voltage and current matrices. The inverse relationship is given by

$$\begin{aligned} [v^{(m)}(t)] &= [S]^{-1}[v(t)] \\ [i^{(m)}(t)] &= [Q]^{-1}[i(t)] \end{aligned} \tag{3.28}$$

The modal signals are assumed to have a single propagation velocity for each mode. The aerial modes will not cause a significant error over the frequency range considered and hence can be assumed frequency independent. However, for a single phase to earth fault, the dominant mode of propagation is the earth mode (model). The earth mode parameters depend on the earth resistivity and may cause significant variations in the propagation velocity [61]. The ground mode has lower velocity and greater attenuation and distortion than the aerial modes (mode2 and mode3) because of the frequency dependence of their parameters. The velocity of waves in aerial modes is close to the speed of light. The velocity and attenuation of the aerial modes for a fully transposed single circuit three phase system are identical. In the studies reported in this thesis, a fully transposed transmission system is assumed and the modal transformation matrices mentioned in Appendix B are used for the transformation like many others did [5, 31, 34, 33, 35]. Since the earth mode is frequency dependent and the velocity varies with the frequency, the earth mode was found to be difficult to use for the fault analysis. Hence for deriving the relaying signals, the aerial mode 2 will be used.

Travelling Waves in a Three Phase System

To derive the travelling wave signals in a three phase system, the modal components of the incremental voltage and current are used. The incremental voltage, Δv and current, Δi components are calculated separately for each phase to find the deviation from steady state components. The modal components of the incremental voltage and current signals are found by using a modal transformation matrix described in Appendix B. For example, if the Clarke transformation is considered,

$$\begin{bmatrix} \Delta v^{(1)} \\ \Delta v^{(2)} \\ \Delta v^{(3)} \end{bmatrix} = \frac{1}{3} \begin{bmatrix} 1 & 1 & 1 \\ 2 & -1 & -1 \\ 0 & \frac{1}{\sqrt{3}} & -\frac{1}{\sqrt{3}} \end{bmatrix} \begin{bmatrix} \Delta v_a \\ \Delta v_b \\ \Delta v_c \end{bmatrix} \tag{3.29}$$

and

$$\begin{bmatrix} \Delta i^{(1)} \\ \Delta i^{(2)} \\ \Delta i^{(3)} \end{bmatrix} = \frac{1}{3} \begin{bmatrix} 1 & 1 & 1 \\ 2 & -1 & -1 \\ 0 & \frac{1}{\sqrt{3}} & -\frac{1}{\sqrt{3}} \end{bmatrix} \begin{bmatrix} \Delta i_a \\ \Delta i_b \\ \Delta i_c \end{bmatrix} \tag{3.30}$$

The modal voltage components $\Delta v^{(m)}$ and $\Delta i^{(m)}$ for each mode m can be used to derive the forward and backward waves for individual modes of propagation. The backward relaying signal $S_1^{(m)}$ for mode m is given by

$$S_1^{(m)} = \Delta v_R^{(m)} + Z_c^{(m)} \Delta i_R^{(m)} \tag{3.31}$$

and the forward relaying signal $S_2^{(m)}$ for mode m is given by

$$S_2^{(m)} = \Delta v_R^{(m)} - Z_c^{(m)} \Delta i_R^{(m)} \tag{3.32}$$

where $\Delta v_R^{(m)}$ and $\Delta i_R^{(m)}$ are the incremental voltage and current quantities of mode m at relay location R. Z_c^m is the surge impedance for mode m.

The wave components S_1^m and S_2^m can be used in the same way as in a single phase transmission line model described in section 3.2.2. Here onwards in this thesis, the notation S_1 and S_2 will indicate the backward and forward relaying signals that belong to the aerial mode 2.

3.2.4 Fault Direction

Travelling Wave Functions

The travelling wave functions S_1 and S_2 calculated using incremental components of the voltage and current signals must ideally have zero magnitude when the power system operates under steady state conditions. Even with the numerical errors associated with the calculations in practice, they show extremely low values. However, when a fault occurs in the system, the voltage and current signals deviate significantly from their steady state values and hence S_1 and S_2 will show large magnitudes. A change in magnitude of the travelling wave signals (from near-zero values) could indicate a disturbance on the line. Depending on the fault direction and relay location, the sequence in which the signals S_1 and S_2 become non-zero can vary. The direction of the fault can be determined by the sequence in which S_1 and S_2 exceed a predetermined threshold. *If S_2 exceeds a certain threshold before S_1, then the fault is in the backward direction, else the fault is in the forward direction.*

Discriminant Functions

The backward and forward travelling wave functions S_1 and S_2 are dependent on the fault inception angle ϕ. In an unlikely situation when a fault occurs near a voltage zero (ie. fault inception angle is close to zero), the signals S_1 and S_2 will have small magnitudes. Under such conditions, it might be difficult to detect a fault only using the S_1 and S_2 signals. Identification of fault conditions and direction can be improved by using a method that will be independent of the fault inception angle. To improve the reliability in fault detection, a *discriminant function* which does not depend on ϕ can be used. The discriminant functions

are calculated using the travelling wave functions and their differentiations [29]. The backward discriminant function D_B and forward discriminant function D_F for a single phase system are given by,

$$D_B = (\Delta V_R + Z_c.\Delta I_R)^2 + \frac{1}{\omega^2}\left[\frac{d}{dt}(\Delta V_R + Z_c.\Delta I_R)\right]^2 \tag{3.33}$$

$$D_F = (\Delta V_R - Z_c.\Delta I_R)^2 + \frac{1}{\omega^2}\left[\frac{d}{dt}(\Delta V_R - Z_c.\Delta I_R)\right]^2 \tag{3.34}$$

The discriminant functions are initially termination independent and the performance of the functions do not depend on the fault inception angle. D_B and D_F are zero for a healthy line and show very high values in case of a fault. The highly decisive nature of these functions can be utilized to classify forward and reverse faults. *If D_F exceeds a certain threshold value before D_B, it is a backward fault, otherwise it is a forward fault.*

3.2.5 Determination of Fault Location

The travelling wave relaying signals S_1 and S_2 can be used to determine the direction of the fault. The relay is set up to operate on a forward fault. However, the relay must be able to determine whether the disturbance occurred within its zone of protection. To determine whether the fault is within the zone of protection, the distance to the fault can be used. The distance to the fault is evaluated using the time difference between an identified forward wavefront at the relay point and the corresponding wavefront reflected from the fault point. To match the two wavefronts correlation techniques are used. The correlation techniques provide a method to distinguish the required wavefront from other surges on the line. Recently, there has been an increasing interest in applying wavelet transform methods to detect transients. However, it is difficult to find a clear method of choosing a suitable mother wavelet which could identify different fault conditions. Due to the robust and simple implementation of the correlation algorithm, a cross-correlation function will be used to calculate the distance to the fault in the proposed method.

When a fault occurs, the fault generated wavefronts will propagate along both directions of the line, as shown in Fig.3.3. The first wavefront f_1 reaches the relay location at time τ_1. Since signal S_2 is still low at this time, a forward fault is detected. When the signal S_2 goes above a certain threshold at time τ_2, a forward wavefront is detected at R. Once a forward fault is detected, the relay starts storing the forward travelling wave signal S_2. This wavefront S_2 is stored in a window of N samples as a reference signal. The storage time is selected so that the stored signal will contain both pre-fault and post-fault information. The wavefront f_2 will reflect at the fault point and a portion of the wavefront will return to the relay location at time τ_3. The reflected wave front is identified by matching the backward relaying signal S_1 to the stored signal S_2. To identify the correct wavefront, the cross-correlation is found between the stored and returning signals [5]. The time τ_3 at which the reflected wave S_1 matches the stored signal S_2 is estimated by finding the instant at which the cross-correlation of the two signals shows a peak value.

The distance to the fault can be calculated by,

$$x_f = \frac{\tau_3 - \tau_2}{2}.a \tag{3.35}$$

where a is the velocity of propagation of waves on the line. If the distance x_f is less than the line length, the fault falls within the protection zone of the relay.

3.2.6 Correlation Techniques

Correlation is a measure of a linear relationship between two variables. Correlation can be readily applied to both random variables and deterministic functions. Correlation methods are widely used in applications where a signal has to be detected in the presence of noise (see Appendix C). The correlation technique can be applied to both analog and discrete signals.

Correlation in the Analog Domain

The purpose of autocorrelation is to analyze the relation between the values of the same random process at different times. The autocorrelation function of a time invariant signal $x(t)$ is defined as

$$R_x(\tau) = \lim_{T\to\infty} \frac{1}{T} \int_0^T x(t).x(t+\tau)dt \tag{3.36}$$

This reveals the presence of a recurrence in a random signal. For a periodic signal, the autocorrelation function is also periodic. $R_x(\tau)$ is an even function;

$$R_x(\tau) = R_x(-\tau) \tag{3.37}$$

The auto-covariance $\Phi_x(\tau)$ of signal $x(t)$ shows the correlation of the signal $x(t)$ at different times, if the signal is made to be of zero mean.

$$\Phi_x(\tau) = R_x(\tau) - \overline{x}^2 \tag{3.38}$$

The value of the autocorrelation function without a delay, $R_x(0)$, gives the time average of the square of each value of x, known as mean-square of x.

$$R_x(0) = \frac{1}{T} \int_0^T x^2(t)\ dt \tag{3.39}$$

The mean square value of the signal can be used to normalize the autocorrelation result since

$$R_x(0) \geq R_x(\tau) \tag{3.40}$$

The cross-correlation function provides the relation between two signals which may be time shifted. The cross-correlation function of two time invariant signals $x(t)$ and $y(t)$ is given by

$$R_{xy}(\tau) = \lim_{T\to\infty} \frac{1}{T} \int_0^T x(t).y(t+\tau)dt \tag{3.41}$$

The cross-covariance function is the cross-correlation of two signals with the mean values of the signals removed. The cross-covariance function of two signals $x(t)$ and $y(t)$ is

$$\Phi_{xy}(\tau) = \lim_{T\to\infty} \frac{1}{T} \int_0^T [x(t) - \overline{x}].[y(t+\tau) - \overline{y}]dt \tag{3.42}$$

where the mean values of the signals $x(t)$ and $y(t)$ during the time period T are given by

$$\overline{x} = \frac{1}{T} \int_0^T x(t)dt \tag{3.43}$$

$$\overline{y} = \frac{1}{T} \int_0^T y(t)dt \tag{3.44}$$

and $[x(t) - \overline{x}]$, $[y(t) - \overline{y}]$ give the deviation of the signal from the mean value within the period concerned. The covariance function shows the similarity between the high frequency components of the signals $x(t)$ and $y(t)$.

If the signals are assumed to be time invariant, (3.42) can be further simplified to (see Appendix C)

$$\Phi_{xy}(\tau) = R_{xy}(\tau) - \overline{x}.\overline{y} \tag{3.45}$$

If $y(t)$ is time variant,

$$\Phi_{xy}(\tau) = R_{xy}(\tau) - \overline{x}.\overline{y}(\tau) \tag{3.46}$$

where

$$\overline{y}(\tau) = \frac{1}{T} \int_0^T y(t+\tau)dt \tag{3.47}$$

The correlation coefficient σ_{xy} is a normalized version of the cross-covariance, and is defined as the covariance divided by the product of the standard deviations of x and y.

$$\sigma_{xy}(\tau) = \frac{R_{xy}(\tau) - \overline{x}.\overline{y}}{\sqrt{\left(R_x(0) - \overline{x}^2\right)\left(R_y(0) - \overline{y}^2\right)}} \tag{3.48}$$

Here, $-1 \leq \sigma_{xy} \leq 1$. When $|\sigma_{xy}| \simeq 1$, x and y are said to be highly correlated.

Correlation in the Digital Domain

In the digital domain, sampled values of the signals are used in place of continuous signals. The same definitions used in the analog domain can be extended to the digital domain. The autocorrelation of function $x(k)$ is given by

$$R_x(\tau) = \frac{1}{N}\sum_{k=1}^{N} x(k\Delta t).x(k\Delta t + \tau) \tag{3.49}$$

where $\tau = m.\Delta t$ and m is the number of samples the two waveforms are shifted from each other. Here, Δt is the sampling interval and N is the total number of samples in the time interval T.

The cross-correlation function of the two signals $x(k)$ and $y(k)$ is given by

$$R_{xy}(\tau) = \frac{1}{N}\sum_{k=1}^{N} x(k\Delta t).y(k\Delta t + \tau) \tag{3.50}$$

The cross-covariance function of the mean removed signals $x(k)$ and $y(k)$ is given by

$$\Phi_{xy}(\tau) = \frac{1}{N}\sum_{k=1}^{N} [x(k\Delta t) - \overline{x}].[y(k\Delta t + \tau) - \overline{y}(\tau)] \tag{3.51}$$

where

$$\overline{x} = \frac{1}{N}\sum_{n=1}^{N} x(n\Delta t) \tag{3.52}$$

$$\overline{y}(\tau) = \frac{1}{N}\sum_{n=1}^{N} y(n\Delta t + \tau) \tag{3.53}$$

The cross-covariance function $\Phi_{S_1S_2}$ can be effectively used to find a match between the relaying signals S_1 and S_2. The relaying signals S_1 and S_2 have different mean values on which the travelling wave signals are superimposed. If the cross-correlation output between the two signals is considered, it will be difficult to find the correct match due to effect

of mean values. Hence the mean values are removed to obtain a meaningful correlation between the two signals. The wavefronts reflected from the fault location will have a sign opposite to the forward travelling wavefront. In order to obtain a positive peak from $\Phi_{S_1S_2}$ at the time when the two signals match, the sign of S_2 is changed before correlating with S_1. The discrete cross-covariance function (3.54) between the stored signal S_2 and the reflected signal S_1 is given by,

$$\Phi_{S_2S_1}(\tau) = \frac{1}{N}\sum_{k=1}^{N} -[S_2(k\Delta t) - \overline{S_2}].[S_1(k\Delta t + \tau) - \overline{S_1(\tau)}] \tag{3.54}$$

where

$$\overline{S_2} = \frac{1}{N}\sum_{n=1}^{N} S_2(n\Delta t) \tag{3.55}$$

and

$$\overline{S_1(\tau)} = \frac{1}{N}\sum_{n=1}^{N} S_1(n\Delta t + \tau) \tag{3.56}$$

where $\overline{S_1}$ and $\overline{S_2}$ are the mean values of the signals S_1 and S_2 in their respective sample groups. The time shift τ corresponding to the peak value of $\Phi_{S_1S_2}$ can be used to calculate the distance to the fault. The literature on travelling wave protection uses the term *cross-correlation* to refer to *cross-covariance* mainly because both are used to find correlation between two signals. Although the two terms have distinct meanings, adhering to the standard usage, the term *cross-correlation* will be used in the rest of the thesis to refer to *cross-covariance*.

3.3 Theory of Impedance Measurement Algorithm

3.3.1 Background

Any disturbance on an EHV transmission line has to be identified and cleared from the system in a time which will preserve system stability. At high voltages, the fault has to be detected at least within one power frequency cycle and the faulted section has to be

then isolated. Distance protection schemes based on impedance measurement have long been used to achieve fast fault detection times. With the introduction of digital techniques to protection, new methods of estimating impedance emerged [16, 17]. In a digital relay, the fundamental frequency component of the voltage and current signals are calculated using frequency analysis methods. The high-speed microprocessors today are capable of calculating impedance in real-time at high sampling rates.

The basic principle behind impedance relaying is to calculate the impedance "seen" at the relay location using fundamental frequency components of the voltage and current signals [14]. The voltage and current signals must be sampled at a sampling frequency greater than twice the frequency of the fundamental component, f_m. The sampling frequency, f_s has to be synchronized to any variation in the power frequency for proper estimation of the fundamental frequency component and in order to avoid ripples. The signal component with frequencies above f_m is considered as high frequency noise for the impedance algorithm. In order to remove the noise, the signals are filtered before sampling. A bandpass filter can be used to remove most of the noise, but this may introduce additional delay in the process. The most commonly used are the anti-aliasing filters, which is essentially a low pass filter. In addition to the high frequency noise, there can be unwanted noise due to the exponentially decaying components, especially in the current, and sub-harmonics.

Fourier transform based methods can be used to derive the fundamental components of the voltage and current signals. A one cycle DFT is capable of calculating the fundamental components, while rejecting any harmonic of the power frequency (see Appendix D). The introduction of the FFT has made it possible to calculate the fundamental frequency and the harmonic components on a real time basis.

3.3.2 Impedance Relay Implementation

The task of the impedance relay is to calculate the impedance from the voltage and current phasors and determine whether the impedance falls within a safe region. If the impedance

seen by the relay is less than its reach setting the relay operates. The most widely used distance relays are based on mho characteristics (see Appendix D). The impedance relay calculates the impedance as seen at the relay location. Under a three phase short-circuit or phase-phase fault condition, the impedance measured by the relay is equal to the positive sequence impedance of the line between the fault point and the relay location. A standard distance relay implementation will have six impedance measuring elements - three for phase to ground faults and three for phase to phase faults.

Before voltage and current signals are sampled, an anti-aliasing filter removes the high frequency noise. The fundamental frequency components are extracted from the voltage and current samples using a DFT filter. Then these fundamental frequency components will be used to derive the sequence components (see Appendix D). The zero sequence current is required in the calculation of line to ground impedance and the positive and negative sequence components may be useful for directional elements. The impedance seen by the ground element of a three phase system with phases a, b, and c is given by,

$$Z_n = \frac{V_n}{I_n + kI_0} \tag{3.57}$$

where $n = a, b$, or c and I_0 is the zero sequence current. The factor k compensates for the difference between the positive and zero sequence impedances of the fault loop and allows the relay to measure the positive sequence impedance to the fault. The factor k is calculated from

$$k = \frac{Z_0 - Z_1}{Z_1} \tag{3.58}$$

where Z_0 and Z_1 are the zero sequence and positive sequence impedance of the line respectively.

The impedance measured by the phase elements of the relay is evaluated from

$$Z_{nm} = \frac{V_n - V_m}{I_n - I_m} \tag{3.59}$$

where $n, m = a, b, c$. The value of Z_{nm} will be the positive sequence impedance to the fault when there is a short circuit between phases n and m.

3.3.3 Impedance Zone

The calculated impedance is a complex quantity; the real part gives the resistive component and the imaginary part shows the reactive component of the impedance. When the resistance R and reactance X are known, the impedance trajectory can be established on an X-R plane. The zone of protection can be described as a mho circle as in Fig.3.5(a) along with a straight line representing the impedance of the transmission line.

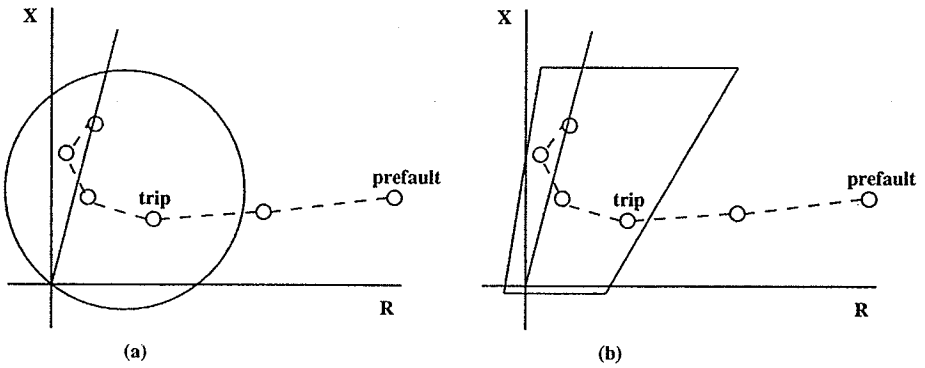

Figure 3.5: Mho and quadrilateral characteristic of impedance relay

Under normal operating conditions, the measured impedance stays outside the mho circle. This is shown as the *pre-fault* point on Fig.3.5. This is an impedance resulting from a load flow condition and can be calculated from the voltage and current samples. Under fault conditions, the impedance will fall back inside the mho characteristic. A trip signal can be issued once the impedance is inside the circle. The impedance locus shows the sequence of impedances calculated, when the impedance changes from the pre-fault value to the post-fault value. The mho circle characteristics can be replaced with quadrilateral characteristics shown on Fig.3.5(b) to achieve a more flexible protection zone.

A block diagram of the impedance measurement algorithm is shown on Fig.3.6. It indicates different stages involved in a digital impedance relay.

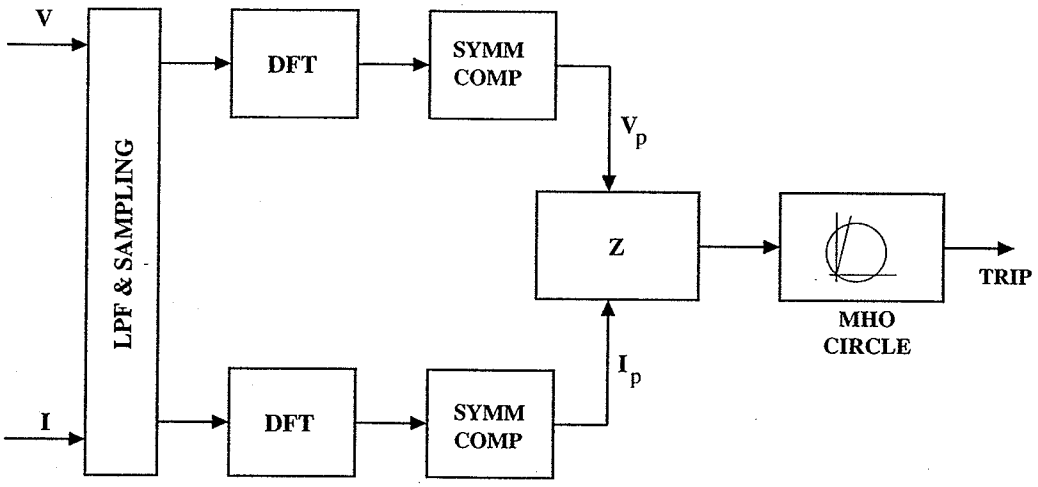

Figure 3.6: Block diagram of a digital impedance relay

3.4 Combined Algorithm

3.4.1 Concept

The motivation behind combining the travelling wave information and the impedance measurement in a single protective relay was discussed before under section 1.3. A protection scheme based on travelling wave information could fail to detect a disturbance on a transmission line under certain fault conditions. If the fault is too close to the relay location, it will be difficult to distinguish the successive reflections of the wavefronts between the relay location and fault point due to the bandwidth limitations in the measuring instruments. On the other hand, if a single phase to ground fault occurs (in the rare occasion) when the voltage at the fault location is near or equal to zero, the travelling waves generated will not contain steep wavefronts. Hence it will be difficult to detect such disturbances on the line. However, a distance protection scheme based on impedance measurement will move quickly inside its protection zone for a close-up fault. It is capable of detecting a close-up fault within a few milliseconds. The need for speeding up the distance relay is towards the reach point of the relay. In addition, impedance relays can detect faults occurring at the instant of a zero-crossing.

A protection scheme which makes use of the positive features of both of these algorithms will be able to rapidly detect all faults on a transmission line. When the travelling wave relay detects distinct wavefronts it responds quickly while the impedance relay will act as a backup in case the travelling wave relay cannot detect steep wavefronts. This will improve the reliability of the relay while achieving very rapid fault detection in most cases. The travelling wave algorithm not only detects faults fast, but is also capable of calculating the distance to the fault accurately. Since the relay operates with the information available at only one end of the line, it reduces the reliance on a communication channel for the vast majority of faults on the line. The two algorithms use the voltage and current samples available through a single set of transducers. There is no need for separate transducers and A/D converters for the two algorithms. Hence the overall cost of the combined scheme will be low. The combined features of the two algorithms make it an ultra-high-speed and reliable relay.

3.4.2 Key Issues

As discussed before, a protection scheme based on travelling waves may mal-operate under certain conditions. The magnitude of the high frequency transients initiated by a single-phase-to-ground fault depends on the fault inception angle of the phase voltage and fault resistance. The travelling waves do not contain steep wavefronts if a line to ground fault occurs near a voltage zero. Dommel and Michels [29] suggested a discriminant function (as described in section 3.2.4) to identify faults that occur near voltage zero. The value of the discriminant function does not depend on the fault inception angle. Mansour [33] later developed a microprocessor relay based on the discriminant functions to detect faults with small inception angles. However, the discriminant function does not provide a means for identifying the fault location.

The other problem area associated with travelling wave protection is related to the faults close to the relay station. For faults very close to the relay, the travel time becomes

very small. The signals contain very high frequencies and the relay requires high fidelity transducers having a wide bandwidth and a linear output throughout the dynamic range. The small travel times make it difficult to identify adjacent wavefronts and find a matching reflection through correlation.

On the other hand, the protection resolution for close-up faults will be affected by the duration of the stored reference S_2. The duration of S_2 (as described in 3.2.5) is inversely proportional to the wave transit time. The optimum duration (or the number of samples N) of the stored section of S_2 is a concern. As N increases, the protection scheme's ability to distinguish between a reflection from the fault and a reflection from a remote discontinuity reduces. On the other hand, when N decreases, the protection scheme's ability to distinguish between waves reflected from the fault and reflections from discontinuities beyond the faults increases. But a low value of N increases the risk of mal-operation on non-fault transients. Shehab-Eldin and McLaren suggested a composite correlation reference [34] which includes both a short section and a long section of reference S_2 to detect close-up faults. This method still showed difficulties in identifying faults very close to the relay due to bandwidth limitations of the transducers and identifying faults with small inception angles.

However, the impedance relay is capable of identifying close-up faults as well as faults with small inception angles. The measured impedance moves rapidly inside the protection zone if the fault is close to the relay location. Hence impedance measurement is a good alternative for detecting close-up faults. By combining the impedance measurement with the travelling wave algorithm in a single relay it is possible to rectify the problems associated with the travelling wave scheme. The main concern in the combined approach is how to decide which algorithm should issue the trip signal in case a fault is detected by both algorithms.

3.4.3 Decision Process

The decision to use impedance relay output instead of the travelling wave relay output is based on several criteria. If the travelling wave relay does not detect a disturbance (this may happen for faults with small inception angles), the impedance relay automatically acts as a backup. If the fault inception angle is found to be smaller than a certain value or the fault is found to be too close to the relay location or the value of the cross-correlation function is below a certain threshold, the trip decision will be made by the impedance relay. All these scenarios are discussed below.

Fault Inception Angle

The travelling wave relay finds the matching wavefronts to the stored reference signal S_2 through cross-correlation. In the relay, the cross-correlation process is started only when a disturbance in the forward direction is detected. The first backward travelling wavefront, f_1 which appears at the relay location after a disturbance is used to identify a forward fault (as explained in section 3.2.2). The wavefront f_1 contains information about the fault type, fault inception angle, fault direction etc. By analyzing f_1, it is possible to find an approximate value for the fault inception angle.

In (3.15), it was shown that the wave front f_1 of the backward relaying signal S_1 is of the form

$$S_1(t) \approx -2V_p \sin(\phi) \tag{3.60}$$

if the pre-fault voltage at the fault location is $V_p \sin(\omega t + \phi)$ and the transmission line is assumed to be lossless. For a short period of time W, $\hat{f}_1$ may be assumed to stay constant at this value. Now if the mean square value of S_1 within this time period is considered,

$$\begin{aligned} R_{S_1}(0) &\approx \frac{1}{W}\int_0^W 4V_p^2 \sin^2(\phi)\, dt \\ &= 4V_p^2 \sin^2(\phi) \end{aligned} \tag{3.61}$$

A small value of $R_{S_1}(0)$ will indicate a fault with a small inception angle ϕ. If ϕ is close to zero, the travelling wave relay is disabled and impedance relay output can be used to trip the breaker.

Close-up Fault

Since the travel time of wavefronts is very short for a close-up fault, the successive reflections cannot be distinguished in the relaying signals. As a result, the correlation process may not provide a clear peak corresponding to the fault location. However, for a close-up fault, the amplitude of the relaying signal can be high (depending on ϕ) and may increase rapidly following a ramp characteristic within the first few milliseconds. The cross-correlation function output $\Phi_{S_2S_1}$ may show several peaks, but may lack any distinct peak. For a close-up fault, a high dc level can be observed in the correlation output. The mean value $\overline{\Phi}_{S_2S_1}$ of the cross-correlation function can be used to identify such a situation where there are several peaks in the output, but without any distinct peak. The output $\Phi_{S_2S_1}$ is averaged over a time period equal to the travel time Γ of the transmission line being protected. The average value $\overline{\Phi}_{S_2S_1}$ is compared with the root mean square value of the cross-correlation output $\Phi_{S_2S_1rms}$. The ratio λ between $\overline{\Phi}_{S_2S_1}$ and $\Phi_{S_2S_1rms}$ could be used to identify situations when the correlation output does not have a clear peak.

$$\begin{aligned} \lambda &= \frac{\overline{\Phi}_{S_2S_1}}{\Phi_{S_2S_1rms}} \\ &= \frac{\frac{1}{\Gamma}\int_0^{\Gamma}\Phi_{S_2S_1}dt}{\sqrt{\frac{1}{\Gamma}\int_0^{\Gamma}\Phi_{S_2S_1}^2\,dt}} \end{aligned} \tag{3.62}$$

For a fault very close to the measuring location, λ shows a value close to unity. However, the indication given by λ is not always reliable and could show lower values for some close-up faults.

On the other hand, the cross-correlation output of the travelling wave relay will show a short fault distance for a close-up fault (the maximum peak among the several peaks

observed corresponds to this short distance). However, this distance estimation may not be correct due to low sampling resolution (bandwidth limitations of the transducers). Therefore, if the fault distance given by the travelling wave relay is smaller than a certain limit, then the travelling wave relay is disabled. The distance relay based on impedance measurement moves rapidly into the trip zone for close-up faults. When λ is close to unity or the fault distance given by the travelling wave relay is below a certain limit, the travelling wave relay is disabled and the impedance relay output will be activated.

Value of the Correlation Function

In the travelling wave algorithm, the correlation coefficient $\sigma_{S_1S_2}$ is used to find a match between the signals S_1 and S_2. The correlation coefficient $\sigma_{S_1S_2}$ is defined as

$$\sigma_{S_1S_2}(\tau) = \frac{R_{S_1S_2}(\tau) - \overline{S_1}.\overline{S_2}}{\sqrt{\left(R_{S_1}(0) - \overline{S_1}^2\right)\left(sigmaR_{S_2}(0) - \overline{S_2}^2\right)}} \tag{3.63}$$

Here, $-1 \leq \sigma_{S_1S_2} \leq 1$. When $|\sigma_{S_1S_2}| \simeq 1$, S_1 and S_2 are said to be highly correlated. In the algorithm, the calculation of $\sigma_{S_1S_2}$ is started once the reference signal S_2 is stored and will be carried out for a time duration equal to twice the travel time Γ of the line. Hence the operating time of the travelling wave relay depends on the travel time Γ and Γ depends on the total length of the line being protected. The *positive peak* with the maximum amplitude of $\sigma_{S_1S_2}$ within the window 2Γ from the instant S_2 is stored will be used to calculate the fault distance X_f. The magnitude of $\sigma_{S_1S_2}$ can be affected by the fault inception angle, the distortion of waveform due to line attenuation, the phases involved in the faulted network and the fault resistance. To improve the reliability of the relay, only positive peaks above a certain threshold ψ are considered when finding the peak value of $\sigma_{S_1S_2}$ within the time window 2Γ. If $\sigma_{S_1S_2} < \psi$ within the time window 2Γ, the impedance relay will be allowed to make the decision.

3.4.4 Design Considerations

Combining the Algorithms

The derivation of the travelling wave information from the measured voltage and current signals and the calculation of impedance are carried out simultaneously. The travelling wave relay and the impedance relay use the same voltage and current signals, but what is useful for one relay becomes the noise for the other. The travelling wave relay depends on the high frequency transient signals, and hence the 60Hz main frequency component has to be removed from the measured waveforms. On the other hand, the impedance relay uses the fundamental frequency component and the high frequency noise has to be filtered out.

The travelling wave signals contain high frequency transients and hence the voltage and current signals need to be sampled at a high sampling rate. A travelling wave fault detection scheme must consider transient generated frequencies as high as 5kHz [58]. Hence the voltage and current signals will have to be sampled with a sampling rate of at least 10kHz according to the *Nyquist theory* [62]. The frequencies present in the transient signals might vary depending on the fault location and other line conditions [4, 58].

Since only the fundamental power frequency component is of interest for a distance relay based on impedance measurement, the impedance relay does not need such a high sampling rate. When the two algorithms are cascaded, the sampled values used for the travelling wave algorithm may contain frequency components that will become noise to the impedance algorithm. In order to avoid sampling the same signals at two different frequencies, the samples of voltage and current obtained for the travelling wave relay are decimated to achieve a lower sampling rate for the impedance relay. To avoid aliasing, the sampled signals have to be filtered using an anti-aliasing filter with a suitable cut-off frequency before decimation [63]. A one cycle DFT is capable of calculating the fundamental components, while rejecting any harmonics of the power frequency.

Block Diagram

A block diagram of the cascaded algorithm is shown in Fig.3.7. The calculations of the two algorithms are carried out in parallel. The voltage and current signals are sampled at a rate required for extracting transient information from the waveforms. The same voltage and current samples are supplied to both travelling wave relay and impedance relay. The travelling wave algorithm is executed on each sample of the input signal. The input samples to the impedance algorithm are decimated by a decimation factor N_D. The impedance of the line is calculated only once in every N_D samples. This saves the processor time which can be used for the fast travelling wave algorithm.

In the impedance algorithm, the samples are filtered and decimated before extracting the fundamental frequency components using the DFT. The extracted 60Hz signals are used for the impedance calculation. The ground and phase relays calculate the phase to ground impedance and phase to phase impedance respectively. They also check whether the calculated impedance falls within the zone of protection set by the mho characteristics. In the case when the impedance falls within the protection zone, a trip signal is issued.

In the travelling wave algorithm, the *delta filter* removes the fundamental component from the measured waveforms to derive the incremental components of the voltage and current signals. The Clarke transformation is used to obtain the modal quantities. The modal components of the aerial mode 2 are used to derive the travelling wave signals. The *fault detector* checks for possible disturbances in the forward direction. A disturbance is detected when the values of the relaying signals S_1 or S_2 goes above a certain threshold. The direction of the fault is determined by the sequence in which S_1 and S_2 exceed the threshold value. In the case when it identifies a forward fault, both *correlator* and *wavefront analyzer* are activated. The wavefront analyzer checks the conditions on (3.61) and (3.62). This block determines whether the fault inception angle is small or the fault is close to the relay location.

The correlator stores a reference signal of the forward travelling wavefront S_2 and a

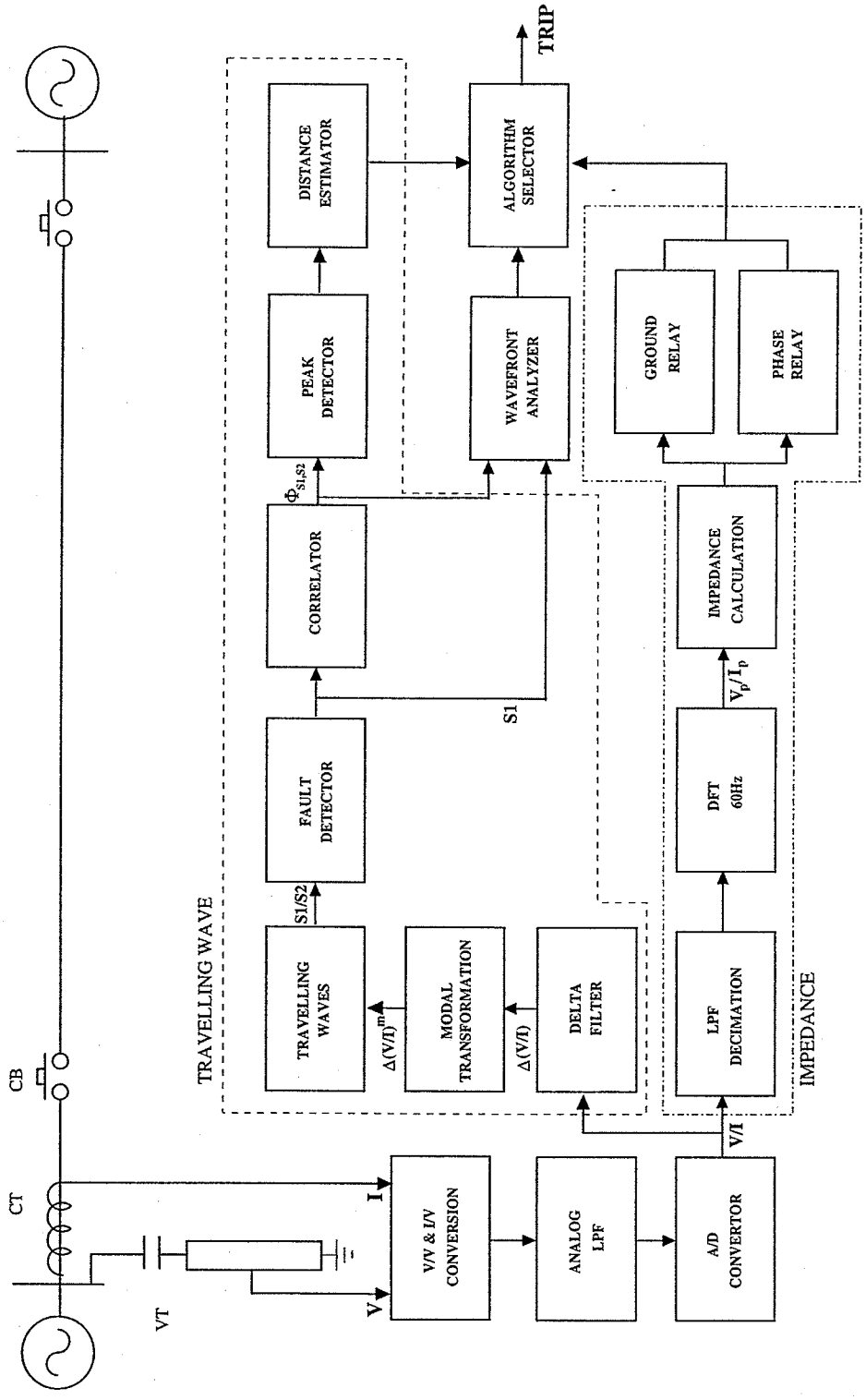

Figure 3.7: Block diagram of the hybrid relay

timer is activated (say at time t_1). Then it finds the cross-correlation between the stored reference S_2 and the reflections of the wavefronts S_1 from the fault. The correlator passes the correlation coefficient $\rho_{S_1S_2}$ to the *peak detector.* The peak detector finds the maximum positive peak within a time period set according to the travel time of the line and register the time (say t_2) at which the maximum peak is detected if the peak is above the threshold ψ. The *distance estimator* uses the times t_1 and t_2 as inputs and estimates the distance to the fault. If the distance is within the protection zone, a trip signal is issued.

For the protection zone of the travelling wave relay, there is a lower limit and a higher limit. The lower limit is set to avoid discrepancies arising from distance calculations of close-up faults and the higher limit is set to avoid faults on the adjacent line being recognized as internal faults. The wavefront analyzer investigates the initial wavefront S_1 and estimates whether the fault originated with a small inception angle or the fault is too close to the relay location for the travelling wave relay to give an accurate result. Depending on the decision of the wavefront analyzer, the *algorithm selector* determines which algorithm can be confidently used to issue the trip signal. Even if the wavefront analyzer decides to use the travelling wave relay, in the case where the fault distance falls below the lower limit, the trip decision is left to the impedance relay.

3.5 Operating Principle of the Hybrid Algorithm

The distance protection scheme based on impedance measurement moves rapidly into the trip zone for close up faults. The need for speeding up is towards the reach point of the relay. The travelling wave relay is capable of quickly detecting faults close to the reach point of the impedance relay as well as faults beyond the reach point depending on the maximum distance setting of the travelling wave based algorithm. The maximum setting of the distance which can be accurately calculated depends mainly on the accuracy of the measuring transducers. The remaining fraction of the line beyond this setting can only be covered in a zone 1 time by some kind of inter-trip scheme. Hence the travelling wave

information will be effectively used to identify faults towards the reach point of the line while impedance measurement will be utilized to handle the faults close to the relay location. The output of the two algorithms can be combined in different configurations to satisfy various protection requirements while improving the reliability and speed of the overall scheme. In this thesis, we look at two methods (or two algorithms) of combining the travelling wave information with the impedance measurement to achieve reliability and speed in the proposed cascaded protection scheme.

3.5.1 Algorithm One

The first algorithm investigates how the speed of the primary protection can be improved while maintaining a high reliability level. Here, the trip decision is always made by the travelling wave relay except under the following conditions:

- the fault detector completely fails to identify a disturbance on the line. This could happen when the fault inception angle is zero and the fault is away from the relay location.
- the wavefront analyzer decides that the initial wavefronts do not carry enough information to detect a fault condition. This could happen when the fault inception angle is near zero.
- the wavefront analyzer may decide that a fault is too close to the relay location for the travelling wave measurement.
- the fault distance calculated by the travelling wave relay is smaller than the lower limit (the upper limit is higher than the reach of the impedance relay)
- the cross-correlation output doesn't show a clear peak above the set threshold and is hence unable to estimate the distance to the fault.

Under any of the above circumstances, the impedance relay acts as a backup to the travelling wave relay. A flowchart explaining the first algorithm is shown in Fig.3.8. The impedance is calculated after every N_D^{th} sample. The figure is self-explanatory. If for any reason the travelling wave relay does not detect the fault condition, the impedance relay acts as a backup.

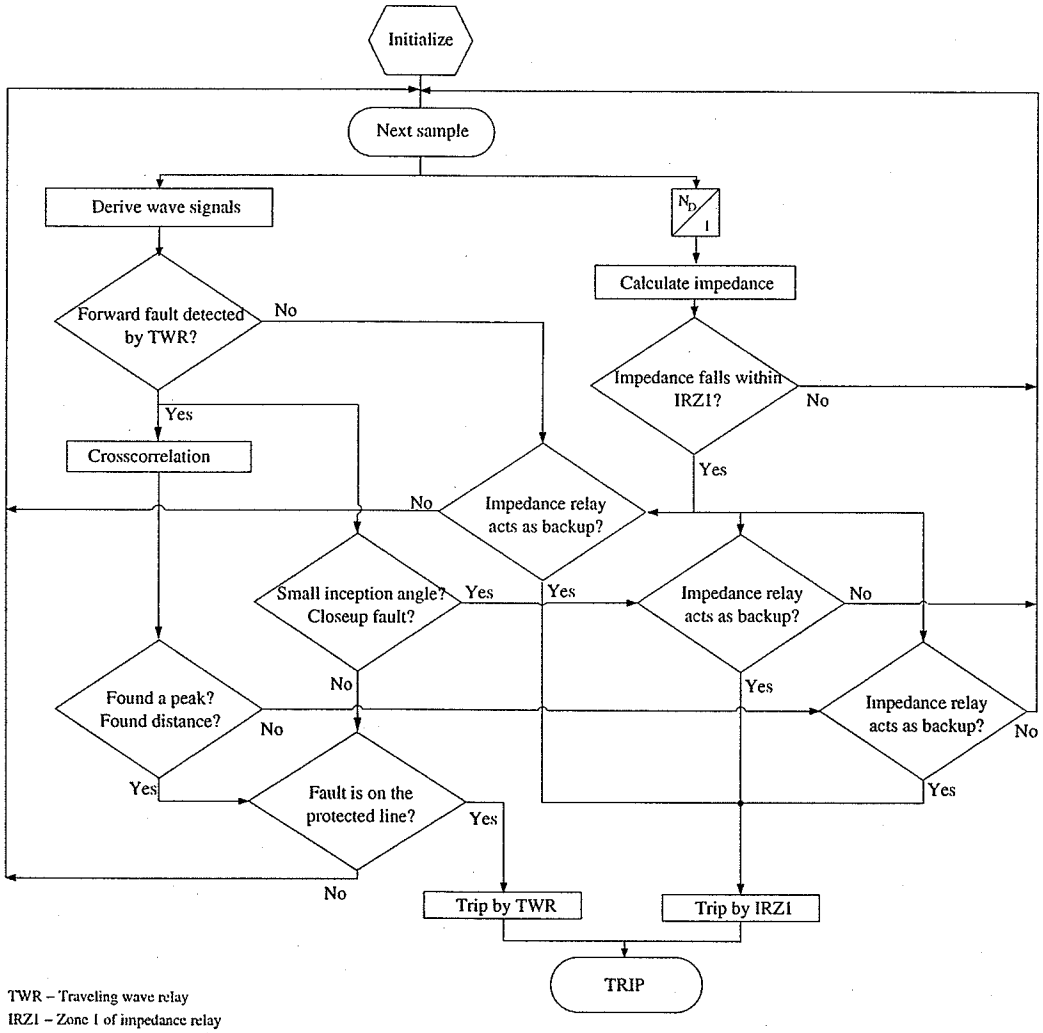

Figure 3.8: Flowchart for algorithm 1

3.5.2 Algorithm Two

The second algorithm investigates methods of improving the relay reach and reliability of the combined algorithm. Here, the trip decision is always *"triggered"* by the zone 2 element of the impedance relay. The main objectives of the second algorithm are:

- to improve the reliability of the combined protection scheme;
- to increase the relay reach;
- to accelerate the zone 2 protection of the impedance measurement technique;
- to increase the reliability by reducing the dependency on an end-to-end communication channel.

The measured impedance enters the zone 2 of the impedance characteristic before reaching the zone 1. Therefore, for faults that occur in zone 1, the combination of zone 2 element and travelling wave information could provide faster operating times than that provided with the zone 1 of the impedance relay alone. The zone 2 element prevents possible mal-operation of the travelling wave relay from non-fault transients caused by switching operations. Since the zone 2 element triggers the cascaded algorithm, the reliability of the protection scheme is very high, but the fault detection time will be shorter than the primary protection of the impedance relay.

The faults that occur at the far end of the line have long travel times. The transient waves generated by such faults will have a low bandwidth. The bandwidth requirement of measuring transducers are low for such faults. When a fault occurs towards the end of the line, the travelling wave relay can calculate the distance to the fault accurately. Therefore, the relay reach of the combined scheme can be extended almost to the far end of the line. The resolution of the distance measurement will depend on the sampling rate of the waveforms. With the high sampling rates used in the travelling wave algorithm, it is

possible to extend the relay reach to about 90%-95% in long EHV lines depending on the accuracy of the measuring transducers used.

The standard practice in distance protection is to set the primary reach to about 80% of the line length. A fault on the remaining 20% of the line will fall into zone 2 of the protection scheme. The zone 2 element in a distance relay involves an added delay to allow a primary element in the adjacent line to operate first for a fault on the adjacent line which falls within the zone 2 reach. However, this delay can be too long to maintain the stability of a highly loaded system. A directional protection scheme with two relays at the opposite ends of the line connected through an end-to-end communication protocol will be a solution to improve the fault isolation time. A transfer-trip or permissive signal is used to command the relay at the remote end of the transmission line to trip the breakers open. The transfer-trip signal travels via the communication network and when received by the remote end relay a breaker trip signal is issued.

However, the reliability of teleprotection schemes will depend on the reliability of the communication channel. Besides, the communication equipment can be very expensive. As an alternative solution, the output of the travelling wave relay is utilized to accelerate the zone 2 element of the impedance relay in the hybrid algorithm. When the calculated distance of the travelling wave relay shows a fault on the protected line and the measured impedance enters zone 2 of the impedance characteristic, the zone 2 element is accelerated. This method not only eliminates the necessity of the costly communication channel, but is also capable of achieving faster tripping times compared to a teleprotection scheme. An analog teleprotection scheme using frequency-shifting techniques to transmit the transfer-trip signal can have back-to-back latencies greater than 10 milliseconds. Adding the operating time of the remote relay and the propagation delay of the communication channel to this latency results in higher values for the fault detection time than the combined algorithm.

The Fig.3.9 shows a flow chart of the protection algorithm. Zone 2 acts as the "starter" element for the travelling wave technique. If the travelling wave relay is unable to detect

a fault (in the rare event of a line to ground fault that occurs when the line voltage at the fault location is zero), the zone 1 or the zone 2 element of the impedance relay will detect the fault depending on the fault location. If the travelling wave relay fails to detect the fault in the second zone, the zone 2 element will have the standard (eg. 30 cycle) delay. The hybrid algorithm operates faster than the zone 1 or zone 2 element of the impedance relay alone. The travelling wave relay enables a *"fast zone 2 element"* and allows the impedance relay to detect faults quickly on almost the full length of the line. The overall result is a secure and fast protection scheme.

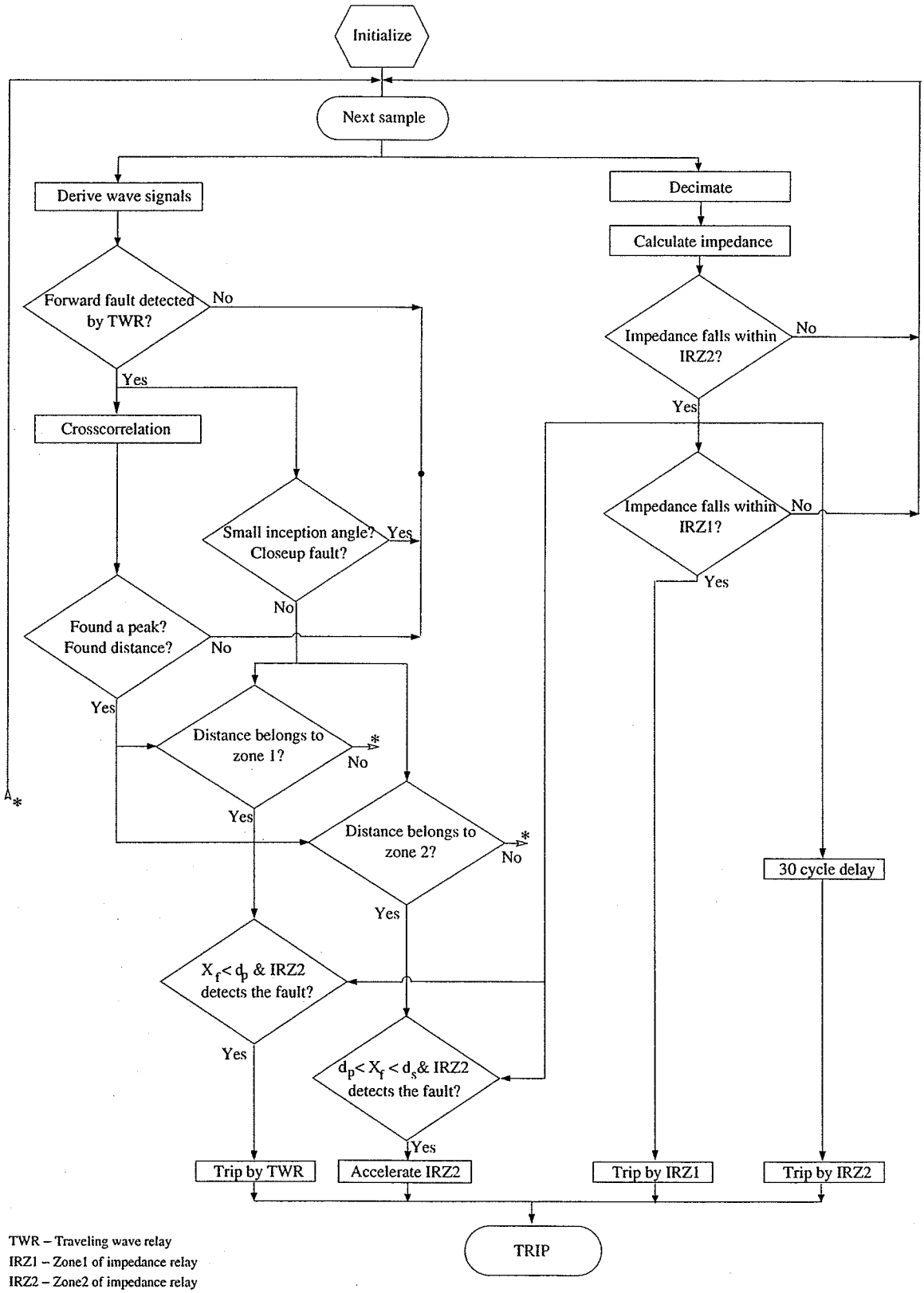

Figure 3.9: Flowchart for algorithm 2

Chapter 4

Simulation Studies

4.1 Introduction

The ideal approach to study the transient phenomena in a power system is to capture and record the transients using wide bandwidth transducers and recording equipment and then analyze these waveforms. However, capturing transient signals this way representing all possible scenarios is not realistic. An alternative technique is to simulate the power system using a suitable electromagnetic transient program (EMTP). The EMTP programs available in the market today represent the power system components with realistic models. These models usually match the main characteristics of the components while keeping the complexity of the models to a minimum. The power system simulation programs not only present a convenient way to generate the signals required to analyze a certain feature (eg. the protection scheme in this case), but also allow the user to study the worst case scenarios that are unlikely to be generated in the real world.

In order to verify the concept of the hybrid relay discussed in the previous chapter, simulation studies were carried out on a three phase power system using an EMTP program. A power network can have many possible system configurations. The main objective here was to select a more practical system configuration to identify the feasibility of the proposed protection scheme. Rather than testing the protection scheme on many different configura-

tions, it was decided to choose a single configuration based on a real system and prove the concept with different fault situations. Since the main application of the hybrid protection scheme is in EHV long transmission systems, a model based on 500 kV system from Manitoba to Minnesota was used for simulation studies. The 500 kV system was modelled as a simple power system represented by a single circuit, three phase transmission line with lumped parameter equivalent sources at each line end. The simulations were carried out using PSCAD/EMTDC ^{TM} [12] software. This chapter presents the details of the power system configuration chosen, the simulation studies carried out and the simulation results.

4.2 System Configuration

The three phase power network chosen for simulation studies is *based on* Manitoba Hydro's Dorsey-Forbes-Chisago network which spans from Southern Manitoba to Minnesota. A detailed diagram of the power network with its main electrical components is shown in Fig.4.1. The two major 500 kV transmission lines connect the Dorsey and Forbes, and Forbes and Chisago substations respectively. The Dorsey-Forbes line is 537 km long and the Forbes-Chisago line is 224 km long. The Chisago substation is connected to King/Kohlman with a 345 kV double transmission line. The Dorsey-Forbes-Chisago EHV long transmission network gives a model of a real system for testing the performance of the proposed hybrid scheme.

For simulation purposes, only the 500 kV transmission system was considered. For simplicity, the series compensation on the two lines were removed. The 345 kV system was replaced with its lumped parameter equivalent source at the Chisago busbar. When evaluating the surge propagation along a transmission line, the significantly shorter delay within the windings of a transformer and generator enable these elements to be considered as lumped parameter approximations [6]. Hence the power system was represented by a single circuit, three phase transmission line with its lumped parameter equivalent sources at each end. The generators were modelled in their three phase equivalent circuit in which the posi-

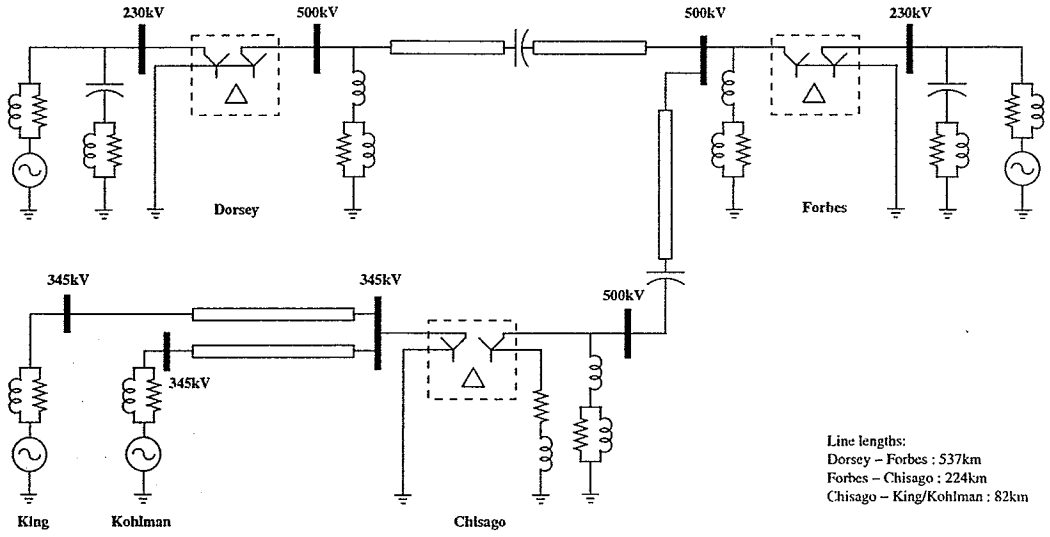

Figure 4.1: Network diagram for 500 kV system

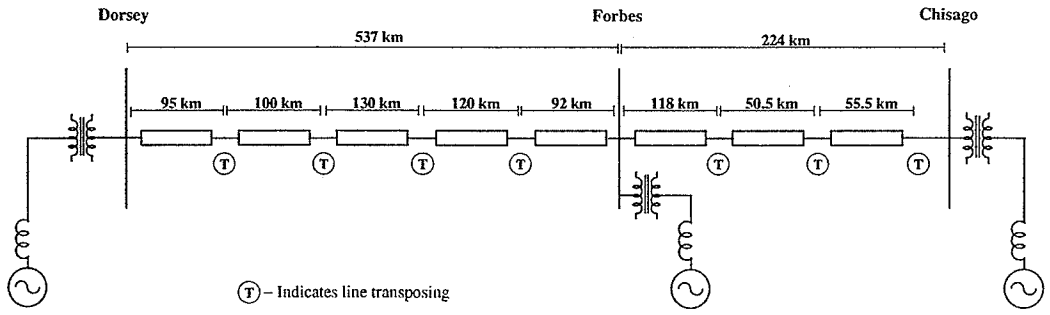

Figure 4.2: Line transposing intervals of the 500kV line

tive sequence lumped reactance was calculated from the fault levels (short circuit capacity). This short circuit capacity value can be varied according to the simulation requirements. The overhead transmission lines were assumed to be uniformly distributed along its length and the line impedance values were calculated, for all frequencies chosen, from the line physical construction by taking into account the effects of line spacing, conductor geometry, conductor internal impedance, and earth return path. The line was considered fully transposed since the physical line transpositions in the 500 kV line were incorporated in the simulation model. The line transposing positions are shown in Fig.4.2.

The simplified circuit equivalent used for simulations is shown in Fig.4.3. The trans-

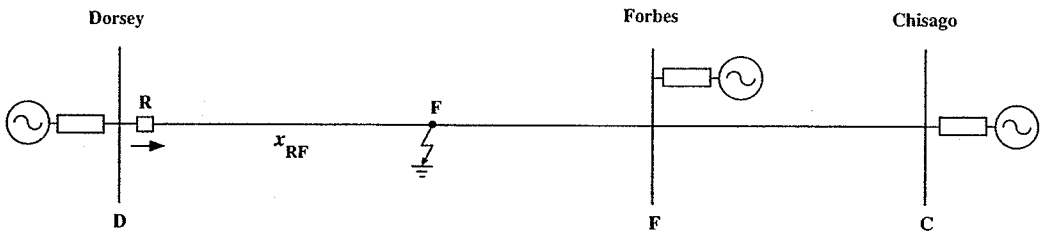

Figure 4.3: The 500kV three phase power system used for simulations

mission lines were represented with the frequency dependent model available in PSCAD. The pre-fault conditions were set by using data available from load flow calculations. The calculations are done in the pu system using a base of 100MVA and system nominal voltage of 500kV. The line configuration and parameters are given in Appendix E.

4.3 Protection Simulation

The different components of the hybrid relay shown in Fig.3.7 were implemented as library modules in PSCAD. The modules were programmed using FORTRAN [64] and interfaced to PSCAD. The PSCAD simulation provides an ideal environment because it analyzes the discrete numerical data exactly as expressed in the equations describing the protection algorithm without the distortion or noise associated with the hardware. The voltage and current signals measured at different locations are available in their discrete format and hence the error associated with A/D conversion was not considered for simulation. The PSCAD simulation calculate the voltage and current values at a rate of 256 samples per 60 Hz cycle (15.36 kHz), or in other words, the simulation time step is $65.1\mu s$. A sample time of $65.1\mu s$ means that the travelling wave protection has a distance resolution of $9.8km$ at the velocity of light. Faults can be applied and timed at any point in the system during the simulation. The fault path is simulated by a constant resistive element in which the fault resistance could be varied according to the requirement. Multi-phase faults are assumed to occur simultaneously on all the faulted phases. The point on wave at the fault inception can be chosen at will for single phase to ground faults.

PSCAD generates instantaneous voltage and current signals at different locations. The voltage and current measurements taken at the relay location are used in the protection algorithm. The calculations of both travelling wave and impedance algorithms are carried out in parallel. The signals sampled at 15.36kHz are low pass filtered and re-sampled at 480Hz before using them for the impedance calculations. A third order Butterworth filter was used for filtering. The down-sampling provides 8 samples per a 60Hz cycle for the impedance estimation. The procedures involved in the simulation of the travelling wave and impedance algorithms are described separately below.

4.3.1 Travelling Wave Algorithm

The program calculates the instantaneous values of the incremental components of the voltage and current waveforms. The incremental signals are generated by subtracting the measured signals taken exactly one cycle before from the present samples. The incremental voltage and current phase signals are decoupled into three independent modes (mode 1, mode 2 and mode 3) using the Clarke transformation matrices given by (3.29) and (3.30). Since the three phase system is fully transposed and has balanced line terminations, the effects of frequency dependence of the modal decomposition matrices is ignored. Mode 1 is the earth mode and mode 2 and mode 3 are aerial modes. The earth mode is frequency dependent, highly attenuated and has a slower velocity compared with the aerial modes. The distance obtained using earth mode was found to be inaccurate. The aerial modes are not much affected by the varying ground resistivity over a wide frequency band and give sufficiently accurate results [59]. In our implementation, the relaying signals of mode 2 are used for the travelling wave algorithm. Mode 2 has a propagation velocity of $295km/ms$ and a modal surge impedance of 276Ω.

Fig.4.4 shows the three phase voltage and current waveforms, the incremental phase components, and the incremental modal quantities for a three phase to ground fault at a distance 325 km away from the relay location ($x_{RF} = 325km$) on line DF in Fig.4.3. The

incremental components clearly show the presence of travelling wavefronts in the voltage and current signals.

The incremental components of the aerial mode 2 are used to derive the relaying signals S_1 and S_2.

$$S_1^{(2)} = \Delta v^{(2)} + Z_c^{(2)}.\Delta i^{(2)} \tag{4.1}$$

$$S_2^{(2)} = \Delta v^{(2)} - Z_c^{(2)}.\Delta i^{(2)} \tag{4.2}$$

where $Z_c^{(2)}$ is the surge impedance of mode 2.

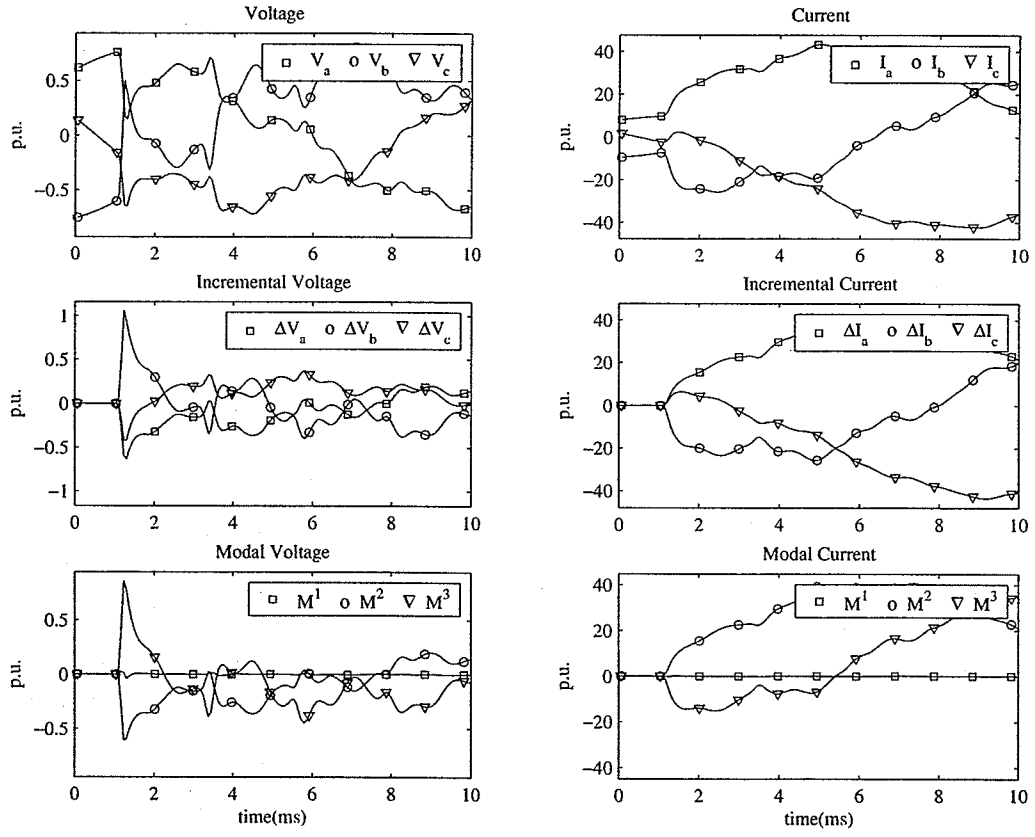

Figure 4.4: The fault transients generated by a three phase to ground fault: $x_{RF} = 325km$

The fault detector checks for possible disturbances on the transmission line by checking the sequence in which the relaying signals S_1 and S_2 go above a predetermined threshold.

When the fault detector identifies a disturbance in the forward direction, it issues a *forward trigger* signal that triggers the correlator. The correlator stores a section of the forward relaying signal S_2. A storage window of 10 samples, $(N = 10)$, or in other words a sample window of duration $t_w = 0.651ms$ was found to be optimal for detecting most of the fault conditions.

The storage window includes some samples before and some samples after the fault disturbance to ensure the best representation of the wavefront. The literature [36] and the simulations showed that a storage window containing 3 samples before $(n_b = 3)$, and 7 samples after the disturbance $(n_a = 7)$ was capable of producing clear peaks in the cross-correlation output. The correlator finishes storing a section of the relaying signal S_2 at time τ_1. The correlator finds the cross-correlation between the stored signal S_2 and sections of backward relaying signal S_1.

The sections of the relaying signals S_1 and S_2 have different mean levels on which the required travelling wave components are superimposed. To find a useful correlation, the mean values of the signals S_1 and S_2 are removed before finding the cross-correlation. The cross-correlation function is then normalized to find the correlation coefficient. The correlation output is calculated for a time period equal to twice the travel time of the line being protected, 2Γ from the instance the correlator finishes storing the signal S_2.

Fig.4.5 shows the relaying signals, the forward trigger signal and the correlator output for the above fault. The forward trigger signal is kept high for a time period equal to 2Γ plus the storage time of the signal S_2, ie a total duration of $[2\Gamma + (n_a/N)t_w]$. For the line DF, $2\Gamma = 3.64ms$.

The peak detector finds the positive peaks of the correlator output above a certain threshold. The threshold was set to 0.25 p.u. to eliminate false peak identification due to the effect of noise. The maximum positive peak of the correlator output within the time period 2Γ is used by the distance estimator to calculate the distance to the fault. The time at which the correlator output becomes maximum, τ_2 corresponds to the distance to

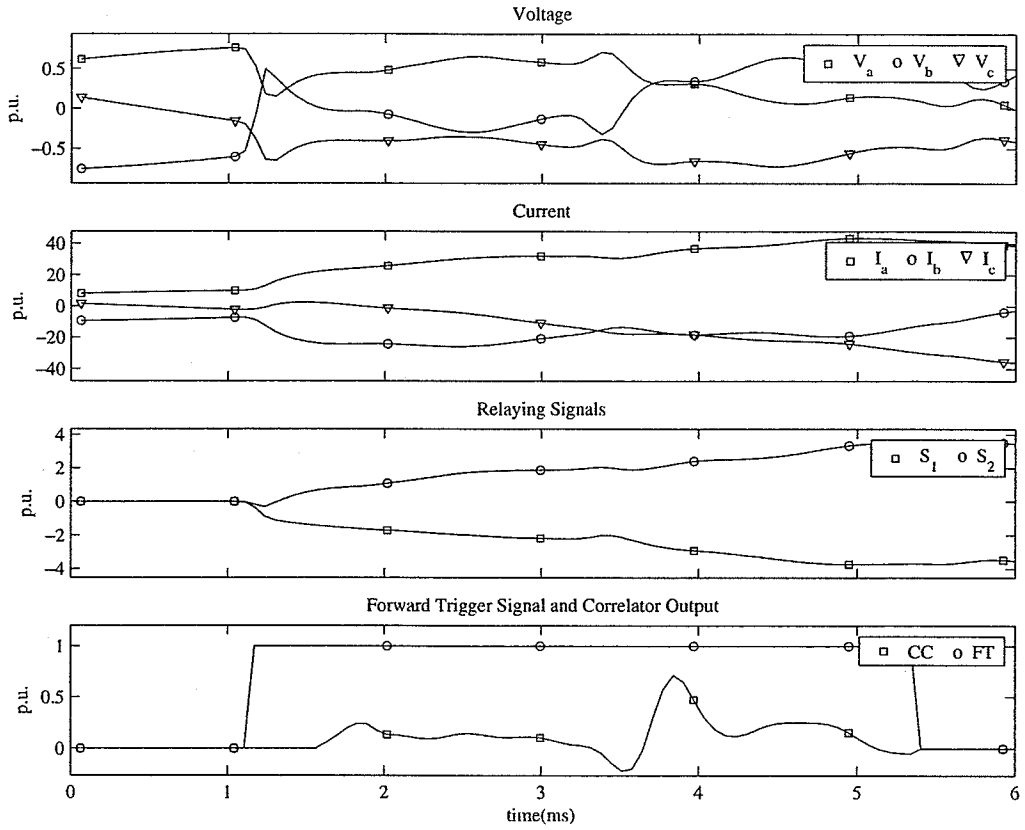

Figure 4.5: The relaying signal for a three phase fault: $x_{RF} = 325km$

the fault. For the three phase fault described above, $\tau_1 = 1.63ms$, $\tau_2 = 3.84ms$, and the calculated distance to the fault $x_{RF} = 325.98km$.

4.3.2 Impedance Measurement Algorithm

The apparent impedance seen at the relay location is calculated using the voltage and current signals. In our simulations, we use 8 samples of voltage and current signals per 60Hz cycle for impedance estimation. That means, the samples used for travelling wave algorithm are decimated by a factor of 32. Instead of using a DFT (as shown in Fig.3.7), the FFT block component available in the PSCAD program was used to extract the fundamental 60Hz components of voltage and current signals. Separate FFT blocks were used to find the 60Hz voltage, 60Hz current and symmetrical components. The fundamental compo-

nents were then used to calculate the line-to-ground impedance (ground relay) for each phase and line-line to impedance (phase relay) for each line pair. The ground and phase relays check whether the calculated impedance falls within the protection zone. For the simulations, the protection zone was specified by mho characteristics. The settings for the mho characteristics were calculated as follows:

Zero sequence resistance of the line, $R_0 = 0.3211 \times 10^{-3}\ \Omega/m$

Zero sequence reactance of the line, $X_0 = 0.1218 \times 10^{-2}\ \Omega/m$

Positive sequence resistance of the line, $R_1 = 0.1756 \times 10^{-4}\ \Omega/m$

Positive sequence reactance of the line, $X_1 = 0.3378 \times 10^{-3}\ \Omega/m$

For line DF, the positive sequence impedance, $Z_1 = 9.43 + j181.4\ \Omega$

Positive sequence impedance for primary protection (80%) $= 7.54 + j145.12\ \Omega$

Sequence compensation factor, $k = (Z_0 - Z_1)/Z_1 = 2.56$

Fig.4.6 shows the impedance loci for the ground elements and phase elements. Since the fault involves the three phases and the ground, all six impedance elements (A-G,B-G,C-G,A-B,B-C,and C-A) fall within the mho characteristics.

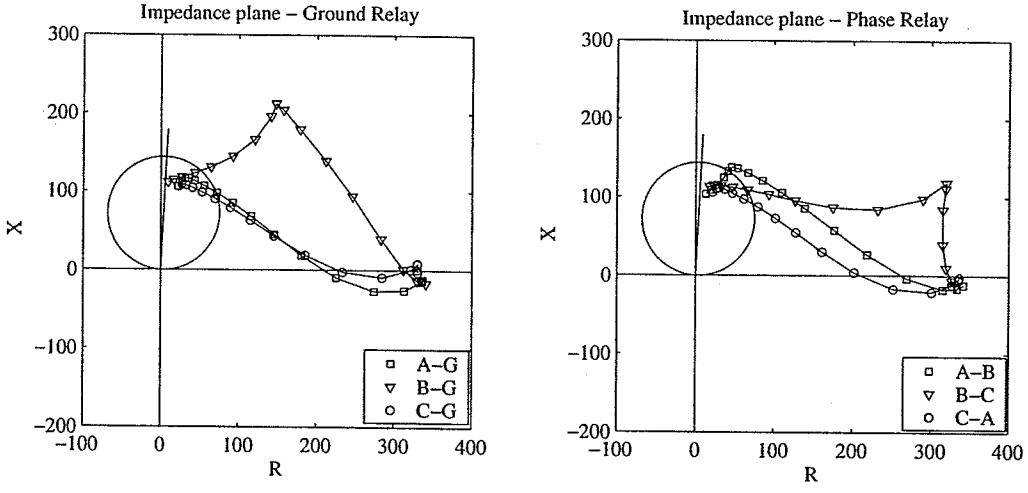

Figure 4.6: The impedance loci for the three phase fault: $x_{RF} = 325km$

4.3.3 Combining the Algorithms

Fig.4.7 shows the three phase voltage and current signals and the trip signals issued by the travelling wave and impedance algorithms separately for the three phase to ground fault discussed above. The travelling wave relay estimates the distance to the fault to be 325.9 km. Since this is within the protected line length, a trip signal is issued by the travelling wave relay 5.4ms after the fault inception. The impedance relay detects the fault 11.7ms after the fault inception. The wavefront analyzer analyzes the first wavefront that appeared at the relay location to see whether a steep wavefront was created by the fault transients. For this fault, the wavefront analyzer decides that the travelling wave algorithm can make a reliable estimation of the fault distance. Since the fault distance is within the reach, the hybrid algorithm issues a trip signal without waiting for the decision of the impedance relay. The combined algorithm speeds up the trip decision by 6.3ms in comparison to the case when only the impedance relay was present.

4.4 Simulation Cases

The operating principle of the hybrid algorithm was explained in the above section using a three phase to ground fault example. However, the most frequent disturbances present in transmission networks are the single line to ground faults. The operating principle of the hybrid relay is similar for single-phase-to-ground faults, but special cases can be found when the fault inception angle becomes very small. In order to show the operating strategy of the hybrid relay, several examples are considered here. The reach of the impedance relay is set to 80% of the line length while the travelling wave algorithm accepts disturbances between 15% and 95% of the line.

Fig.4.8 shows the waveforms related to a phase B to ground fault at $x_{RF} = 270km$. The fault inception angle, $\phi = 60^0$. The fault detector identifies a forward disturbance at 0.92ms after the fault inception. The correlator shows a peak at 3.39ms which corresponds to a

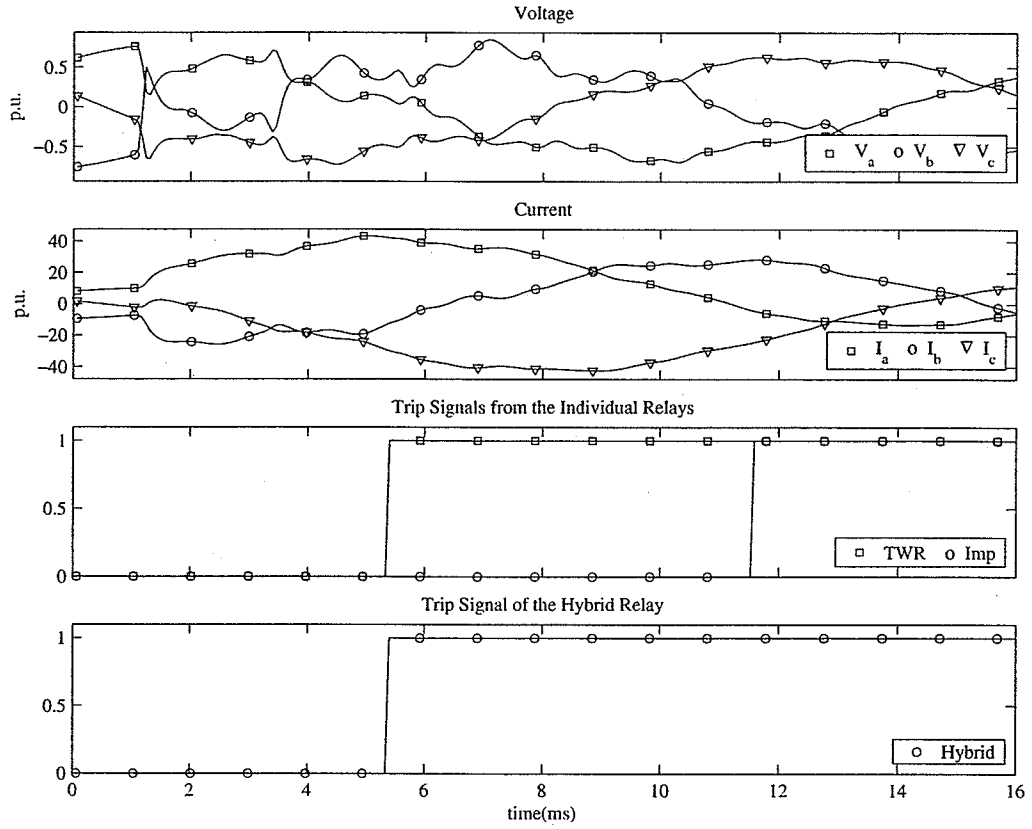

Figure 4.7: The trip signals issued for the three phase fault: $x_{RF} = 325km$

fault distance of 277 km. The wavefront analyzer approves the decision of travelling wave algorithm and hence a trip signal is issued at 5.2ms. For comparison, the fault identification time of impedance relay is also provided. The impedance relay identifies the fault at 13.2ms.

Fig.4.9 shows the waveforms related to a phase C to ground fault at $x_{RF} = 195km$. The fault inception angle, $\phi = 3^0$, which is very small. The fault generated transients do not carry any steep wavefronts. The fault detector fails to identify a forward disturbance. However, the measured impedance moves inside the protection zone and the impedance algorithm detects the fault. The impedance relay identifies the fault after 10.9ms. This shows that although the travelling wave relay alone would have failed to identify the fault, the hybrid relay is capable of identifying faults with small inception angles.

Fig.4.10 shows the waveforms of another special case. A phase A to ground fault is

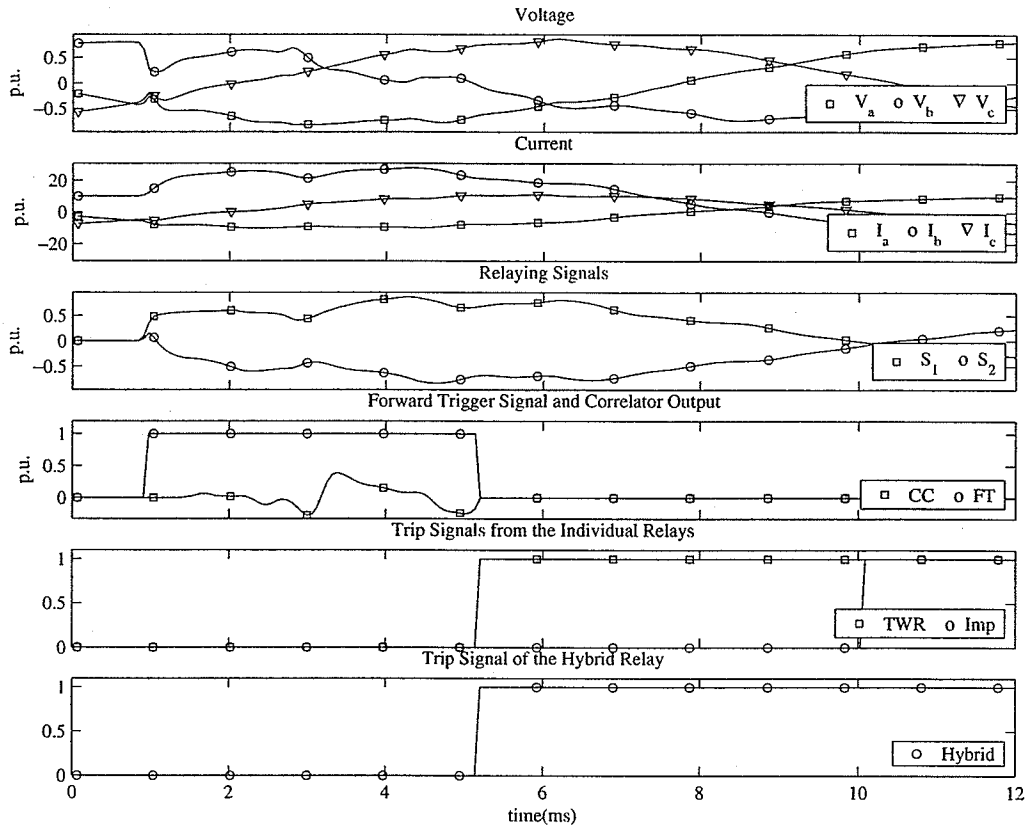

Figure 4.8: The relaying signal for a phase B to ground fault: $x_{RF} = 270km, \phi = 60^0$

applied at $x_{RF} = 220km$. The fault inception angle, $\phi = 154^0$. The fault detector identifies a forward disturbance at 0.76ms. However, the correlator does not show a peak above the set threshold level. The peak at 2.9ms corresponds to a fault distance of 229 km, which is the correct fault distance, but since the peak was below the correlator threshold that value is not considered. However, the measured impedance moves inside the protection zone and the impedance algorithm identifies the fault at 11.9ms.

Simulations were done to observe the behavior of the algorithm under close-up faults. One such example is shown in Fig.4.11. A phase B to ground fault is applied just 25 km away from the relay location when the voltage of line B is at its maximum. The wavefronts from the fault appear at the relay location within the first $100\mu s$. The calculated distance is 38.4 km and this is below the lower limit of 78 km. Hence the travelling wave relay

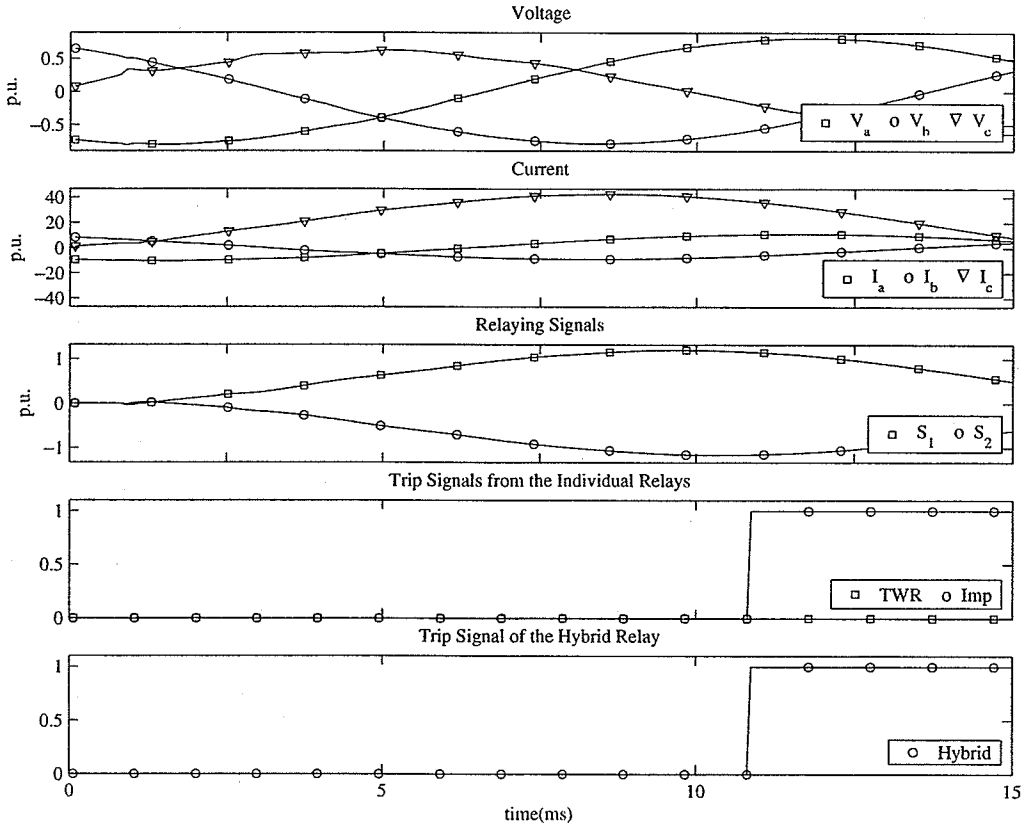

Figure 4.9: The relaying signal for a phase C to ground fault: $x_{RF} = 195km, \phi = 3^0$

is disabled. The measured impedance rapidly moves inside the protection zone and the impedance algorithm identifies the fault at 5.3ms.

The waveforms for a fault outside the reach of both travelling wave and impedance relay, but on the protected line is shown in Fig.4.12. A three phase to ground fault occurs close to the Forbes busbar, 525 km away from the relay location R. The peak of the correlator output at 3.58ms corresponds to a distance of 526.3 km, but since this is outside the setting, a trip signal is not issued by the hybrid relay. The impedance loci on Fig.4.13 show that the calculated impedances fall outside the protected zone.

Table 4.1 summarizes simulation results of different fault scenarios. Line-to-ground, line-to-line, and line-to-line-to-ground faults were applied at different fault locations both inside and outside the protected zone. The results show that the travelling wave relay always

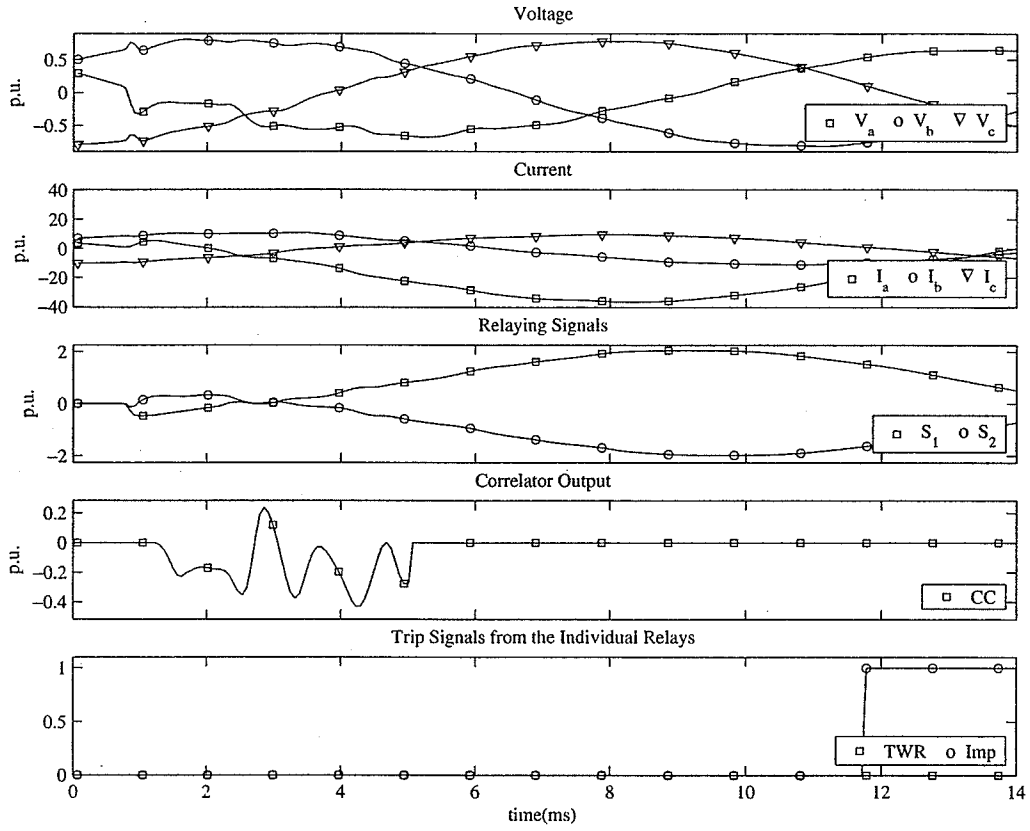

Figure 4.10: The relaying signal for a phase A to ground fault: $x_{RF} = 220km, \phi = 154^0$

detects the faults quickly when steep wavefronts are present. The impedance relay is slow compared to the travelling wave algorithm, but detects faults under all possible scenarios within its reach. The overall performance of the hybrid relay is superior to either travelling wave or impedance relay alone.

4.5 Accelerating Zone 2 Protection

In section 3.5.2, we discussed how the hybrid relay arrangement could be used to accelerate the zone 2 protection of a distance relay. The hybrid relay is a single-ended scheme, or in other words, the relay uses the information from only one end of the line. The idea of using a single-end information is to get rid of the expensive communication channel. In order to study the behavior of the hybrid relay scheme in the proposed algorithm, simulations

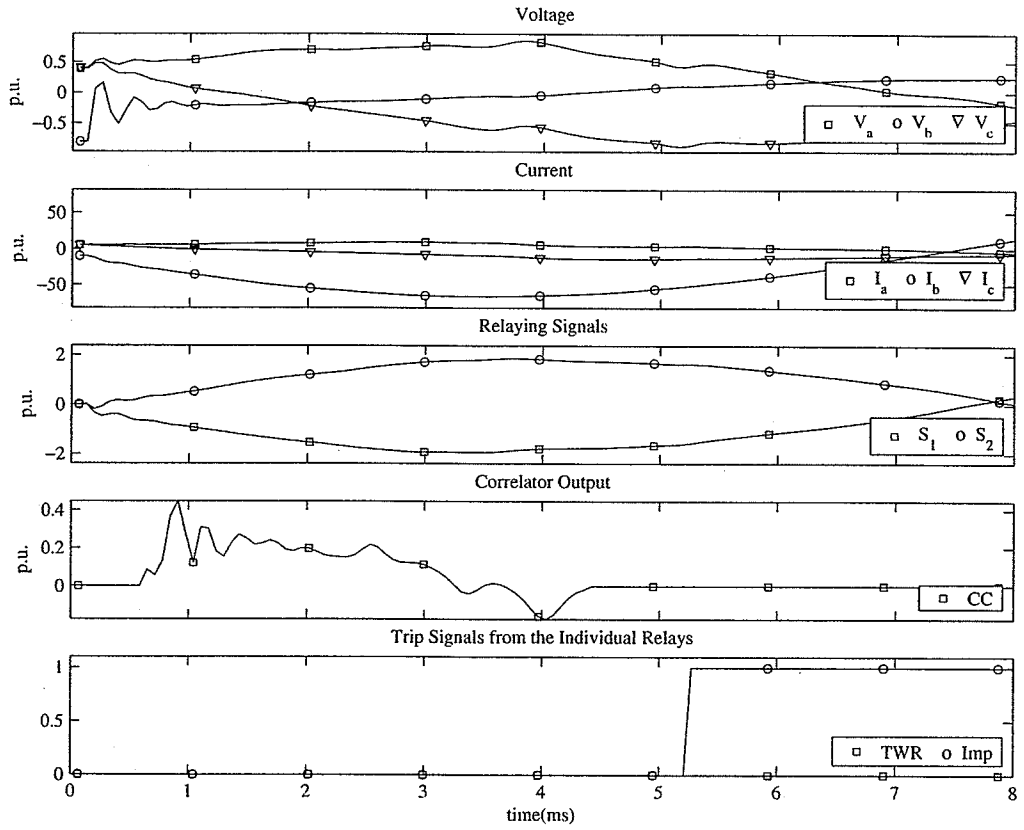

Figure 4.11: The relaying signal for a close-up B to ground fault: $x_{RF} = 25km, \phi = 90^0$

were carried out on the 500kV three phase power network mentioned before. The Zone 1 reach of the distance relay was set to 80% of the line length and the Zone 2 reach was set to 120%. To compare the results with the performance of a standard teleprotection relaying scheme, a teleprotection system was simulated on the same power network. Two distance relays, R_1, R_2 at the two ends of the Dorsey-Forbes line were connected by a transfer-trip teleprotection system as shown in Fig.4.14. An analog teleprotection scheme using frequency-shifting techniques to transmit the transfer-trip signal can have back-to-back latencies greater than 10 milliseconds. For the simulations, we set the transfer trip latency at 10ms. The propagation delay of the communication channel was introduced as a fixed delay. For the line DF, the propagation delay is about 1.8ms if other possible delays are ignored.

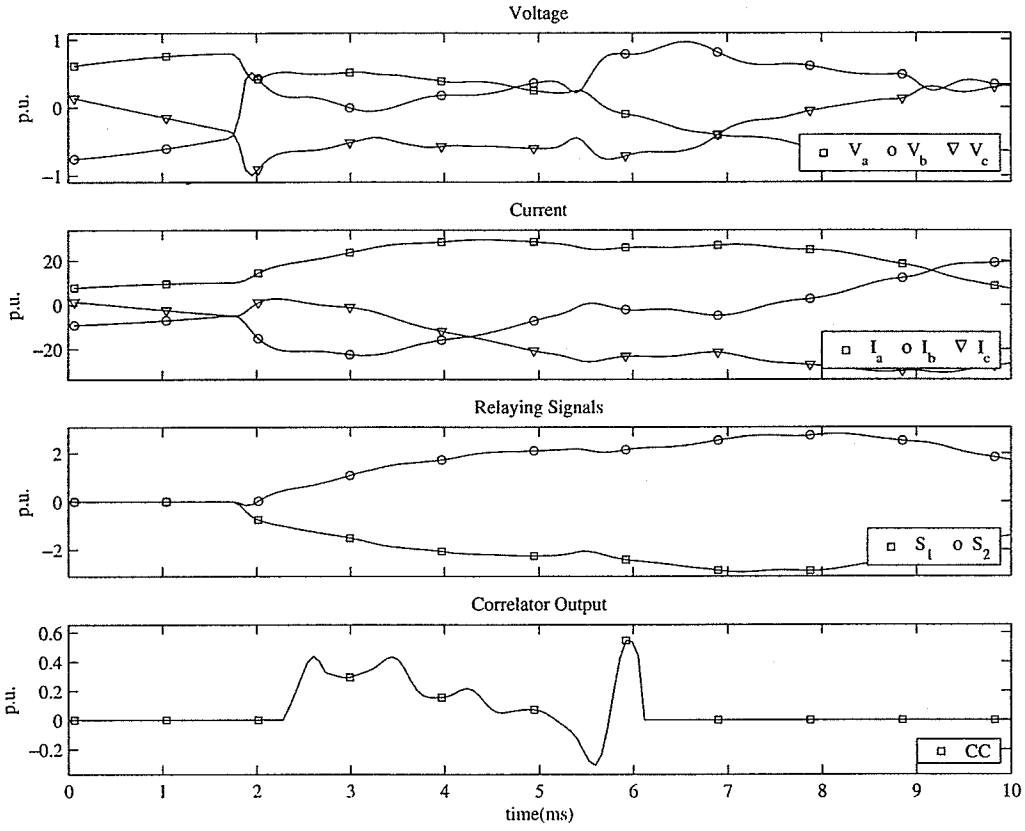

Figure 4.12: The relaying signal for three phase to ground fault: $x_{RF} = 525km$

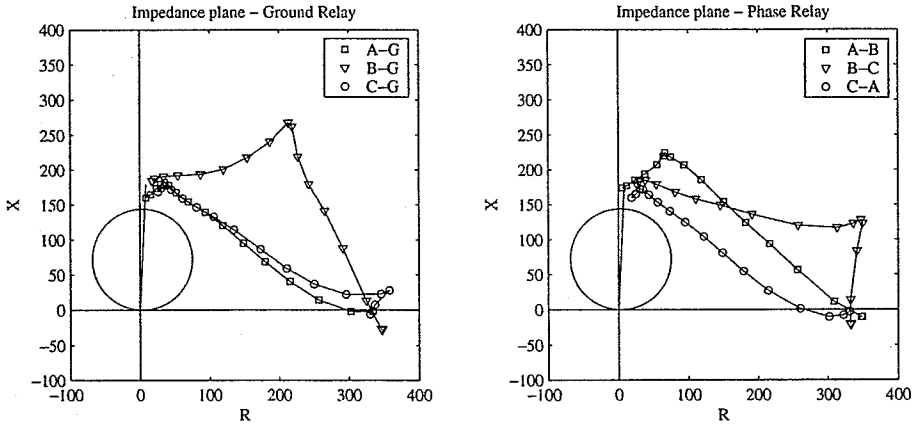

Figure 4.13: The impedance loci for three phase to ground fault: $x_{RF} = 525km$

Table 4.1: Simulation Results I

Fault	x_f	ϕ^o	t_p	t_{tw}	t_z	t_h	x_{tw}
A-G	325	90	3.84	5.4	14.5	5.4	325.4
B-G	270	60	3.39	5.2	10.3	5.2	277.2
C-G	195	4	-	-	10.9	10.9	-
AB-G	425	-	4.9	5.8	13.5	5.8	421
A-G	220	154	2.9†	-	11.9	11.9	229†
AC	490	-	5.5	5.96	-	5.96	488
ABC-G	325	-	3.84	5.4	11.7	5.4	325.4
B-G	25	270	-	-	5.3	5.3	-
C-G	245	45	3.0	5.1	9.3	5.1	239.2
AC-G	95	-	1.6	4.7	7.2	4.7	95.7
ABC-G	525	-	5.9‡	-	-	-	526.3‡

x_f = The distance to the fault

ϕ = The fault inception angle

t_p = The time at which the peak of correlator output occurs

t_{tw} = The fault detection time of the travelling wave relay

t_z = The fault detection time of the impedance relay

t_h = The time at which the hybrid relay issues the trip signal

x_{tw} = The distance calculated by the travelling wave relay

†*The correlator peak is below threshold*

‡*The calculated distance outside the reach*

Let us consider a three phase to ground fault to demonstrate the operating principle of the algorithm. The fault occurs at a location 500 km away from D towards F. The voltage and current signals seen by the relays R_1, and R_2 are shown in Fig.4.15.

The loci of the impedance seen by the two relays R_1 and R_2 are shown in 4.16. The impedance calculation of the relay R_1 falls inside zone 2 while the impedance loci of the relay at the other end enters inside zone 1.

Fig.4.17 shows the relaying signals of the travelling wave relay, the correlator output, and the various trip signals issued by relays at both ends of the line. The fault detector detects a forward fault 1.7ms after the fault occurred. The correlator output shows a peak

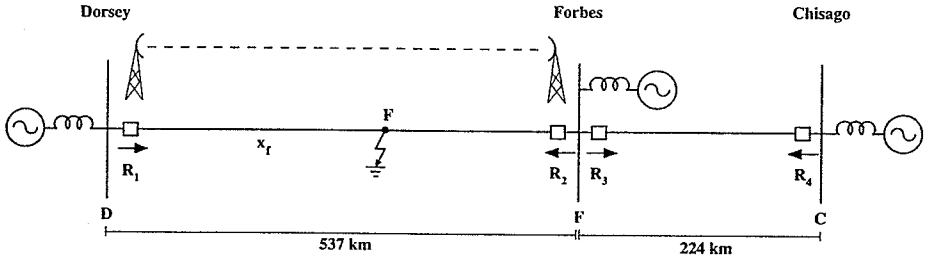

Figure 4.14: The 500kV line with two relays connected by a communication channel

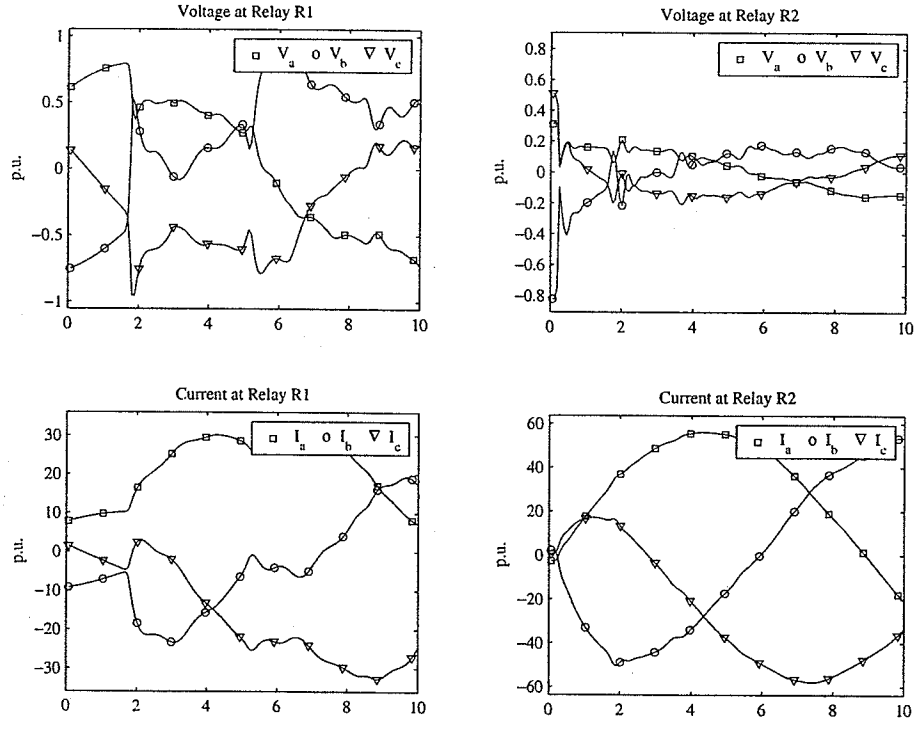

Figure 4.15: The fault transients generated by three phase to ground fault: $x_{RF} = 500km$

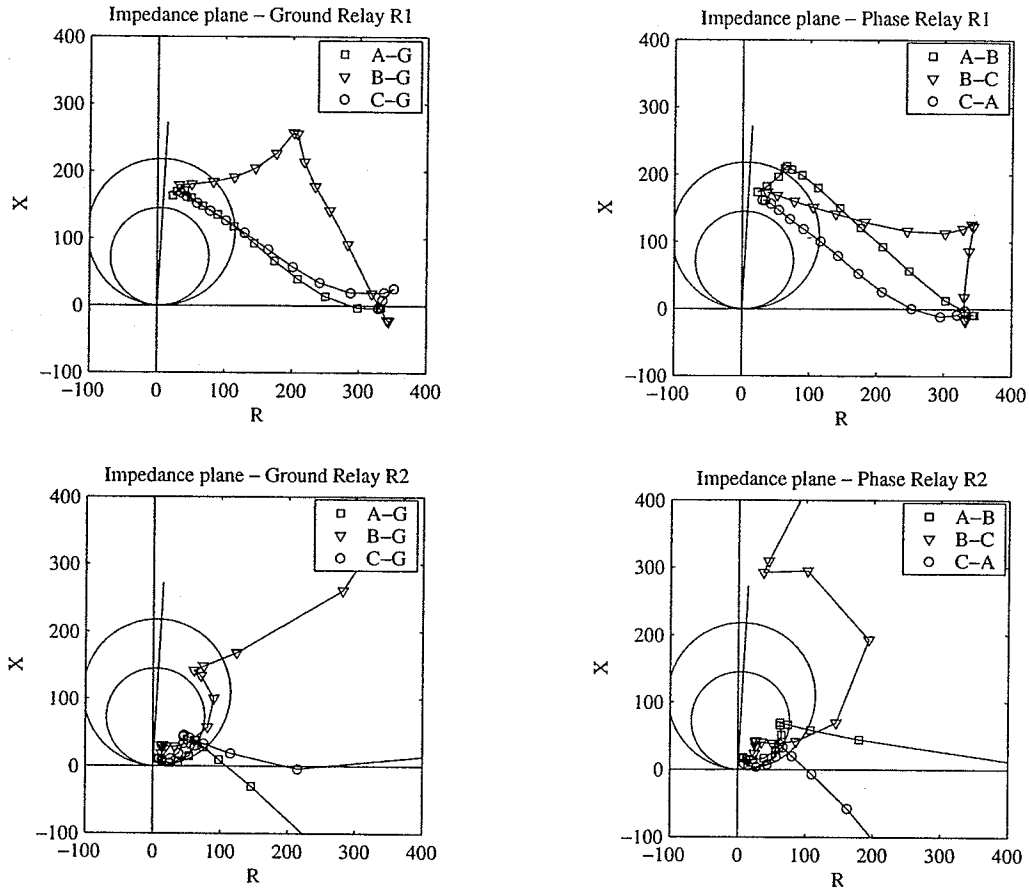

Figure 4.16: The impedance loci for three phase fault: $x_{RF} = 525km$, (a) R_1 (b) R_2

signal at 5.6ms which corresponds to a distance of 507 km. Since the calculated distance is on the line, the travelling wave relay issues a trip signal at 6.0ms, but the hybrid relay waits for the trip signal from the zone 2 element of the impedance relay. The calculated impedance enters the zone 2 of relay R_1 at 10.5ms and hence the hybrid relay issues a trip signal at 10.6ms. The impedance calculated by relay R_2 at the remote end falls within its zone 1 after 8.5ms. After the delay involved in communicating the trip signal, the transfer trip signal arrives at relay R_1 at 20.5ms.

Table 4.2 summarizes simulation results of different fault scenarios of algorithm 2. Line-to-ground, line-to-line, and line-to-line-to-ground faults were applied at different fault locations both inside and outside the protected zone. The simulation results show that the

hybrid relay can detect faults faster than a teleprotection scheme when steep wavefronts are present in fault transients. When a fault on the line falls in zone 2 of the impedance relay and the travelling wave relay does not detect the fault, a 30 cycle delay is introduced to the zone 2 trip signal. By using some kind of an inter-trip signal, such faults can be cleared within a satisfactory time. The overall performance of the hybrid relay is superior to either travelling wave or impedance relay alone.

Table 4.2: Simulation Results II

Fault	x_f	ϕ^o	t_p	t_{tw}	t_{z2}	t_{z1}	t_h	t_r	t_{tp}	x_{tw}
A-G	325	35	3.83	5.4	8.4	9.5	8.4	10.5	22.5	325.4
B-G	500	270	5.8	6.0	14.7	-	14.7	6.4	18.3	507.1
C-G	420	-3	-	-	10.2	16.5	16.5	11.2	23.2	-
A-G	470	174	-	-	10.1	-	411	10.1	22.0	-
B-G	445	240	5.0	5.8	13.6	-	13.6	7.4	19.4	449.7
C-G	95	50	1.5	4.6	9.0	11.1	9.0	-	-	95.7
AC-G	525	-	5.9	6.0	12.2	-	12.2	5.9	17.9	526.2
ABC-G	500	-	5.7	6.0	10.5	-	10.6	8.4	20.4	507.1

x_f = The distance to the fault

ϕ = The fault inception angle

t_p = The time at which the peak of correlator output occurs

t_{tw} = The fault detection time of the travelling wave relay

t_{z2} = The fault detection time of the zone 2 of the impedance relay R_1

t_{z1} = The fault detection time of the zone 1 of the impedance relay R_1

t_r = The fault detection time of the zone2 of the impedance relay R_2

t_h = The time at which the hybrid relay issues the trip signal

t_{tp} = The time at which the transfer trip signal of R_2 is received by R_1

x_{tw} = The distance calculated by the travelling wave relay

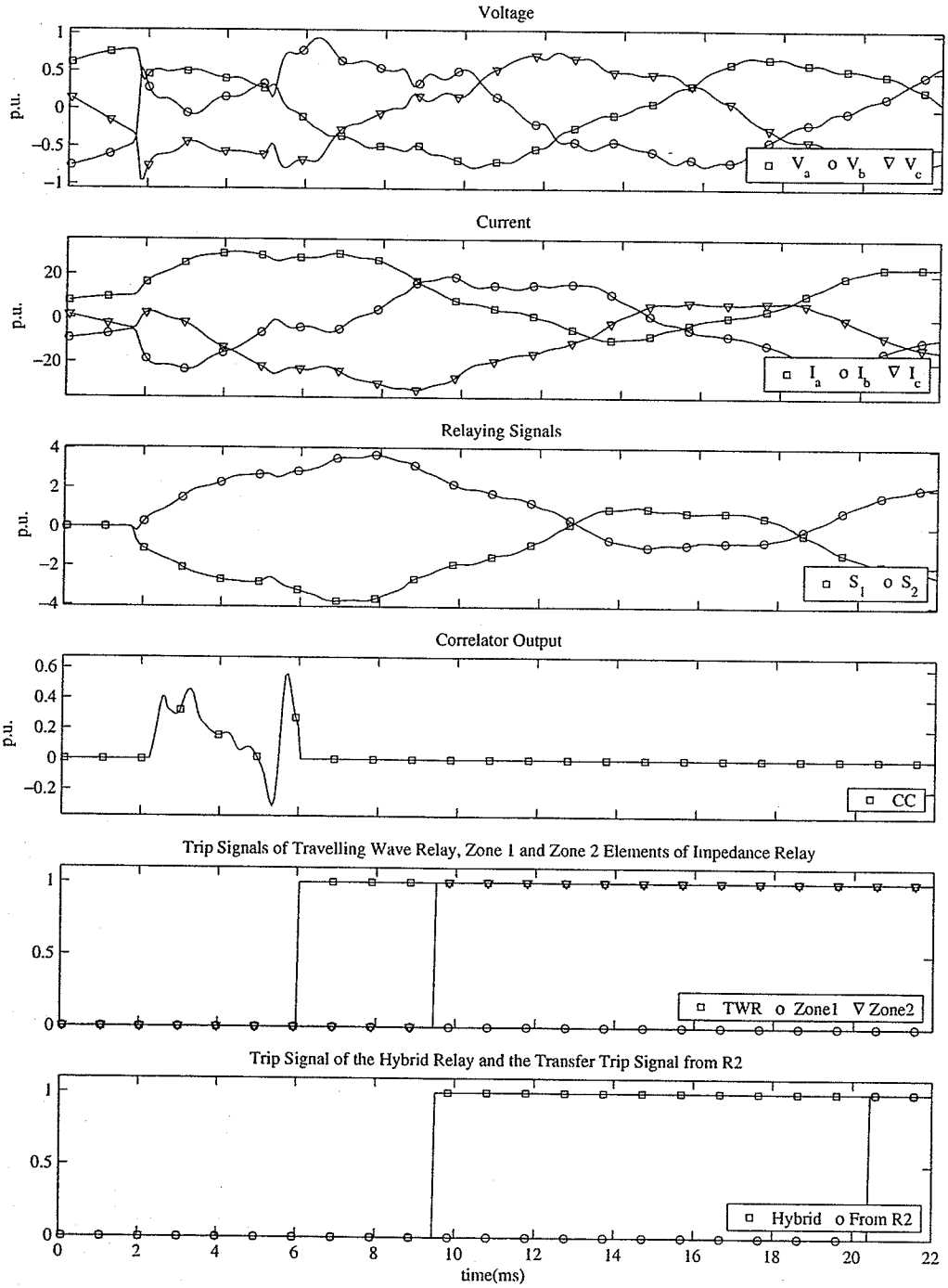

Figure 4.17: Relaying signals of the three phase to ground fault: $x_{RF} = 500km$

Chapter 5

Laboratory Prototype

5.1 Introduction

A laboratory prototype of the hybrid relay algorithm was developed to test the real-time performance of the relay. One of the main aspects of the design was to keep the cost of the relay as low as possible. Choosing and designing hardware and software capable of handling the extensive calculations in real time while keeping the cost low was a difficult task. It was decided to develop the prototype with the hardware resources readily available in the industry, identify their limitations and study the requirements for the final product. Several configurations were attempted and numerous technical difficulties had to be addressed before the final implementation. The simulation algorithms had to be modified and special calculation procedures had to be chosen to decrease the processing time. In this chapter, the hardware and software aspects of the laboratory prototype implementation are discussed. The biggest challenge faced during the implementation was capturing voltage and current signals at high sampling rates required for the travelling wave relay and hence more emphasis will be made to the details of the data acquisition system.

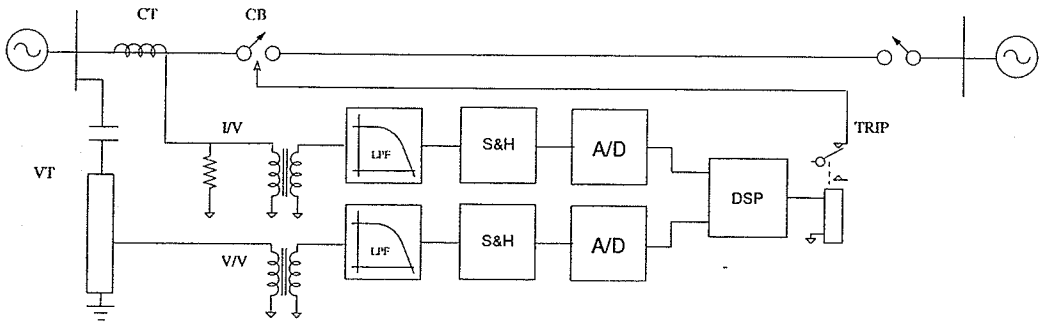

Figure 5.1: A typical digital relay configuration

5.2 Design Considerations

5.2.1 System Requirements

The simulations in the previous chapter were done in an ideal environment. The voltage and current signals measured at the relay location were in their discrete format and hence the error associated with the measuring process was not considered. Some knowledge about signal acquisition for digital relaying is useful for the design process. Fig.5.1 shows the main components associated with signal measurement.

The current and voltage at the relay point are measured with current transformers (CT's) and voltage transformers (VT's) respectively. The current transformers usually have a bandwidth of several hundred kilohertz [8]. In EHV lines, the voltage is usually measured using capacitive voltage transformers (CVT's). CVTs have a limited bandwidth and show a linear frequency range of about 1kHz [9]. Hence the measured voltage waveforms will lack the information of the high frequency transients. The recently developed optical voltage transformers (OVT) have high bandwidths and are capable of reproducing a fairly accurate replica of the high frequency wavefronts [65]. For transient based protection schemes used in EHV lines, OVT must be preferred over CVT. The magnitudes of the measured signals on the secondary side of the voltage and current transducers are further reduced using secondary transformers in order to bring the signal levels down to acceptable levels for microprocessor relays. All these stages in the measuring process introduce noise to the

measured signal. In order to improve the signal to noise ratio, high fidelity transducers must be used.

No signal is truly deterministic and therefore in practice has infinite bandwidth. However, the energy of higher frequency components becomes increasingly smaller so that at a certain value it can be considered to be irrelevant. For an impedance relay the signals above 60Hz become noise, but a transient-based relay needs information contained in the high frequency transients. The signals used for the travelling wave relay need not have an upper limit for the frequency since the correlator compares the shape of the stored reference with the reflected signals. However, analog to digital conversion will introduce an aliasing effect due to the sampling of the continuous signals. In order to reduce the effect of aliasing, the signals used for the travelling wave relay should have an upper limit in the bandwidth.

The amount of aliasing that can be tolerated is eventually dependent upon the resolution of the system. If the system has low resolution, then the noise floor is already relatively high and aliasing does not have a significant effect. However, with a high resolution system, aliasing can increase the noise floor considerably. One way to prevent aliasing is to increase the sampling rate. However, the maximum sampling rate is limited by the type of data converter used and also by the maximum clock rate of the digital processor receiving the data. Therefore, to reduce the effects of aliasing, analog filters must be used to limit the input signal spectrum.

For faults on a high voltage transmission line, the transient signals can have a bandwidth as high as 5kHz [58]. It was decided that considering frequencies below 5kHz is quite adequate for travelling wave measurements. Hence signals above 5kHz will have to be filtered out in the prototype implementation. Hence the sampling rate has to be at least 10kHz. For the implementation, it was decided to consider a sampling rate of at least three times the Nyquist rate. In order to calculate the fundamental frequency component using an Fast Fourier Transform (FFT) algorithm, the number of a samples within one 60Hz cycle has to be a power of two. It is quite adequate to use 8 samples/cycle to calculate

the 60Hz signals. With a sampling rate of about 15kHz and a suitable decimation factor, 8 samples/cycle can be obtained. It was found that a decimation factor of 32 and a sampling rate of 256 samples/cycle (15.36kHz) was suitable for our application.

The voltage and current transducer outputs are captured by the sample and hold circuit at pre-specified time instances. These samples are then converted to discrete values by an analog to digital converter (ADC). The ADC chosen must have a linear gain throughout the input voltage range, and should not have any offset or non-linearity errors. When nonlinearity errors are present, the values on the actual transfer function of the ADC can deviate from a straight line. The analog input to an ADC is a continuous signal with an infinite number of possible states, whereas the digital output is by its nature a discrete function with a number of different states determined by the resolution of the ADC. Hence some information can be lost and distortions may be introduced into the signal. This is known as quantization noise. A high resolution ADC minimizes the effect of quantization noise. However, the cost of the ADC increases with the increase in resolution. Analysis of the waveforms showed that an ADC having a 12-16bit resolution can provide adequate resolution while keeping the cost down.

The travelling wave algorithm needs to analyze information as high as 5kHz. Hence an ADC which supports a sampling rate of at least 10kHz per channel has to be chosen. For a three-phase system, the A/D board must have at least six analog input channels to measure the three voltage and three current signals. All six channels must be sampled simultaneously to facilitate the recognition of the relative position of the wavefronts. In addition, the system must have a digital output to be used for the trip signal.

The sampled voltage and current signals are then sent to the microprocessor for processing. A high-speed digital signal processor (DSP) capable of handling the extensive calculations involved in the hybrid algorithm has to be chosen to implement the proposed system. The processor must be able to carry out the calculations of the two algorithms in parallel in real time. Rather than considering a configuration with parallel processors, it

was decided to go for a fast single digital signal processor board due to the simplicity in handling data. A parallel processor configuration would require special software routines to handle the inter-processor communication and hence the implementation can become very complex.

5.2.2 Relay Test Setup

Fig.5.2 shows a typical laboratory test setup of a digital relay. The waveforms related to fault situations are generated by an EMTP software like PSCAD if data recorded in a real system is not available. The voltage and current waveforms are then regenerated as analog signals using a playback system such as Real Time Playback (RTP) [66]. The waveforms from the playback generator are sampled and converted to discrete values by the ADC (data converter). The sampled data is then processed in the DSP which performs the relay algorithms. A host processor is used for configuring the DSP and monitoring the relay status. When a fault is identified, a trip signal is sent back to the playback generator which accepts it as a digital input and records the trip time.

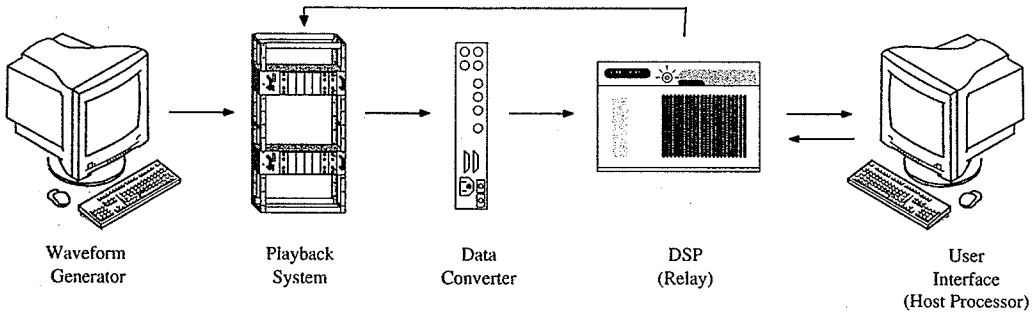

Figure 5.2: Laboratory test setup of a digital relay

5.3 Choice of Hardware and Software

One of the main objectives of the hardware implementation was keeping the cost of the final product as low as possible. At the same time, the chosen hardware must be capable of handling high sampling rates and processing requirements. Hardware already available in the

laboratory was examined first to assess their capabilities and identify the special hardware and software requirements that could emerge when the two algorithms are combined. Once the resources already available in the laboratory were found to be inadequate, alternatives were considered. The configuration selected not only depends on the speed of the signal processor, but also on the availability of data acquisition systems, user-friendliness of the software and previous experience on the products from a particular manufacturer.

The sections to follow discuss the different configurations considered for the implementation of the relay prototype, and the reasons for the failure of some of them. Four different configurations were tested during the development phase:

1. Spectrum Dakar board with DL3-A1 ADC
2. Texas Instruments TMS320C6711 DSK with THS1206 ADC
3. Texas Instruments TMS320C6711 DSK with TLV2548 ADC
4. Texas Instruments TMS320C6711 DSK with ADS8364 ADC

5.4 Spectrum Board Configuration

5.4.1 Spectrum Dakar F5 Carrier Board

Spectrum Dakar F5 board [67] provided as a grant by the Canadian Microelectronics Corporation (CMC) under a product evaluation program was considered as an option to implement the relaying algorithm. This board was used to identify the main requirements of the real-time prototype. Dakar F5 is a configurable DSP platform based on Spectrum Signal Processing Inc.'s Dakar boards and has an embedded Texas Instrument (TI) TMS320C44 processor [68]. The board is supported with Spectrum Signal Processing Inc.'s Software Development Kit (SDK) [69]. The configuration utility tool box [70] was used to generate configuration files for the DSP system. The code was generated using Texas Instruments Code Composer Studio (CCS) integrated development environment (IDE) [71]. The CCS

allows the users to edit, build, debug, profile and manage projects with its MS-Visual C++ like single unified environment [72].

Specifications for Dakar F5:

- Embedded TMS320C44 50MHz processor
- Up to 50 MFLOPS, 25 MIPS performance
- Scalability up to 4 parallel processors
- 2 general-purpose timers
- 6 channel DMA coprocessor
- 1MByte SRAM memory for Node A embedded processor
- 32-bit PCI interface with 132 MBytes/s peak transfer rate
- 10 external COMM ports (8-bit parallel communication ports)
- JTAG real time debugging interface
- On-board DSP-LINK3[1]connector module
- TIM-40[2]compliant code boot-strapping through onboard EPROM

5.4.2 Spectrum DL3-A1

Choosing a signal acquisition system with six or more analog inputs and which could be interfaced with the Dakar F5 board was challenging. Finally, Spectrum Signal Processing Inc.'s DL3-A1 DL3ADA100 Analog Module [73] was selected as the analog to digital converter. This is an add-on board that connects to Dakar board via a DSP-LINK3 module connection [74]. The module acts as a slave on the DSP-LINK3 bus. The DL3-A1 provides four analog input channels and two analog output channels. The objective was to stack two DL3-A1 analog modules in parallel on the two DSP-LINK3 ports to obtain the six inputs.

[1]DSP-LINK3 is an open standard for 32-bit 40 MByte/s I/O interface from Spectrum Signal Processing Inc

[2]TIM-40 modules define a family of DSP modules, based on TMS320C4x processors, designed for use in multiple DSP systems

The analog front end of the DL3-A1 has built-in adjustable input anti-aliasing filters and output smoothing filters. The gain and offset of the input signals can also be adjusted.

Specifications of DL3-A1:

- Four analog input channels and two analog output channels
- 100kHz, 16-bit converter
- DSP-LINK3 interface
- Triggered by on-board timer or external trigger input
- Input/output range: $\pm 10V$
- DC or AC coupled input configuration
- Offset and gain adjustment
- Input anti-aliasing filters (6 pole Butterworth : 340Hz-49kHz)
- Output smoothing filter (single pole : 50kHz)

5.4.3 Limitations of Dakar Configuration

The Dakar board configuration showed several difficulties during the implementation of the relay algorithms. The communication between the host processor and the DSP was intricate. The data handling functions available in the SDK were integer based and exchange of floating point numbers involved longer time periods due to the conversion time delays. The library module provided with the SDK was not sufficient for certain requirements such as handling the interrupts. The processor speed (MFLOPS) of C44 was found to be inadequate to handle the calculations of both algorithms in parallel. In addition, interfacing the DL3-A1 analog module to the Dakar board as expected was not feasible. We realized that the stacking of analog modules to obtain six channels could cause contention in the DSP-LINK3 bus. Hence, it was decided to search for another DSP configuration.

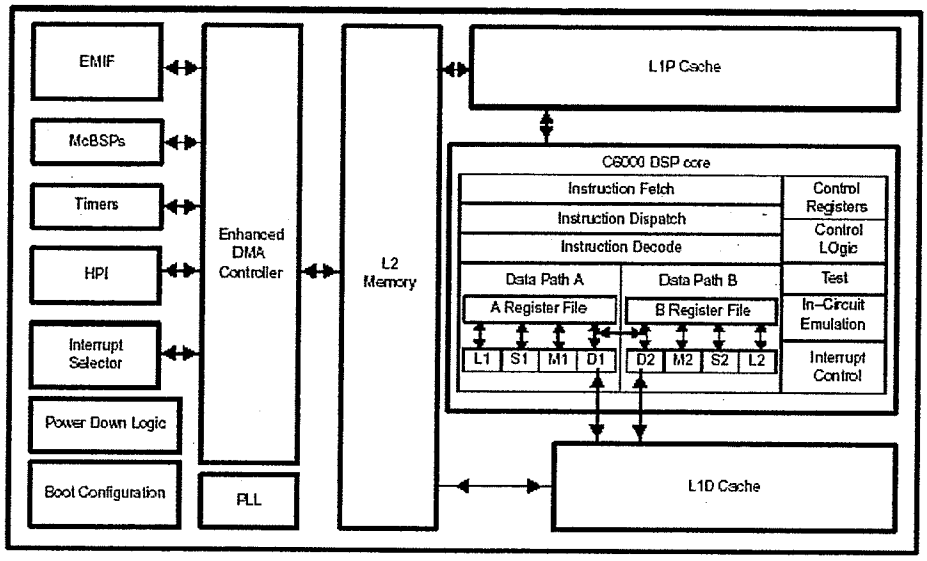

Figure 5.3: Functional block diagram of the C6711

5.5 Texas Instruments C6x Configuration

5.5.1 C6711 DSK

Texas Instrument's C6711 Digital Signal Processor Starter Kit (DSK) was considered as an alternative to the Dakar board. DSK provides an excellent basis for developing prototypes. The C6711 DSK has an embedded TMS320C6711 floating point digital signal processor [75, 76]. The TMS320C6711 processor is based on very-long-instruction-word (VLIW) architecture and is faster than the TMS320C44 processor. In addition, the C6711 DSK costs less compared to the Dakar board and has a lot more attractive features [77].

The C6711 DSK is a parallel port interface platform and the host machine is connected to the DSK through the HPI. The basic functional block diagram of the TMS320C6711 is shown on Fig.5.3 [3].

The C6711 DSK provides dual DSP clock support (see Appendix F), which allows the CPU to run at one frequency and the EMIF to operate at another frequency. This is

[3]The figure was obtained from [78]

important in interfacing daughtercards to the DSP at data rates required by the application. One of the McBSP ports is connected to an onboard codec and the other can be used to interface a daughtercard connected to the expansion peripheral interface. The EDMA controller is directly connected to the two McBSP ports and EMIF. This allows the EDMA controller to control and access a daughtercard without interrupting the CPU, a very useful feature that helps to reduce the workload of the CPU.

Specifications of C6711 DSK:

- 150 MHz clock speed
- Operating speeds up to 900 MFLOPS
- PPC interface to standard parallel port on a host PC (EPP or bi-directional SPP)
- Eight 32-bit instructions/cycle
- 6 ALU's and 2 multipliers
- 16MB of 100MHz SDRAM
- 32-bit external memory interface (EMIF)
- 16-bit host-port interface (HPI) access to all DSP memory
- 16 EDMA channels with simultaneous data handling capabilities
- 2 multi-channel buffered serial ports (McBSP)
- 2 general-purpose timers
- Phase-locked-loop (PLL) clock generator
- 128KB of EPROM
- HPI and 32-bit ROM boot modes
- L1/L2 memory architecture
- 16-bit audio codec
- Expansion memory and peripheral connectors for daughterboard support

5.5.2 Programming the DSK

The software development for the laboratory prototype involved several tasks:

- developing a software interface for the communication between the host and the DSP
- interfacing a chosen ADC to the DSK for the real time signal acquisition
- creating efficient relay algorithms to improve DSP performance
- developing a graphical user interface (GUI) to monitor the relay performance and adjust the relay settings.

A host (a stand-alone PC) can access the HPI of the C6711 DSK through its parallel port. The host-DSP software interface had to have provisions for downloading the DSP code, reading DSP memory locations and interrupt information, and uploading and downloading data between the host and the DSP. The C6711 DSK allows interfacing both serial and parallel data acquisition daughtercards. Serial daughtercards are interfaced through the multi-channel serial ports (see Appendix F) while parallel daughtercards are connected through the external peripheral interface (EPI) by configuring the EPI pins to act as general purpose input/output (GPIO) pins. The relay algorithms were optimized for fast execution and hence the compilers had to be configured to optimize the execution speed.

Code Composer Studio

Texas Instruments Code Composer Studio Integrated Development Environment (CCS IDE) for C6x was used to program the DSK. The CCS extends the basic code generation tools of TI compilers with a set of debugging and real-time analysis capabilities [79]. The CCS IDE supports all phases of the development cycle shown on Fig.5.4. The C6x version of the CCS [80, 81] provided more flexibility and debugging features than the CCS version for C4x chips. The in-built C-compiler and C and Assembly language debuggers

help easy debugging of the codes, code optimization for speed and accessing the CPU registers [82, 83]. Texas Instruments also provided TMS320C6000 Chip Support Library (CSL), which is a set of application programming interfaces (APIs) used to configure and control all on-chip peripherals and run-time support libraries (RSLs) that are used during the execution stage [84, 85].

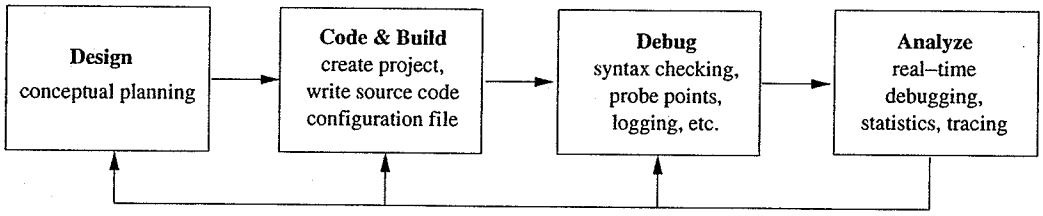

Figure 5.4: CCS development flow

The GUI of the relay runs on a PC. The GUI shows the voltage and current waveforms, protection coordinates of the impedance relay, the relay status and in case of a fault, the trip signals, impedance loci and the estimated distance to the fault. Developing the GUI and interfacing the PC to the DSK required knowledge about Windows programming and parallel port interfacing. At the beginning Visual C++ [86] along with the C6x CCS studio was used to develop the GUI and interface the parallel port of the PC to the HPI of the DSK. Although using Visual C++ was possible, programming the GUI with C++ became strenuous. In order to shorten the relay algorithm development time and the GUI implementation time, an alternative software package called Hypersignal RIDE (RIDE) was used [87].

RIDE

RIDE is a program capable of both simulating algorithms in a graphical environment using a library of software building blocks or from the same environment, running the algorithms directly on a DSP board [87]. RIDE provides libraries for both DSP-based and PC-based analysis. It also supports user-written and user-defined functions or algorithms. RIDE was used for simulation, analysis, and design of the relaying algorithms.

We used a component based approach in developing relaying algorithms which was supported by RIDE. This was accomplished by the utilization of dynamic link libraries (DLLs) that were designed to run with RIDE. These DLLs (or block DLLs) were designed to do specific tasks. The blocks were then connected together according to the data flow between them. Only the required components that were not included in the standard library of general blocks and the standard library of DSP blocks of RIDE [88] were additionally created. Each created block has two parts associated with it; a DLL file that runs on the host and an object code that runs on the DSP. The block DLL is responsible for data transfer from the host to the DSP. The host program or the DLL was created using Microsoft Visual C++ version 6.0 [89]. To create the object code that runs on the DSP, C6x CCS was used [80].

To create the relaying algorithms using RIDE, the real-time function blocks were arranged according to the requirements of the algorithm on a worksheet under the RIDE graphical user environment. The function blocks were connected to establish the data flow and then the parameters of the blocks were set. The parameters were selected to set DSP resources and handle synchronization, interrupt, and profile configurations. The real-time block functions in a worksheet communicate with the DSP board driver and other blocks to transmit data flow information. The DSP board driver performs the linking of DSP object files, downloads code, data, and parameters to DSP memory, controls the execution of the DSP, monitors DSP activity, and provides DSP resource allocation information.

5.5.3 Choice of Analog to Digital Converters for C6711 DSK

To acquire the three voltage and three current signals required for the relay algorithm, an analog to digital converter having six or more channels, which can be interfaced with the C6711 DSK, had to be chosen. Texas Instruments provided several daughterboards which could be directly interfaced with the C6711 DSK through the EMIF and peripheral connecter [90]. However, at the time the search for ADCs started, it was not possible to find

a unit with six or more channels from the selection of TI daughterboards. Hence, third-party companies had to be sought for their products which satisfied the above requirements. The cheapest solution that could be found through web search was Signalware Corporation's AED-106 board. In this board, four Texas Instruments THS1206 data converters [91] were multiplexed in a single configuration and hence provided 16 analog inputs and 24 digital I/O. However, AED-106 was considered expensive for this implementation. That could have made the overall cost of the relay high. Thinking along the design of the AED-106, it was decided to use THS1206 for data acquisition.

5.6 THS1206EVM Analog to Digital Converter

THS1206 is a four channel 12bit 6MSPS simultaneous sampling data converter. An integrated 16 word deep FIFO allows the storage of data in order to take the load off of the processor connected to the ADC [92]. Fast data throughput is achieved with the integrated FIFO.

Specifications of THS1206EVM:

- High-Speed 6MSPS ADC
- 12-bit resolution
- 4 single-ended or 2 differential inputs
- Simultaneous sampling channels
- 16 word, 12-bit integrated FIFO
- Parallel glueless μC/DSP interface

The block diagram of the THS1206 with the inputs and outputs is shown in Fig.5.5 [4]. The THS1206EVM has a parallel interface and is connected to the C6711 DSK through the common connector interface [78]. Interfacing an ADC having a parallel interface to a DSP can become complex compared to an ADC equipped with a standard serial interface and

[4]The figure obtained from [91]

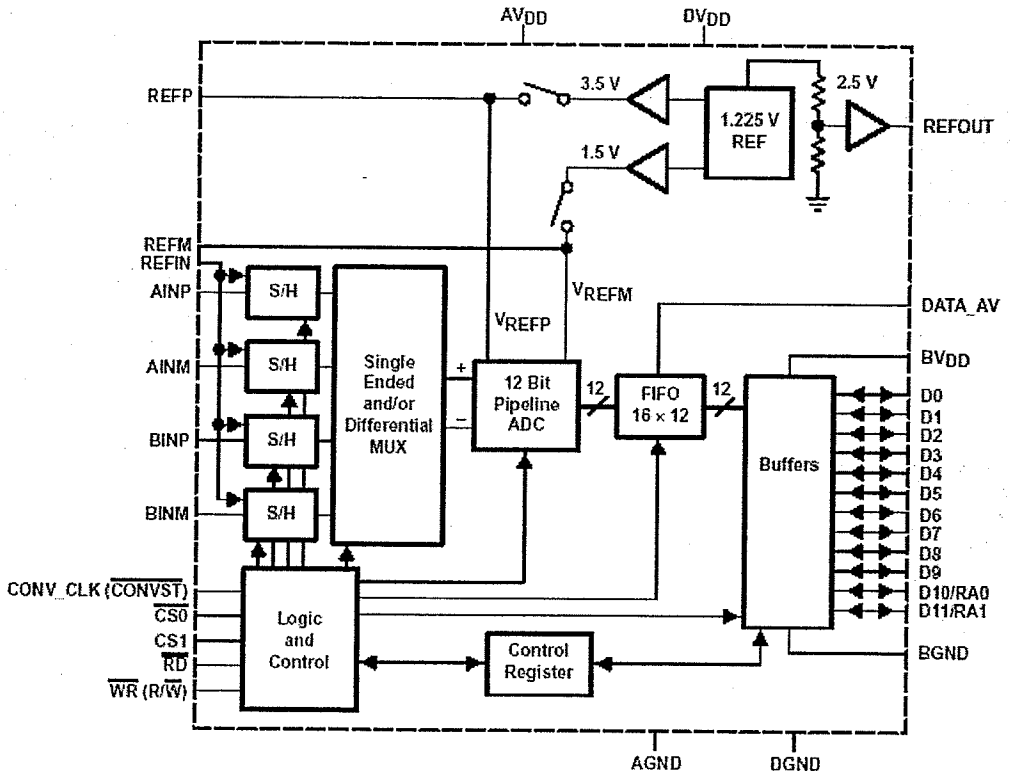

Figure 5.5: THS1206 block diagram

usually there are many ways to build the interface. In our implementation, the read and write inputs (RD, WR) and the programmable control signal DATA_AV were used to read the data from the THS1206 to the DSK [93]. Fig.5.6 shows the signals associated with the connection of EVM to the DSK.

In order to program the THS1206 into the desired mode, two 10-bit wide internal control registers (CR0, CR1) were used. Several steps had to be followed to program the registers. The THS1206 was reset at the beginning of initialization by writing 0x401 to CR1. Then the reset was cleared by writing 0x400 to CR1. The user configuration required for sampling four channels was written to CR0 and CR1 after that. The write access was required to reset and configure the THS1206 to the desired operation mode. The read access transferred converted samples from the THS1206 to the DSP. The conversion clock was generated by

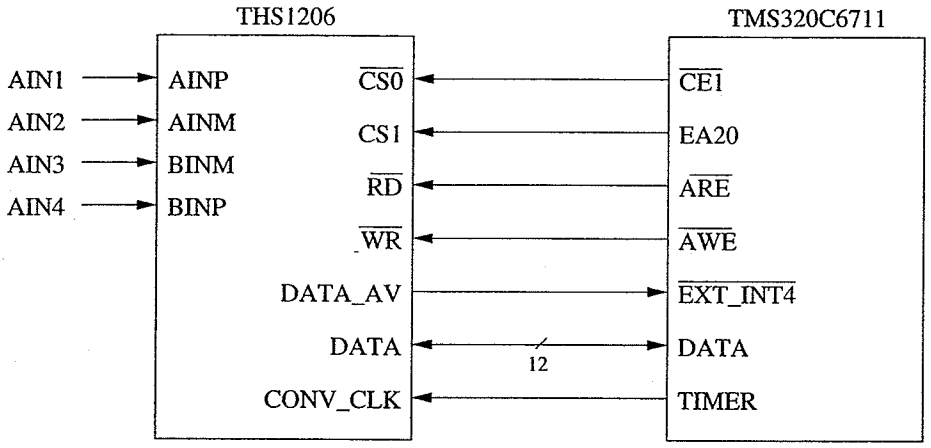

Figure 5.6: Connecting THS1206 to the C6711 DSK

timer0 of the DSK (see Appendix F). It provided a clock signal with a 50% duty cycle. The conversion synchronization was achieved by connecting interrupt EXT_INT4 of the DSK to DATA_AV signal of EVM. When EXT_INT4 becomes active, the DSP is directed to execute the interrupt service routine (ISR) dedicated to the interrupt 4. ISR allows the processor to perform other functions, until an off-chip device needs attention. When an interrupt is detected, the processor checks to see if any interrupts are enabled; if it finds that a particular interrupt is enabled, it looks in the interrupt vector table for the next instruction, which is typically a jump instruction to an ISR. In THS1206, new samples are automatically written to the FIFO with every falling edge of the conversion clock (CONV_CLK). Hence write, read, and trigger pointers were used to control the writing and reading processes. The converted values were written to the circular buffer in a predefined sequence (autoscan mode). The trigger level was set to 4 for the circular buffer in order to obtain the sample values of the four channels at every sampling step to continuously sample the four input channels at 15.36kHz. More information about these registers can be found in [91].

THS1206 was able to read data from four analog input channels at 15.36kHz. However, extending the four channels to six using two boards was not straightforward. The C6711 DSK did not have a method to physically connect two THS1206EVM boards. An intermediate hardware board has to be designed to direct the data from the two boards to

the DSK. To do that, the timing of the DATA_AV signals from the two boards has to be synchronized properly to read the data sampled at the same instant. The DATA_AV signal has to control the data bus to avoid possible bus contentions. Considering all these factors, it was decided to discard the idea of using THS1206EVM and move onto a data converter board with six or more input channels.

At the time of the decision, we could not find a data converter having six or more channels, which could be directly interfaced with the C6711DSK from Texas Instrument or any of their third party hardware manufacturers. However, we realized that Texas Instruments TLV2548EVM with eight analog input channels could be interfaced to the C6711DSK with the use of an off-the-shelf intermediate adaptor board.

5.7 TLV2548EVM Analog to Digital Converter

TLV2548EVM is a 12-bit analog-to-digital converter (ADC) with eight analog input channels, an 8-level FIFO, and four different conversion modes [94].

Specifications of TLV2548EVM:

- Maximum throughput 200-KSPS
- 12-bit resolution
- Built-in reference, conversion clock and 8×FIFO
- DSP-compatible serial interface with SCLK up to 20-MHz
- Hardware controlled and programmable sampling periods
- Programmable auto-channel sweep

The ADC can be interfaced to the C6711DSK using the Multichannel Buffered Serial Port (McBSP) of the DSP. The EVM has three digital inputs and a 3-state output [chip select (CS), serial input-output clock (SCLK), serial data input (SDI), and serial data output (SDO)] that provide a direct 4-wire interface to the serial port. A frame sync (FS) signal is used to indicate the start of a serial data frame. The sample-and-hold function can be

controlled by a special pin, CSTART if required. Functional block diagram of the TLV2548 is shown in Fig.5.7 [5].

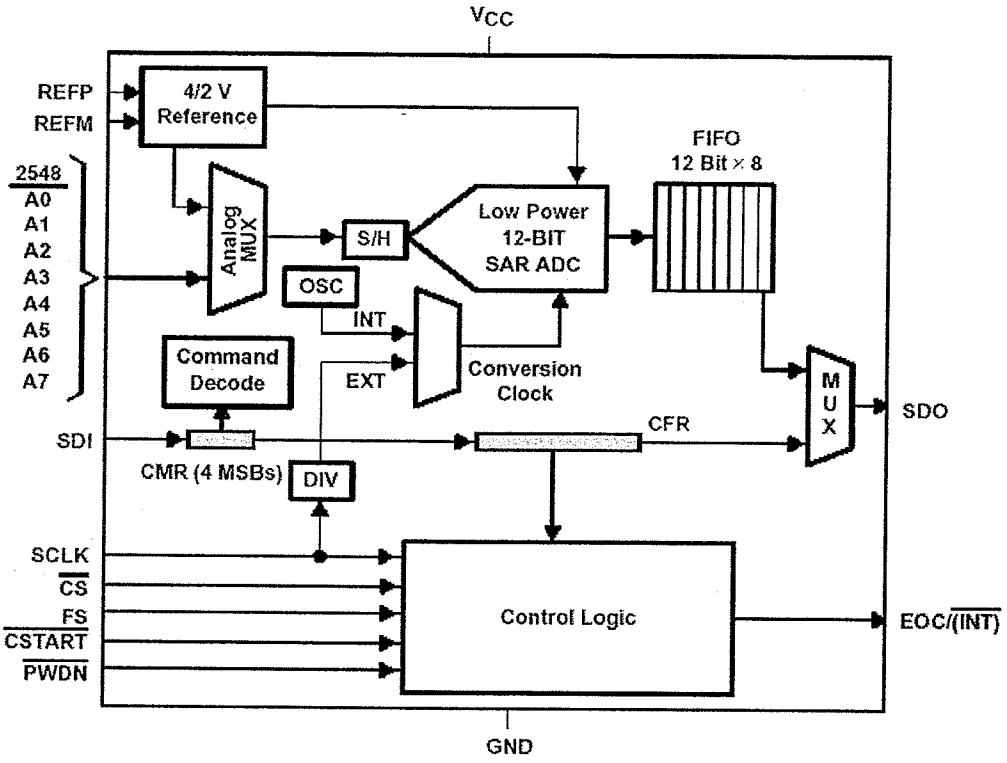

Figure 5.7: TLV2548 functional block diagram

The TLV2548EVM can be directly interfaced with the Texas Instruments TMS320C54x type DSKs [96], but cannot be directly connected to the C6711DSK [97]. In C6711 DSK, two 80-pin headers are used to bring signals to the daughtercards. One of the headers is primarily used for peripheral signals while the other is primarily used for the external memory interface (EMIF). The daughtercard interface on the DSP motherboard has several set requirements concerning signal drive, timing delay, and voltage tolerance [98]. When a daughtercard is connected to a DSP, these requirements have to be satisfied. TLV2548 has a serial interface. Most currently-used data converter EVMs that feature a serial interface use the first serial port (McBSP1) when interfacing to the DSP. The 80-pin EPI header

[5]The figure obtained from [95]

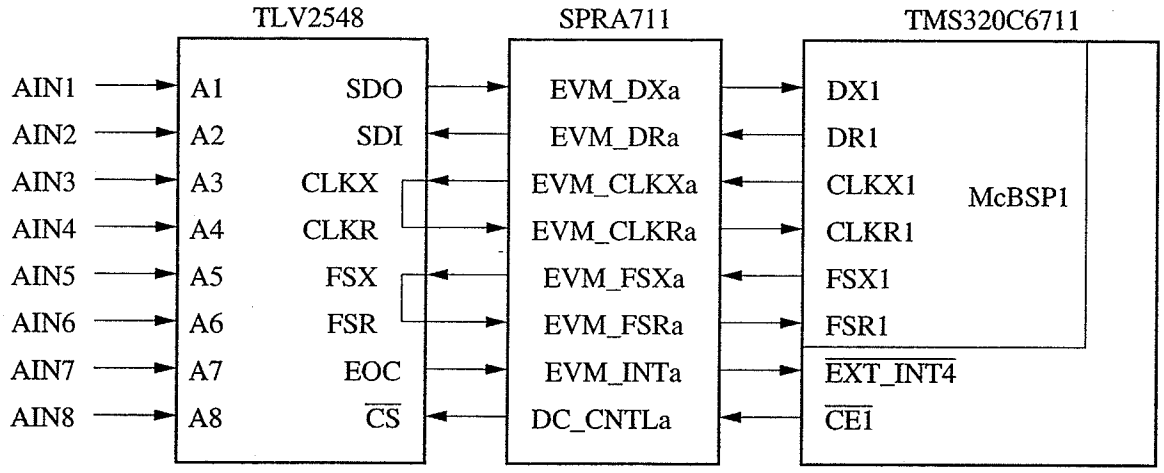

Figure 5.8: Connection between TLV2548EVM and C6711DSK

on the DSK provides access to McBSP1, but TLV2548EVM is not compatible with this interface. Hence an off-the-shelf adaptor board, SPRA711, provided by Texas Instruments was selected and modified to interface the signals between the EVM and the DSK.

The SPRA711 [99] is a cross-platform daughtercard adapter board designed to be used in conjunction with the data converter EVM's from Texas Instruments. This allows daughtercards designed for one motherboard to be used on the others. The interface is developed according to the TMS320 Cross-Platform Daughtercard Specification [98]. The interface provides a serial interface to the daughtercard. The C6711 DSK provides two 7-signal serial ports to the daughtercard. This includes clock (CLKX, CLKR), frame (FSX, FSR), and data signals for both the transmit and receive data streams, as well as a clock input to operate the serial port asynchronously to the DSP. In addition, the adaptor board allows the daughtercard to access the two timer outputs (TOUT), external interrupt signals (EXT_INT), and other general purpose input/output (I/O) signals. Of the two serial interfaces present on the DSK, one is dedicated to the daughtercard and one is selectable between the daughtercard and system hardware. With switches available on the DSK, the McBSP port used to access the daughtercard can be chosen. In this design, McBSP port 1 was used.

Fig.5.8 shows how the TLV2548EVM was connected to the C6711DSK through the SPRA711. The McBSP drives serial-line transmit clock CLKX and transmit frame sync FSX signals, and accepts receive clock CLKR and receive frame sync FSR signals as inputs. Serial lines CLKX and CLKR, as well as FSX and FSR, are connected together on the TLV2548EVM. An interrupt signal is issued by the EVM at the end of each conversion. The TLV2548 interrupt line was tied to INT4 of the DSP [100] in our application. A low sampling rate (1920Hz) was attempted at the beginning and it was increased to a higher value (15.36kHz) later.

The McBSP was used to generate the required clock pulses for the conversion using the sample rate generator (SRG) (see Appendix F). The SRG is composed of a three-stage clock divider that allows programmable data clocks (CLKG) and framing signals (FSG). These McBSP internal signals were programmed to drive receive and transmit clocking (CLKR/X) and framing (FSR/X). The sample rate generator register (SRGR) controls the operation of the various functions of the SRG. The transmit control register (XCR) and receive control register (RCR) were programmed to set the mode of the transmitter and receiver. The McBSP had to be initialized in order to use it as a serial buffer [101]. Fig.5.9 shows the sequence in which the McBSP serial port was initialized and how the TLV2548 was programmed to sample six analog input channels. Different steps and the register contents associated with each step are described in sequence.

In the step 1, EXT_INT4 was enabled and assigned to the ISR associated with reading data from the EVM. In the next step, the McBSP1 was initialized. The transmitter, the receiver, the frame-sync generator, and the sample rate generator were first disabled by asserting the serial port reset state (MCBSP1_SPCR = 0x0). The McBSP configuration registers were programmed while the serial port was in the reset state. The pin control register (McBSP1_PCR), receive control register (McBSP1_RCR), transmit control register (McBSP1_XCR), and sample rate generator register (McBSP1_SRGR) of serial port 1 were programmed as follows:

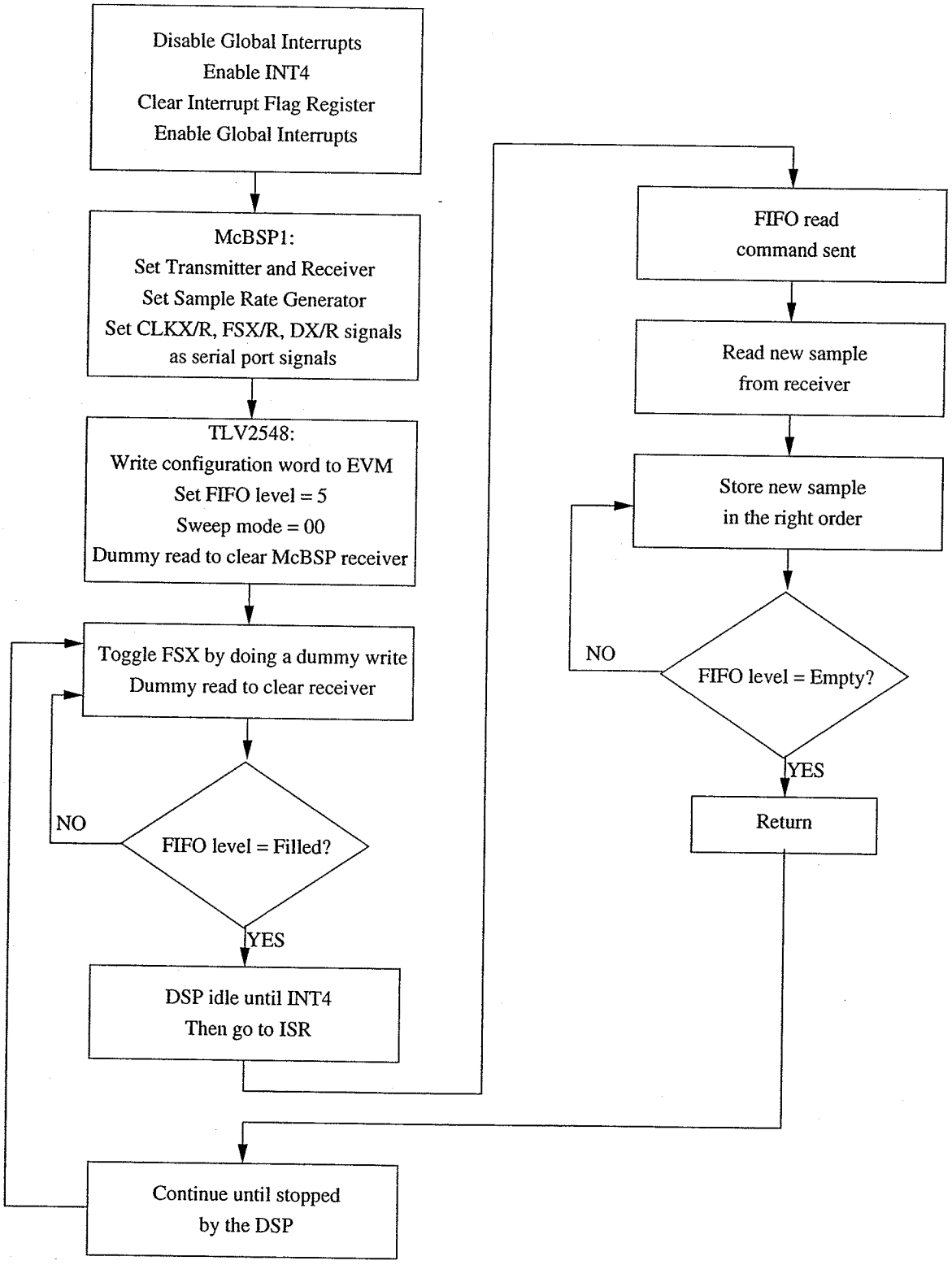

Figure 5.9: Interfacing the TLV2548 to the McBSP

McBSP1_PCR = 0x00000A00:

- DX, FSX, CLKX are serial-port pins
- DX is the data-transmit pin
- FSX is the frame-sync pin, and is driven by the SRG
- FSR is an input pin driven by an external source
- CLKX is an output pin driven by the internal SRG
- CLKR is an input pin driven by an external clock
- FSX and FSR are active high
- The transmit data is sampled on the rising edge of CLKX
- The receive data is sampled on the falling edge of CLKR

McBSP1_RCR = 0x00420040:

- Receive one 16-bit word per frame
- Single phase - only one data word per FSR
- Last four LSBs are zero-padded
- Data transfer to start with the MSB
- 1-bit data receive delay
- Data sent out by ADC immediately after FSR falling edge

McBSP1_XCR = 0x00420040:

- Transmit one 16-bit word per frame
- Single phase - only one data word per FSX

- Last four LSBs are zero-padded
- Data transfer to start with MSB first
- 1-bit data transmit delay
- Data sent to ADC immediately after FSX

McBSP1_SRGR = 0x301C0111:

- SRG clock is derived from the internal clock
- FSX is driven by the SRG clock
- Frame-sync pulse width (FWID) = 1 CLK period
- SCLK = (CPU clock / (1+CLKGDV)). Desired SCLK = 6.25MHz. Since the CPU clock is equal to 75 MHz, CLKGDV = 11 to generate the required SRG clock frequency
- To generate the required frame sync (FSG = 215.5kHz), FPER = 28

After setting the McBSP1 registers, the transmitter, the receiver, the frame-sync generator, and the sample rate generator were enabled (McBSP1_SPCR = 0x0C50023).

The next step was configuring the TLV2548EVM. TLV2548 can be controlled by writing a 16-bit word through SDI. Different commands can be used to select the channels, read data from the EVM configuration register (CFR), write values to CFR or read data from the FIFO. TLV2548 uses the first 4 bits as command bits. Table 5.1 shows the command set associated with the TLV2548.

The EVM is configured at initialization by writing the first bits as 0xA and the following 12 bits contain the configuration data. Table 5.2 shows the configuration register bit definitions.

To read the six channels continuously from the ADC, the CFR was programmed as follows:

Table 5.1: TLV2548 command set

SDI [15-12]	COMMAND
0000	Select analog input channel 0
0001	Select analog input channel 1
0010	Select analog input channel 2
0011	Select analog input channel 3
0101	Select analog input channel 5
0110	Select analog input channel 6
0111	Select analog input channel 7
1000	SW power down (analog + reference)
1001	Read CFR register data shown as SDO $D[11-0]$
1010	Write CFR followed by 12-bit data
1011	Select test, voltage = (REFP+REFM)/2
1100	Select test, voltage = REFM
1101	Select test, voltage = REFP
1110	FIFO read, FIFO contents shown as SDO $D[15-4]$, $D[3-0] = 0000$
1111	Reserved

TLV2548_CFR = 0xA8C1:

- Internal 4V reference voltage
- Short sampling
- Conversion clock source = SCLK
- Sweep mode
- Sweep auto sequence 0-1-2-3-4-5-6-7
- EOC/INT pin used as INT
- FIFO trigger level 3/4 (for six channels)

The EXT_INT4 of the DSP was used to serve the interrupt signal issued by the EVM when the FIFO trigger level was reached.

Table 5.2: TLV2548 configuration register bit definitions

Bit	Definition	Selection
D11	Reference select	0: External 1: Internal
D10	Internal reference voltage select	0: Internal ref = 4 V 1: Internal ref = 2 V
D9	Sample period select	0: Short sampling 12 SCLKs (1x sampling time) 1: Long sampling 24 SCLKs (2x sampling time)
D(87)	Conversion clock source select	00: Conversion clock = internal OSC 01: Conversion clock = SCLK 10: Conversion clock = SCLK/4 11: Conversion clock = SCLK/2
D(6,5)	Conversion mode select	00: Single shot mode 01: Repeat mode 10: Sweep mode 11: Repeat sweep mode
D(4,3)	Sweep auto sequence select	00: 0-1-2-3-4-5-6-7 01: $0-2-4-6-0-2-4-6$ 10: $0-0-2-2-4-4-6-6$ 11: $0-2-0-2-0-2-0-2$
D2	EOC/INT pin function select	0: Pin used as INT 1: Pin used as EOC
D(1,0)	FIFO trigger level (sweep sequence length)	00: Full (INT generated after FIFO level 7 filled) 01: 3/4 (INT generated after FIFO level 5 filled) 10: 1/2 (INT generated after FIFO level 3 filled) 11: 1/4 (INT generated after FIFO level 1 filled)

The TLV2548EVM caused two unexpected problems: First, when the sampling rate was increased from a low sampling rare (1920Hz) to a high sampling rate (15360Hz), the processor was unable to handle the high sampling rate. Secondly, the sampled signals obtained from the waveforms generated by the Real Time Playback (RTP) [66] were distorted. In order to accommodate the high sampling rates, it was decided to read the EVM data using the direct memory access channels (DMA) instead of using the processor. An extra analog buffer circuit had to be introduced to the front end of the EVM to reduce the distortions.

The DMA controller of C6711 can be used for background off-chip data accesses to maximize the achievable bandwidth [78, 100]. The CPU can be used for non-periodic accesses to individual locations. This prevents the real-time system's performance degradation.

Although the CPU and the DMA controller function independently of one another, it is necessary to properly schedule and configure them in order to minimize conflict and waiting while meeting real-time requirements. After referring to several application notes from the Texas Instruments [96, 103, 104] and attempting to program the DMA to read from the TLV2548, we realized that the DMA cannot access six different channels at the same time in the sweep mode. The DMA could access the six channels under single-shot mode by reading one channel at a time and then rotating between the channels. However, this method did not achieve the high sampling rates required due to latency involved in switching between channels. Hence the idea of improving the data transfer speed through the DMA had to be abandoned.

During this period, Texas Instruments introduced the ADS8364, a new ADC EVM with six analog input channels which could be directly interfaced to the C6711DSK. Due to the difficulties associated with interfacing the TLV2548EVM, it was decided to use the ADS8364EVM to acquire the voltage and current signals.

5.8 ADS8364EVM Analog to Digital Converter

The ADS8364 is a high-speed, 6-channel, 250kHz, simultaneous sampling parallel ADC with the 6 channels grouped into three pairs for high-speed simultaneous signal acquisition. ADS8364EVM can be directly connected to the C6711DSK through the 80-pin interface connectors [105].

The ADS8364 contains six 16-bit ADCs that can operate simultaneously in pairs. The three hold signals (HOLDA, HOLDB, and HOLDC) initiate the conversion on the specific channels. A simultaneous hold on all six channels can occur with all three hold signals strobe together. The converted values are saved in six registers. For each read operation, the ADS8364 outputs 16 bits of information. The Address/Mode signals (A0, A1, and A2) select how the data is read from the ADS8364. These Address/Mode signals can define a selection of a single channel, a cycle mode that cycles through all channels, or a FIFO mode

Table 5.3: ADS8364EVM address map

Mode	Address
Select Channel A0	0xA000 0020
Select Channel A1	0xA000 0024
Select Channel B0	0xA000 0028
Select Channel B1	0xA000 002C
Select Channel C0	0xA000 0030
Select Channel C1	0xA000 0034
Select Cycle mode	0xA000 0038
Select FIFO mode	0xA000 003C

that sequences the data determined by the order of the hold signals as shown in Table 5.3 [106].

Specifications of ADS8364EVM:

- 250KSPS throughput
- 6 independent fully differential 16-bit inputs
- 4 μs total throughput per channel
- Direct connection to C6x DSK platforms through the 80-pin interface connectors
- High-speed parallel interface
- Built-in reference

For this design, the address 0xA0000020 was used as the base address. Channel A0 could be accessed from this location, with channels A1 through C1 located at the base address + (0x04)n. The signals ADD, A0, A1, A2, RESET, HOLDA, HOLDB, and HOLDC are accessible through the data bus and control word. The HOLDA, HOLDB, and HOLDC hardware pins on the ADS8364 are controlled by the CLKR1, FSX1, and FSR1 pins (as GPIO) of McBSP1. When the MSB is HIGH, the device is in the configuration mode. MSB LOW will start conversion or reset the part. The EVM uses four address lines to access the data converter. The lower address lines control the A0, A1, and A2 pins of the ADC,

while the upper most address line is sent through a single gate inverter to act as chip select (CS). Fig.5.10 shows a block diagram representing how the ADS8364 was connected in the implemented system using software control mode with the C6711DSK.

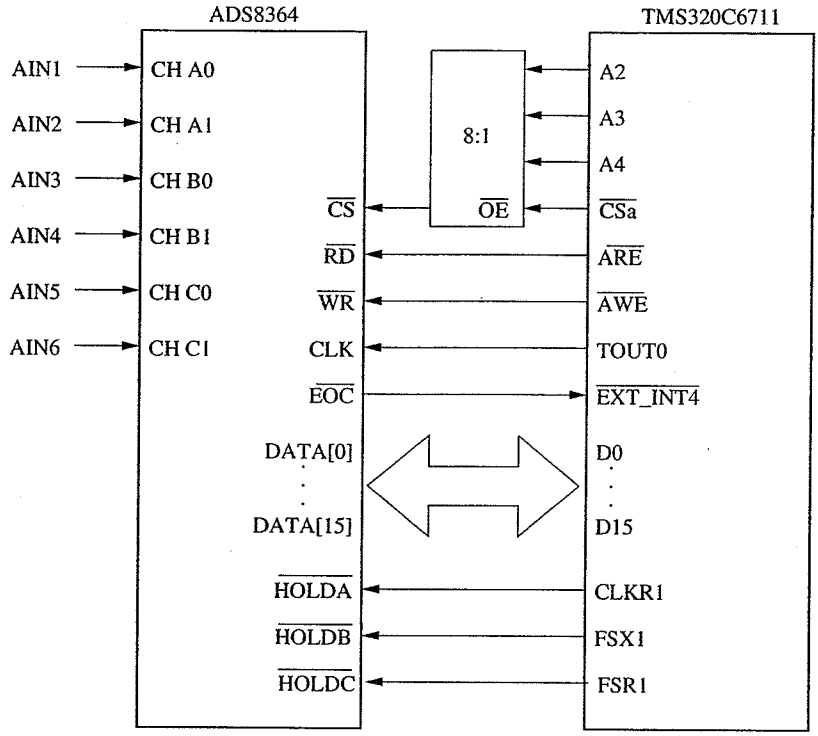

Figure 5.10: Connecting the ADS8364EVM to the DSK

The ADS8364 can operate from a maximum clock frequency of 5 MHz. The sample/conversion process is completed within 20 conversion clock cycles. All six channels of the ADS8364 can be sampled/converted simultaneously, providing a maximum 250 KSPS throughput rate. In our implementation, the ADS8364 was operated from a 307.2kHz clock, providing 256 samples per 60Hz cycle per channel. The McBSP1 of the TMS320C6711 was used as a general-purpose I/O port to interface the ADS8364. The McBSP was used to control the HOLDx pins, the ADD pin and the RESET pin. The first data (FD) signal was used as an input to the McBSP to indicate when data from channel A1 was present. The DSKs read enable (RE), write enable (WE), and daughtercard chip select (DC_CSa) were all used in the parallel interface.

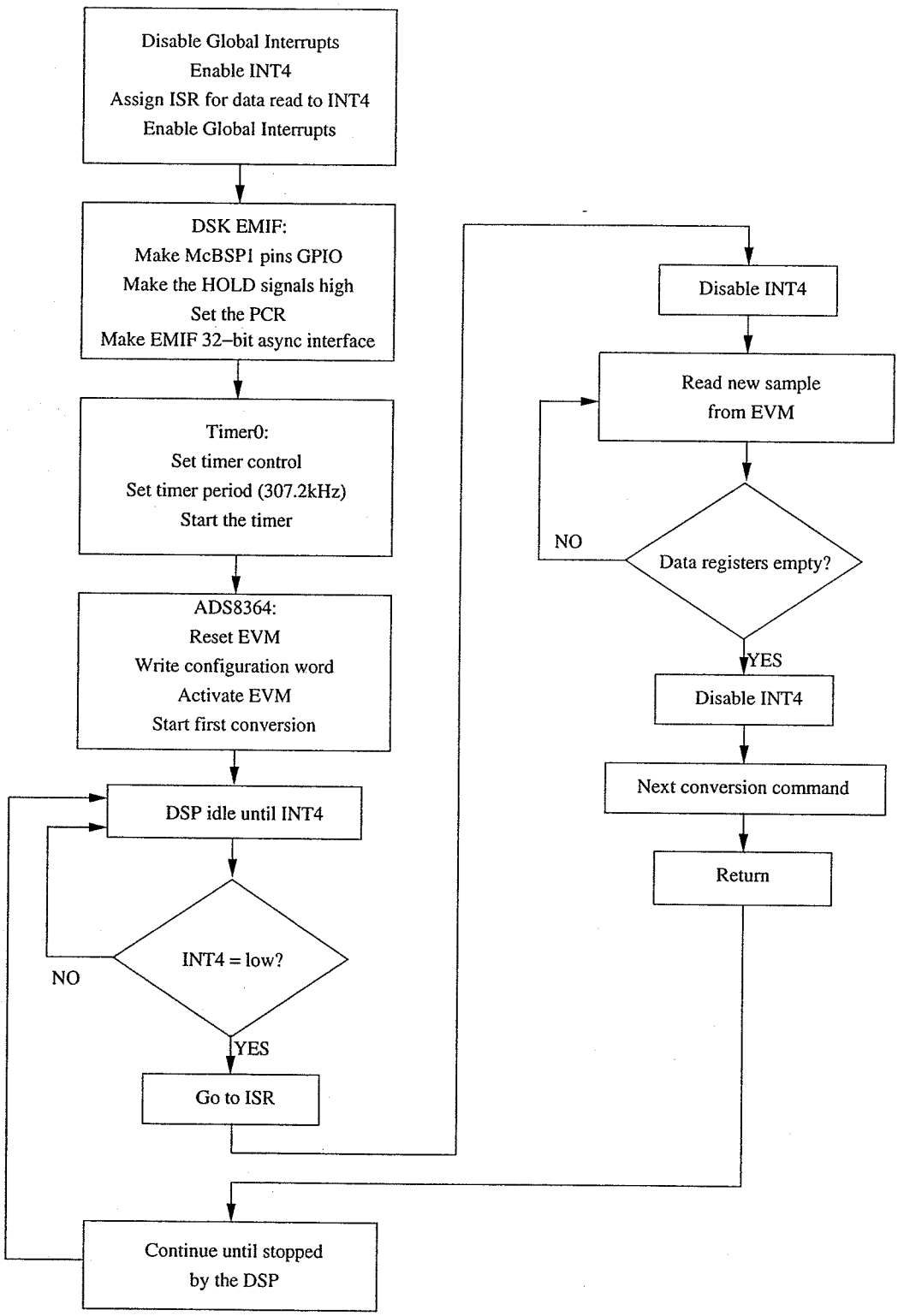

Figure 5.11: Interfacing the ADS8364 to the C6711 DSK

The different steps involved in interfacing the ADS8364EVM to the DSK are shown in Fig.5.11. In the first step, the external interrupt 4 of the processor was assigned to the ISR that handles reading data from the EVM. The EOC signal is active low once for each channel pair converted and in our implementation the EOC signal was routed to EXT_INT4 on the C6711 DSK. In the next step, the McBSP1 port on the DSK was configured as a general-purpose I/O port. To set up McBSP1 as a GPIO port SRGR and SPCR were cleared (McBSP1_SRGR = 0x0; McBSP1_SPCR = 0x0) and then, PCR was set for the desired functions:

McBSP1_PCR = 0x3F0F:

- FSX is a general purpose I/O
- FSR is a general purpose I/O
- CLKX is a general purpose I/O
- CLKR is a general purpose I/O
- DX is a general purpose output
- DR is a general purpose input
- HOLDx lines are set
- ADD line is cleared

In the next step, the conversion clock was set. The DSKs internal timer, TOUT0, was used as the conversion clock source for the ADS8364EVM. The clock was set for 50/50 duty cycle and a division multiple of 244. This provided approximately a 307.2kHz conversion clock to the converter.

The last step of the initialization was configuring the EVM. The data inputs and commands associated with the EVM are given in Table 5.4. The commands are set by writing to the base address of the ADC (ADC_BASE). First the ADS8364 was reset to ensure that

Table 5.4: ADS8364 data input/command

Command	D7	D6	D5	D4	D3	D2	D1	D0
Convert	0	×	×	×	RESET	HOLDA	HOLDB	HOLDC
Configuration	1	×	×	BIN/2s	ADD	A2	A1	A0

the read pointer was pointing to the first data register (ADC_BASE = 0x0007). The EVM was then configured for continuous data sampling in CYCLE mode and binary data output format (ADC_BASE = 0x90). The EVM was then activated and first conversion command was issued to sample all six channels (ADC_BASE = 0x04).

The HOLDx hardware pins are active low sampling triggers. When the three HOLD lines are brought low together, all six analog inputs are simultaneously sampled and the conversion process begins with the next rising clock edge. The conversion results are automatically stored in the data registers starting with channel A0. The conversion is completed after 20 clock cycles, at which time the end of conversion (EOC) pin goes low for 1/2 clock cycle on all three channels. When EOC is detected, the ISR is activated and the sampled data values are read from the EVM. When all six channels have been read, the EVM is issued the next conversion (HOLDx) command. To get the maximum throughput from the ADS8364, the HOLDx command was set to be issued prior to reading the contents of the data registers. This allows the ADC to start a new conversion sequence while the host processor reads the results of the current conversion. ISR makes sure that the read process is completed before the new conversion cycle is finished.

The ADS8364EVM solved the problems associated with capturing voltage and current signals to the C6711 DSK. Several difficulties associated with the three EOC commands had to be solved before the required sampling rate of 15.36kHz could be achieved.

5.9 Hybrid Algorithm Implementation

The C6711 DSK provided a feasible, but inexpensive platform to implement the hybrid relaying algorithm in real-time. The ADS8364EVM was capable of sampling voltage and current signals at the high sampling rates required. As explained before, a modular component based approach was utilized in programming the relaying algorithms using RIDE. In this approach, each step of the relaying algorithm (including signal acquisition and conversion) which could be defined as an individual task was implemented as a block component. Each block component had two parts: a DLL file which runs on the host and takes care of the data transfer from host to the DSP and an object code which runs on the DSP.

The DLL files were compiled using MS Visual C++ [89] and the object files were compiled using Texas Instruments CCS [80]. These blocks were then connected according to the execution order and dataflow requirements of the relaying algorithm. The PC and DSP code run in parallel with the PC side assigned to handle the user interface and the DSP side assigned to perform the relaying functions. The real-time blocks run at full speed on the DSP without requiring any intervention from the PC side during execution. The data can be uploaded to the PC user interface when required.

In the hybrid relay, the relaying functions are performed only when a new set of voltage and current samples is provided by the data acquisition system. The presence of new data is indicated to the DSP by the interrupt EXT_INT4. When the processing of the present set of samples is finished, the processor idles until the next set arrives. The impedance of the line is calculated at a rate lower than that used for the travelling wave relay. The travelling wave relay derives the relaying information 256 times in a 60Hz cycle while the impedance is calculated only 8 times within the same period. This approach saves valuable processor time.

The different execution speeds of individual block components were achieved through synchronization of real-time blocks. Synchronization was implemented using a pair of in-

dependent sync flags on each real-time block for input and output synchronization. An output sync flag was used by each block to indicate when its output data was valid for other blocks to use. A real-time blocks input sync flag was matched with another real-time blocks output sync flag to control its execution. Subsequent blocks that use an input sync will only execute during that specific execution cycle if the previous block or blocks have set their output sync flags. When the project is compiled, the linker builds a main execution loop that sequences through a worksheets blocks in the order that data flows and makes sure that the data is processed according to the sync flags.

The user interface allows the user to change the relay settings and monitor the relay performance. The user interface shows the voltage and current waveforms, impedance loci, the trip signals of the hybrid relay and the calculated distance to the fault. Settings of the travelling wave relay and impedance relay can be adjusted through user-input dialog boxes. The DSP uploads data to the PC only when the processor is not used for calculations. Hence the graphical user interface does not show all values of data, but gives a clear indication about the performance of the relay. A section of the user interface developed using RIDE is shown in Fig.5.12.

5.10 Test Results

A setup similar to the one described in section 5.2.2 was used to test the hybrid relay. Voltage and current waveforms related to different fault conditions were generated and recorded using PSCAD/EMTDC. A 50μs time step was used to record the signals. The waveforms were generated using the same 500kV network used for simulations in section 4.2. The recorded waveforms were then played back using the Real Time Playback (RTP). The RTP produced analog waveforms between $\pm$5V proportional to the voltages and currents. The ADS8364EVM sampled the waveforms at 15.36kHz. The ADC block in RIDE also converted the samples back to the original values using the PT and CT ratios specified by the RTP.

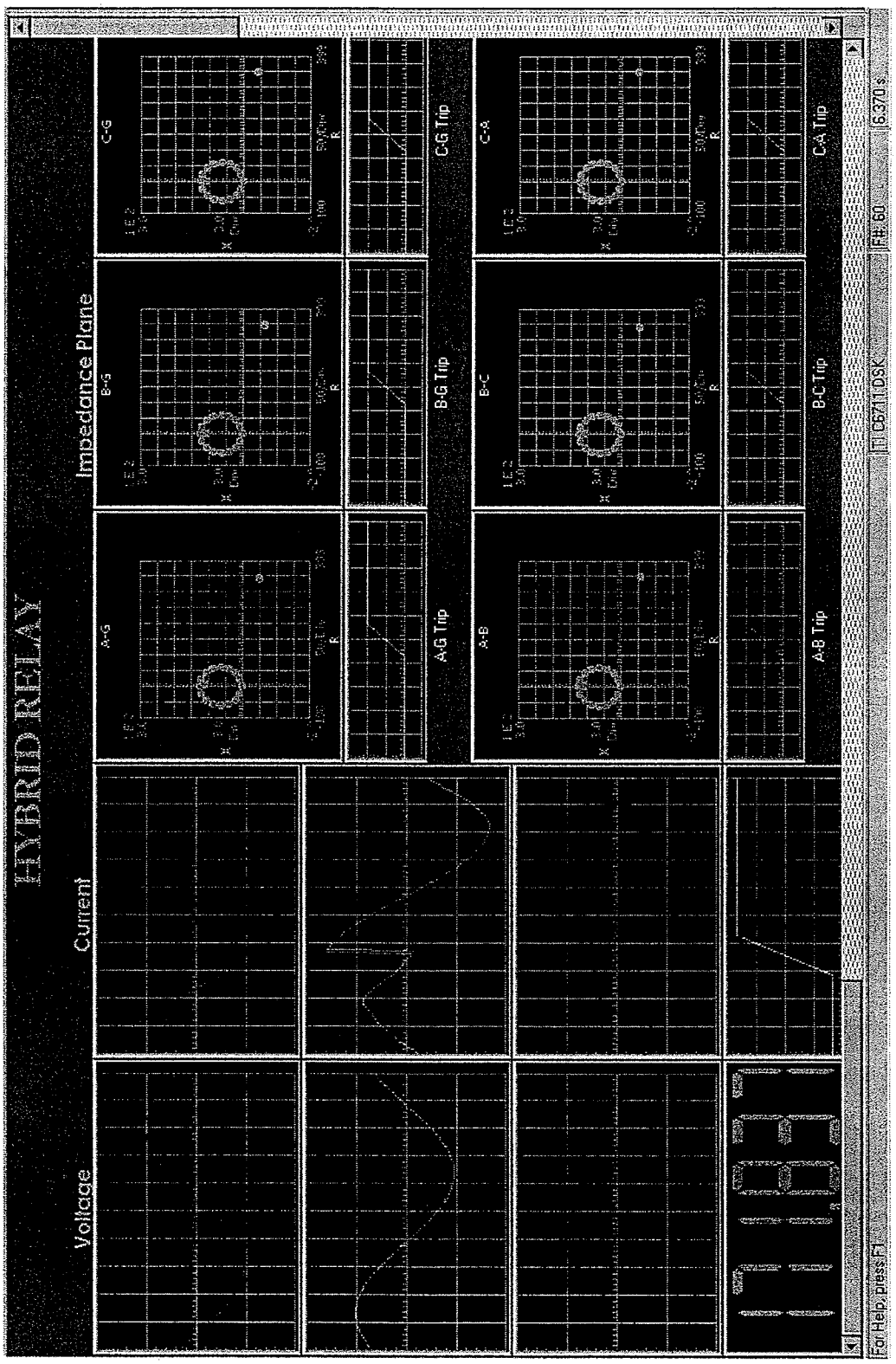

Figure 5.12: Part of the graphical user interface arrangement

The hybrid relay algorithms processed the samples and issued a trip signal if a fault condition within the protection zone was identified. The C6711 DSK does not have a digital output channel. Hence the trip signal was "tapped" from one of the user outputs of the C6711 DSK. This signal was fed back to the RTP to record the trip signal and measure the fault detection time. The user output signal of the DSK is a TTL output (5V). However the RTP required an input voltage of 20V or more to identify a digital input as "high". The TTL output of the DSK was "amplified" using a peripheral drive array integrated circuit Motorola MC1413 before connecting it back to the RTP. The relay prototype and the test setup are shown in Fig.5.13.

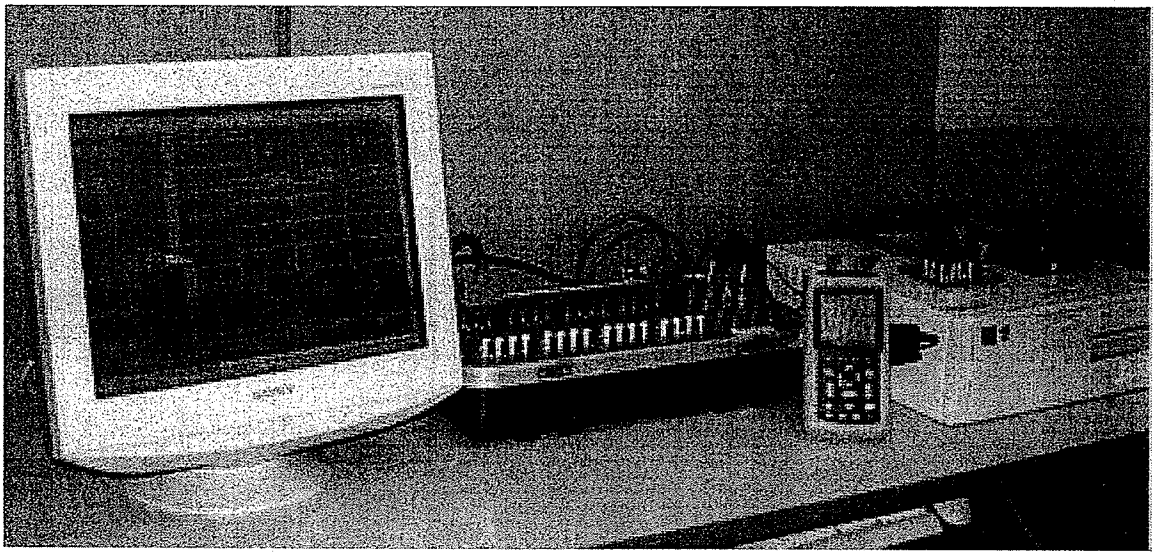

Figure 5.13: The setup used for testing the hybrid relay

Waveforms were generated for single-line-to-ground, line-line, and line-line-ground faults using PSCAD/EMTDC. These waveforms were played back using the RTP and were used for testing the relay. The RTP displays the trip signal along with the waveforms played back and hence can be used to measure the trip time of the relay. The current and voltage waveforms and the relay trip signals captured by the RTP for a three phase to ground fault are shown in Fig.5.14. These waveforms correspond to a fault that occurred 325km away from the relay location R. Out of the two trip signals shown, the bottom one corresponds

to the travelling wave relay trip signal while the top one belongs to the impedance relay. The hybrid trip signal is not shown here, but is used for the tripping of the breakers.

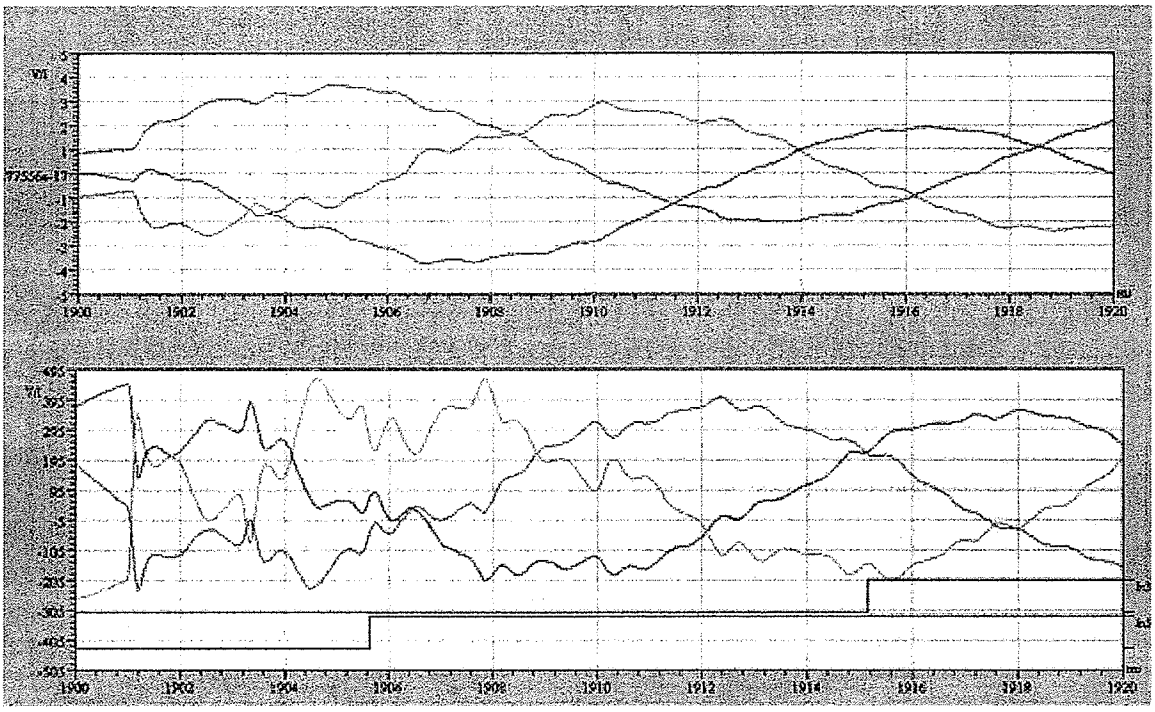

Figure 5.14: The waveforms and trip signals obtained from RTP for a three phase fault

Table 5.5 summarizes the results of the tests carried out on the real-time laboratory prototype. The results confirm that the hybrid algorithm is reliable and detects faults quickly.

Table 5.5: Test Results

Fault	x_f	ϕ^o	t_{tw}	t_z	t_h	x_{tw}
A-G	195	86	5.14	14.84	5.14	201.8
B-G	195	285	5.15	14.4	5.15	201.8
C-G	95	168	-	10.07	10.07	-
A-G	270	36	4.61	13.26	4.61	288.1
B-G	95	252	4.79	11.74	4.79	96.1
C-G	245	45	5.33	13.13	5.33	249.8
AB-G	445	-	5.88	17.05†	5.88	451.4
AC-G	325	-	5.42	15.75	5.42	332.4
ABC-G	325	-	5.47	15.15	5.47	334.2

x_f = The distance to the fault in km

ϕ = The fault inception angle

t_{tw} = The fault detection time of the travelling wave relay

t_z = The fault detection time of the impedance relay

t_h = The time at which the hybrid relay issues the trip signal

x_{tw} = The distance calculated by the travelling wave relay in km

†The impedance relay over-reached.

Chapter 6

Conclusions and Recommendations

Conclusions

The thesis examined how the measured impedance at the relay location and the fault generated high frequency transient wavefronts can be combined in a single relay to find solutions for the negative features associated with each method and improve both speed and reliability of the protection scheme. Distance protection algorithms based on transient signals provide a number of significant advantages but not without some limitations. The travelling waves initiated by a fault depend not only on the fault position but also on the fault type, the fault inception angle, fault impedance and the power system configuration. These factors consequently have an influence on the reliability of the decision made by a travelling wave protection scheme. The first wavefront initiated by a fault that appears at the relay location contains information about the fault direction, fault type and fault inception angle. This initial information can be used to determine whether the travelling wave algorithm will be able to identify a disturbance and classify it as an internal or external fault. Internal and external fault classification is achieved by measuring the distance to the fault. The distance is measured by observing the return of the initial forward wave to the relaying station after being reflected at the fault location. Two main problem areas have been identified with travelling wave protection: close-up faults and single phase faults that

occur near a voltage zero.

Distance protection schemes based on impedance measurement have shown their reliability over several decades. But the fault detection speed of impedance relays cannot be further improved without compromising the reliability of the reach setting. However, impedance relays are capable of detecting faults with small inception angles and the measured impedance quickly moves inside the protection zone for close-up faults. The hybrid protection scheme proposed in this thesis takes advantage of these features so that the impedance relay will detect the fault in case the travelling wave relay fails. The simulations carried out on a simple 500kV three phase power system have shown that the hybrid relay not only improves the speed of fault detection, but also maintains the reliability of the overall scheme.

The thesis also looked at how the zone 2 protection of a distance relay can be accelerated without the aid of a teleprotection scheme. The proposed algorithm improves the reliability of the travelling wave protection algorithm by combining the output of the zone 2 element with the travelling wave distance calculation. Since the zone 2 element of the impedance relay "monitors" the trip decision of the travelling wave relay, possible mal-operation of the travelling wave relay due to switching transients is avoided. Since both algorithms check for the presence of a fault, the inherent redundancy improves the reliability of the relay. However for faults on the line which occur beyond the maximum allowable measurement distance of the travelling wave scheme, a suitable inter-trip scheme will have to be utilized to clear such faults in a timely fashion.

A laboratory prototype of the hybrid relay was implemented on Texas Instruments TMS320C6711 DSK. The voltage and current waveforms were obtained using ADS8364 EVM. The ADC is capable of providing samples at a high sampling rate while the DSK performs the relaying functions of the two algorithms in real-time. The cost of the prototype was kept as low as possible considering the needs of commercial production. The tests carried out in the laboratory using generated waveforms showed the capability of the hybrid

relay prototype in detecting faults quickly with a high reliability.

Suggestions for Further Research

Further work is recommended as an extension of this thesis in the following areas:

1. The current and voltage at the relay point are measured with current transformers and voltage transformers. In EHV lines, the voltage is usually measured using capacitive voltage transformers (CVT). All these transducers have a limited bandwidth, especially the CVT which has a bandwidth of around 1000Hz. Hence the measured signals of the voltage waveform may not include the information of the high frequency transients. This can reduce the relay algorithm's ability to detect faults using travelling waves. However, the current transformers have a fairly high bandwidth of several hundred kilohertz [8]. The measured waveforms of the current will contain most of the high frequency transient components of the wavefront. The possibility of modifying the travelling wave algorithm to detect faults only using current signals has to be studied.

2. In the second algorithm of the hybrid relay, the zone 2 operation is used to monitor the travelling wave relay. The travelling wave relay waits until the measured impedance enters zone 2 before issuing a trip signal. The speed of the hybrid relay can be further improved by reducing this "wait time". Any movement of the measured impedance towards the protection zone can be used as an indication for the presence of a fault. Since the travelling wave relay already determines the location of the fault, the initial movement of the impedance towards the protection zone may be used to trigger the travelling wave trip signal. Since the travelling wave scheme is immune to power swings or load variations, the reliability of the hybrid relay will still be high.

3. The proposed hybrid scheme was only simulated and tested on a simple three phase power network. Further tests have to be carried out to study the behaviour of the

scheme in a complex power system.

4. The hybrid relay was not tested on a system with series compensation. It is evident that series compensation will not cause a significant effect on travelling wave relays because the relay makes its decision before the operation of the series capacitor protection circuit. The high frequency transient signals see the series capacitor as a short circuit and hence will not be much affected. However, the re-insertion of capacitor compensation after an external fault may develop transient signals and requires further study.

5. This thesis did not consider the fault impedance values higher than 25Ω. A high fault resistance affects the reflected wave quantity and increases the transmitted component. A detailed study has to be done how the results of the two algorithms can be effectively combined to detect high impedance faults.

6. The fault which occurs at a fault inception angle near zero requires further investigation. A proper differentiation method of the relaying signals for such cases must be developed to make correct identification of such faults.

7. The hardware implementation requires further improvements in order to simplify the relay functions, improve the speed and lower the cost. Also, the use of high bandwidth field data instead of the off-line simulation data would be very helpful to permit the study of the effect of noise.

Appendix A

Transmission Line Theory

When the length of a transmission line increases, both potential and current at any instant may vary appreciably with the distance along the line. When the lines are too long, the lumped parameter models of transmission lines no longer would give valid results. In such circumstances, distributed parameter model is used. This section will describe the behaviour of voltage and current signals in long transmission lines.

Lossless Line

The propagation characteristics of signals on transmission lines can be determined by a transient solution of the basic equations. First, an ideal lossless line which has no series resistance and shunt admittance will be examined.

Characteristic Equations

Suppose that at some instant, voltage v and current i are distributed along a lossless transmission line of inductance L per unit length and capacitance C per unit length as shown in Fig. A.1. The distributions will be both functions of distance x and time t. The

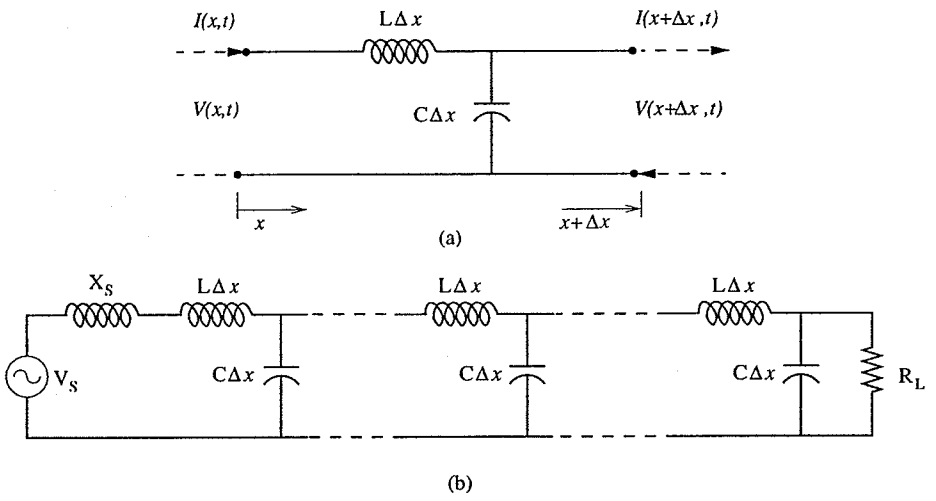

Figure A.1: The distributed parameter model of a transmission line (a) a section of unit length(b) the transmission line

voltage and current distributions are given by,

$$v = V(x,t) \text{ and } i = I(x,t) \tag{A.1}$$

Now, consider two points on the line at distances x and $x+\Delta x$. Then the total capacitance current over the section Δx is

$$I(x,t) - I(x+\Delta x,t) = \int_x^{x+\Delta x} C.\frac{\partial v}{\partial t}.dx$$

Now if Δx is made to tend to zero,

$$\lim_{\Delta x \to 0} \int_x^{x+\Delta x} C.\frac{\partial v}{\partial t}.dx = \Delta x.C.\frac{\partial v}{\partial t}$$

Hence

$$\begin{aligned} \lim_{\Delta x \to 0} \frac{I(x,t) - I(x+\Delta x,t)}{\Delta x} &= C.\frac{\partial v}{\partial t} \\ \frac{\partial i}{\partial x} &= -C.\frac{\partial v}{\partial t} \end{aligned} \tag{A.2}$$

Similarly, the potential difference between the two points at distances x and $x + \Delta x$ is given by the inductive drop over the section Δx, i.e.

$$V(x,t) - V(x+\Delta x,t) = \int_x^{x+\Delta x} L.\frac{\partial i}{\partial t}.dx \tag{A.3}$$

Using the same argument as above, it is possible to show that

$$\frac{\partial v}{\partial x} = -L.\frac{\partial i}{\partial t} \tag{A.4}$$

Differentiating (A.2) with respect to time,

$$\frac{\partial^2 i}{\partial t \partial x} = -C.\frac{\partial^2 v}{\partial t^2} \tag{A.5}$$

and differentiating (A.4) with respect to distance

$$\frac{\partial^2 v}{\partial x^2} = -L.\frac{\partial^2 i}{\partial x \partial t} \tag{A.6}$$

From (A.5) and (A.6),

$$\frac{\partial^2 v}{\partial x^2} = LC.\frac{\partial^2 v}{\partial^2 t} \tag{A.7}$$

and a similar elimination yields

$$\frac{\partial^2 i}{\partial x^2} = LC.\frac{\partial^2 i}{\partial^2 t} \tag{A.8}$$

Solution of the equation

The solution can be found in the same way for both wave equations (A.7) and (A.8). A solution method was introduced by ďAlembert for this type of equations. The wave equation (A.7) is of the form

$$\frac{\partial^2 v}{\partial t^2} = a^2.\frac{\partial^2 v}{\partial x^2} \tag{A.9}$$

where $a = 1/\sqrt{LC}$. (A.9) is first transformed by introducing the new independent variables

$$r = x + at \quad \text{and} \quad s = x - at \tag{A.10}$$

Then voltage v and current i become functions of r and s. Hence using the chain rule, left hand side of (A.4) can be expanded to give

$$\frac{\partial v}{\partial x} = \frac{\partial v}{\partial r}.\frac{\partial r}{\partial x} + \frac{\partial v}{\partial s}.\frac{\partial s}{\partial x} = \frac{\partial v}{\partial r} + \frac{\partial v}{\partial s} \tag{A.11}$$

Squaring (A.11),

$$\frac{\partial^2 v}{\partial x^2} = \frac{\partial^2 v}{\partial r^2} + 2\frac{\partial^2 v}{\partial r \partial s} + \frac{\partial^2 v}{\partial s^2} \tag{A.12}$$

Similarly,

$$\frac{\partial v}{\partial t} = \frac{\partial v}{\partial r}.\frac{\partial r}{\partial t} + \frac{\partial v}{\partial s}.\frac{\partial s}{\partial t} = a\left(\frac{\partial v}{\partial r} - \frac{\partial v}{\partial s}\right) \tag{A.13}$$

Squaring (A.13)

$$\frac{\partial^2 v}{\partial t^2} = a^2\left(\frac{\partial^2 v}{\partial r^2} - 2\frac{\partial^2 v}{\partial r \partial s} + \frac{\partial^2 v}{\partial s^2}\right) \tag{A.14}$$

Substituting (A.12) and (A.14) in (A.9),

$$\frac{\partial^2 v}{\partial r \partial s} = 0 \tag{A.15}$$

Now, (A.15) can be solved with two successive integrations. Integrating with respect to r

$$\frac{\partial v}{\partial s} = w(s) \tag{A.16}$$

where $w(s)$ is an arbitrary function of s, independent of r. Integrating with respect to s

$$\begin{aligned} v &= \int^s w(s)ds + f_2(r) \\ &= f_1(s) + f_2(r) \end{aligned} \tag{A.17}$$

where $f_2(r)$ is an arbitrary function of r. Substituting r and s in (A.17)

$$v(x,t) = A(x-at) + B(x+at) \tag{A.18}$$

where A and B are arbitrary functions. Equation (A.18) is known as the ďAlembert solution of the wave equation. Here $A(x-at)$ represents a wave travelling in the positive x direction, and $B(x+at)$ represents a wave travelling in the negative x direction. These waves are known as *travelling waves* that move with speed a. The voltage and current signals are represented by

$$v(x,t) = f_1(x-at) - f_2(x+at) \tag{A.19}$$

$$i(x,t) = \frac{1}{Z_c} f_1(x-at) + \frac{1}{Z_c} f_2(x+at) \tag{A.20}$$

where f_1 and f_2 replace the arbitrary functions A and B in (A.18). $Z_c = \sqrt{\frac{L}{C}}$ is the surge impedance of the line.

Lossy Line

The distributed parameter model of a transmission line with losses is represented by an inductor of inductance L per unit length in series with a resistor of resistance R per unit length and a shunt capacitor of capacitance C per unit length with a parallel resistor with conductance G per unit length. The distribution of voltage v and current i will be both functions of distance x and time t as in the lossless case. The distributed parameter model of a lossy line for an incremental distance Δx is shown in Fig. A.2.

Now the voltage drop between two points on the line Δx apart is given by

$$V(x,t) - V(x+\Delta x,t) = \int_x^{x+\Delta x} \left(Ri + L.\frac{\partial i}{\partial t} \right) dx \tag{A.21}$$

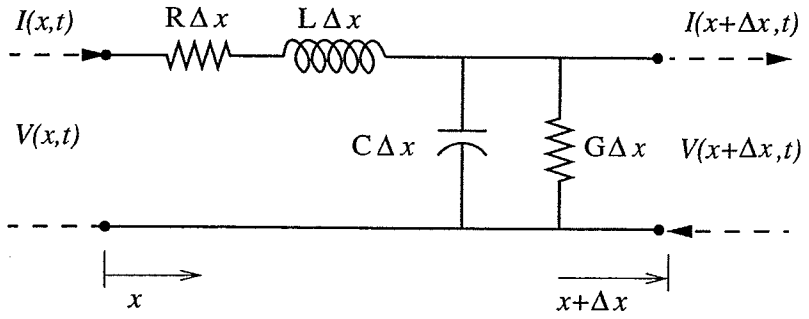

Figure A.2: The distributed parameter model for a lossy line

By simplifying as in the lossless case

$$\frac{\partial v}{\partial x} = -\left(Ri + L.\frac{\partial i}{\partial t}\right) \tag{A.22}$$

The current is shunted through both the capacitor and the conductance. Then the total leakage current over the section Δx is given by

$$I(x,t) - I(x+\Delta x,t) = \int_x^{x+\Delta x} \left(Gv + C.\frac{\partial v}{\partial t}\right) dx \tag{A.23}$$

and this yields

$$\frac{\partial i}{\partial x} = -\left(Gv + C.\frac{\partial v}{\partial t}\right) \tag{A.24}$$

Solving (A.22) and (A.24) in the time domain is very much involved. It will be easier to consider the steady state frequency domain solution for the fundamental frequency of the excitation voltage. Considering a source of

$$X(t) = X\cos(\omega t) = Re[Xe^{j\omega t}] \tag{A.25}$$

the voltage and current distributions are given by

$$V(x,t) = Re[\hat{V}(x)e^{j\omega t}] \tag{A.26}$$

$$I(x,t) = Re[\hat{I}(x)e^{j\omega t}] \tag{A.27}$$

Considering only the real part of the voltage and current

$$\frac{\partial v}{\partial x} = -\left(R + j\omega L\right).i \tag{A.28}$$

and

$$\frac{\partial i}{\partial x} = -\left(G + jwC\right).v \tag{A.29}$$

Differentiating (A.28) and substituting from (A.29) lead to

$$\frac{\partial^2 v}{\partial x^2} = \left(R + j\omega L\right)\left(G + jwC\right).v \tag{A.30}$$

and

$$\frac{\partial^2 i}{\partial x^2} = \left(R + j\omega L\right)\left(G + jwC\right).i \tag{A.31}$$

The coefficient $\sqrt{\left(R + j\omega L\right)\left(G + jwC\right)}$ is known as propagation constant, γ. Then

$$\frac{\partial^2 v}{\partial x^2} = \gamma^2 v \tag{A.32}$$

$$\frac{\partial^2 i}{\partial x^2} = \gamma^2 i \tag{A.33}$$

The solution for (A.32) and (A.33) is given by

$$v_x = V^+ e^{-\gamma x} + V^- e^{\gamma x} \tag{A.34}$$

and

$$i_x = \frac{V^+}{Z_c} e^{-\gamma x} - \frac{V^-}{Z_c} e^{\gamma x} \tag{A.35}$$

where

$$Z_c = \sqrt{\frac{\left(R + j\omega L\right)}{\left(G + jwC\right)}} \tag{A.36}$$

Appendix B

Three Phase Transmission Lines

Derivation of 3-Phase Transmission Line Equations

Equivalent Circuit

A 3-phase transmission line composed of three conductors parallel to the ground is shown in Fig. B.1. The sending end is considered as the generating point while the receiving end normally consists of a load. The voltage and current signals will be functions of position x along the line usually measured from the sending end and time t measured from some reference time.

The equivalent circuit approximation of a differential length of the transmission line

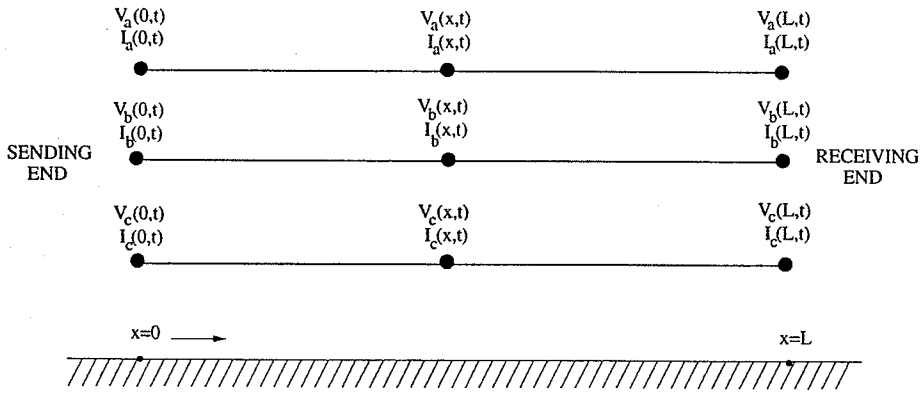

Figure B.1: Representation of a three phase transmission line with an earth return

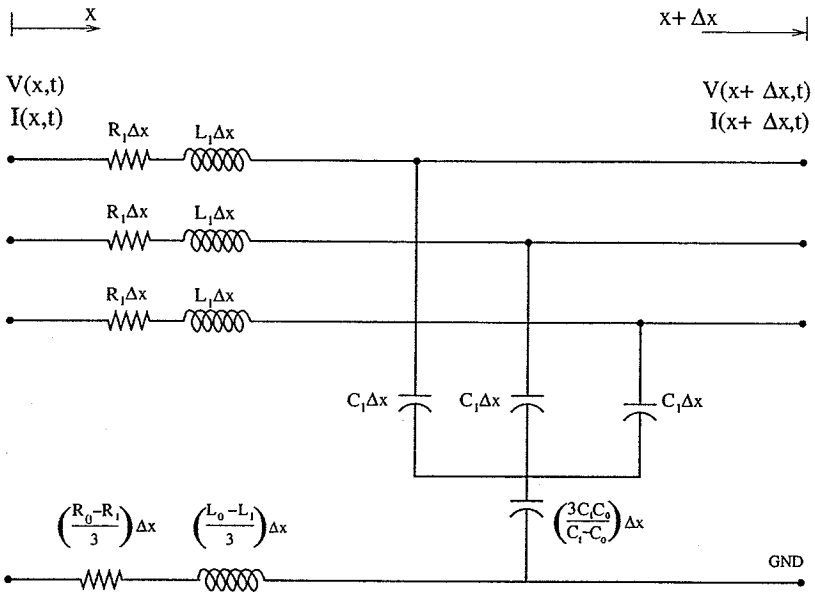

Figure B.2: Equivalent circuit of unit length of a 3-phase transmission line

is shown in Fig. B.2. A uniformly distributed parameter line model is considered which includes the frequency dependent variations in the line parameters and the effect of the earth return. The conductors are described by their positive-sequence parameters, while the effects of ground return are taken care of with zero-sequence parameters.

Voltage-Current Relationship

Applying Kirchhoff's voltage law to the loop formed by each conductor and ground,

$$-\frac{\partial}{\partial x}\begin{bmatrix} V_a(x,t) \\ V_b(x,t) \\ V_c(x,t) \end{bmatrix} = \frac{1}{3}\begin{bmatrix} Z_s & Z_m & Z_m \\ Z_m & Z_s & Z_m \\ Z_m & Z_m & Z_s \end{bmatrix}\begin{bmatrix} I_a(x,t) \\ I_b(x,t) \\ I_c(x,t) \end{bmatrix} \tag{B.1}$$

where

$$Z_s = (R_0 + L_0\frac{\partial}{\partial t}) + 2(R_1 + L_1\frac{\partial}{\partial t}) \tag{B.2}$$

$$Z_m = (R_0 + L_0\frac{\partial}{\partial t}) - (R_1 + L_1\frac{\partial}{\partial t}) \tag{B.3}$$

Also, using Kirchhoff's current law at the junction of each conductor with the capacitive branch to the ground,

$$-\frac{\partial}{\partial t}\begin{bmatrix} V_a(x,t) \\ V_b(x,t) \\ V_c(x,t) \end{bmatrix} = \frac{1}{3}\begin{bmatrix} Y_s & Y_m & Y_m \\ Y_m & Y_s & Y_m \\ Y_m & Y_m & Y_s \end{bmatrix} \frac{\partial}{\partial x}\begin{bmatrix} I_a(x,t) \\ I_b(x,t) \\ I_c(x,t) \end{bmatrix} \tag{B.4}$$

where

$$Y_s = (\frac{1}{C_0} + \frac{2}{C_1}) \tag{B.5}$$

$$Y_m = (\frac{1}{C_0} - \frac{1}{C_1}) \tag{B.6}$$

Taking the *Laplace Transform* of (B.1) and (B.4) results in

$$-\frac{d}{dx}\begin{bmatrix} V_a(x,s) \\ V_b(x,s) \\ V_c(x,s) \end{bmatrix} = \frac{1}{3}\begin{bmatrix} (Z_0+2Z_1) & (Z_0-Z_1) & (Z_0-Z_1) \\ (Z_0-Z_1) & (Z_0+2Z_1) & (Z_0-Z_1) \\ (Z_0-Z_1) & (Z_0-Z_1) & (Z_0+2Z_1) \end{bmatrix} \begin{bmatrix} I_a(x,s) \\ I_b(x,s) \\ I_c(x,s) \end{bmatrix} \tag{B.7}$$

and

$$\begin{bmatrix} V_a(x,s) \\ V_b(x,s) \\ V_c(x,s) \end{bmatrix} = \frac{1}{3}\begin{bmatrix} (\frac{1}{Y_0}+\frac{2}{Y_1}) & (\frac{1}{Y_0}-\frac{1}{Y_1}) & (\frac{1}{Y_0}-\frac{1}{Y_1}) \\ (\frac{1}{Y_0}-\frac{1}{Y_1}) & (\frac{1}{Y_0}+\frac{2}{Y_1}) & (\frac{1}{Y_0}-\frac{1}{Y_1}) \\ (\frac{1}{Y_0}-\frac{1}{Y_1}) & (\frac{1}{Y_0}-\frac{1}{Y_1}) & (\frac{1}{Y_0}+\frac{2}{Y_1}) \end{bmatrix} \frac{d}{dx}\begin{bmatrix} I_a(x,s) \\ I_b(x,s) \\ I_c(x,s) \end{bmatrix} \tag{B.8}$$

where $Z_0 = R_0 + sL_0, Z_1 = R_1 + sL_1, Y_0 = sC_0$ and $Y_1 = sC_1$.

The relationships (B.7) and (B.8) can be written in the general form

$$\begin{aligned} -\tfrac{d}{dx}[V] &= \tfrac{1}{3}[Z_p][I] \\ -[V] &= \tfrac{1}{3}[Z_q]\tfrac{d}{dx}[I] \end{aligned} \tag{B.9}$$

Solution to the equations

By eliminating the current matrix $[I]$ of (B.9), a second order differential equation involving the voltage matrix can be obtained.

$$\frac{d^2}{dx^2}[V] - [\mu][V] = 0 \tag{B.10}$$

where

$$[\mu] = \frac{1}{3}\begin{bmatrix} (Z_0Y_0 + 2Z_1Y_1) & (Z_0Y_0 - Z_1Y_1) & (Z_0Y_0 - Z_1Y_1) \\ (Z_0Y_0 - Z_1Y_1) & (Z_0Y_0 + 2Z_1Y_1) & (Z_0Y_0 - Z_1Y_1) \\ (Z_0Y_0 - Z_1Y_1) & (Z_0Y_0 - Z_1Y_1) & (Z_0Y_0 + 2Z_1Y_1) \end{bmatrix} \tag{B.11}$$

The equation (B.10) does not have a simple solution because the coefficient matrix $[\mu]$ is not diagonal. Using a transformation of variables, the actual voltages V can be transformed to another set of components U.

$$\begin{aligned} [V] &= [T][U] \\ [U] &= [T]^{-1}[V] \end{aligned} \tag{B.12}$$

where $[T]$ is the transformation matrix. Now (B.10) can be written as

$$\frac{d^2}{dx^2}[U] - [\tau][U] = 0 \tag{B.13}$$

where

$$[\tau] = [T]^{-1}[\mu][T] \tag{B.14}$$

With a proper choice of $[T]$, it is possible to make $[\tau]$ diagonal. Now (B.13) can be readily solved since it is a set of an ordinary second-order differential equations with constant coefficients.

With proper transformation, the transmission line components of (B.11) become,

$$[\tau] = [T]^{-1}[\mu][T] = \begin{bmatrix} Z_0Y_0 & 0 & 0 \\ 0 & Z_1Y_1 & 0 \\ 0 & 0 & Z_1Y_1 \end{bmatrix} \tag{B.15}$$

Hence, the three-phase system is now represented with three independent systems or modes. This method is known as modal transformation.

Modal Transformation

Basic Principles

A line consisting of n conductors and ground has n modes of propagation. Each mode has a particular voltage-current relationship, velocity and attenuation constant at any given frequency. To analyze the transient behaviour of a 3-phase system, the voltages and currents are converted into modal quantities. The modal transformation techniques convert a dependent n-line system to n independent modes.

A transformation matrix as in (B.15) is used to find the modal quantities. The transformation of voltage and current signal use two transformation matrices. (B.16) shows the relationship between phase and modal quantities.

$$\begin{aligned} [v(t)] &= [S][v^{(m)}(t)] \\ [i(t)] &= [Q][i^{(m)}(t)] \end{aligned} \tag{B.16}$$

where $[S]$ and $[Q]$ are the voltage and current modal transformation matrices respectively. $[v^{(m)}(t)]$ and $[i^{(m)}(t)]$ are the modal voltage and current matrices. The inverse relationship is given by (B.17).

$$\begin{aligned} [v^{(m)}(t)] &= [S]^{-1}[v(t)] \\ [i^{(m)}(t)] &= [Q]^{-1}[i(t)] \end{aligned} \tag{B.17}$$

The relationship between voltage and current of an n line system is given by (B.18) and (B.19).

$$\frac{d[\overline{V}]}{dx} = -[\overline{Z}][\overline{I}] \tag{B.18}$$

$$\frac{d[\overline{I}]}{dx} = -[\overline{Y}][\overline{V}] \tag{B.19}$$

where the matrices have the dimensions corresponding to the number of modes. Applying modal voltage quantities to (B.18) yields

$$\begin{aligned} \frac{d}{dx}\{[S][\overline{V}^{(m)}]\} &= -[\overline{Z}][Q][\overline{I}^{(m)}] \\ \frac{d}{dx}\{[\overline{V}^{(m)}]\} &= -[S]^{-1}[\overline{Z}][Q][\overline{I}^{(m)}] \\ &= -[\overline{Z}^{(m)}][\overline{I}^{(m)}] \end{aligned} \tag{B.20}$$

where $[\overline{Z}^{(m)}] = [S]^{-1}[\overline{Z}][Q]$. Similarly from (B.19), it is possible to show that

$$\frac{d}{dx}\{[\overline{I}^{(m)}]\} = -[\overline{Y}^{(m)}][\overline{V}^{(m)}] \tag{B.21}$$

where $[\overline{Y}^{(m)}] = [Q]^{-1}[\overline{Y}][S]$.

Modal Transformation Matrices

The modal transformation matrices $[S]$and $[Q]$ can be chosen to give independent modes of propagation. The most commonly used transformations are Karrenbauer, Clarke and Wedepohl transformations.

Karrenbauer Transformation:

$$[S] = [Q] = \begin{bmatrix} 1 & 1 & 1 \\ 1 & -2 & 1 \\ 1 & 1 & -2 \end{bmatrix} \tag{B.22}$$

$$[S]^{-1} = [Q]^{-1} = \frac{1}{3}\begin{bmatrix} 1 & 1 & 1 \\ 1 & -1 & 0 \\ 1 & 0 & -1 \end{bmatrix} \tag{B.23}$$

Clarke Transformation:

$$[S] = [Q] = \begin{bmatrix} 1 & 1 & 0 \\ 1 & -\frac{1}{2} & \frac{\sqrt{3}}{2} \\ 1 & \frac{1}{2} & -\frac{\sqrt{3}}{2} \end{bmatrix} \tag{B.24}$$

$$[S]^{-1} = [Q]^{-1} = \frac{1}{3}\begin{bmatrix} 1 & 1 & 1 \\ 2 & -1 & -1 \\ 0 & \frac{1}{\sqrt{3}} & -\frac{1}{\sqrt{3}} \end{bmatrix} \tag{B.25}$$

Wedepohl Transformation:

$$[S] = [Q] = \begin{bmatrix} 1 & 1 & 1 \\ 1 & 0 & -2 \\ 1 & -1 & 1 \end{bmatrix} \tag{B.26}$$

$$[S]^{-1} = [Q]^{-1} = \frac{1}{3}\begin{bmatrix} 1 & 1 & 1 \\ \frac{3}{2} & 0 & -\frac{3}{2} \\ \frac{1}{2} & -1 & \frac{1}{2} \end{bmatrix} \tag{B.27}$$

The modal quantities evaluated will have 3 modes, two aerial modes and an earth mode.

- *Earth mode* [Mode 1]

This is the zero sequence component of the phase voltages and currents. Its velocity and attenuation will be affected by the resistivity of the earth and hence it is frequency dependent. Velocity at low frequencies may be approximately 75% of the speed of light.

- *Aerial modes* [Modes 2 and 3]

In these modes, the current in the 3 phases tend to cancel. Therefore the effect of earth resistivity in that mode is very small. Hence the aerial modes are almost frequency independent and the velocities approach the speed of light.

Modal Impedance and Velocity

For a three phase system

$$[\overline{V}] = [\overline{Z}_c^{(p)}][\overline{I}] \tag{B.28}$$

where $\overline{Z}_c^{(p)}$is the phase characteristic impedance matrix. Using modal transformation, we get

$$\begin{aligned} [\overline{V}^{(m)}] &= [S]^{-1}[\overline{Z}_c^{(p)}][Q][\overline{I}^{(m)}] \\ &= [\overline{Z}_c^{(m)}][\overline{I}^{(m)}] \end{aligned} \tag{B.29}$$

where $\overline{Z}_c^{(m)}$is the modal characteristic impedance matrix.

For a fully transposed line section (symmetrical configuration), $[\overline{Z}_c^{(m)}]$ is diagonal.

$$[\overline{Z}_c^{(m)}] = \begin{bmatrix} Z_0 & 0 & 0 \\ 0 & Z_1 & 0 \\ 0 & 0 & Z_2 \end{bmatrix} \tag{B.30}$$

where Z_0 is the impedance of the earth mode and Z_1 and Z_2 are the impedances of the aerial modes. In (B.30)

$$\begin{aligned} Z_0 &= Z_{0s} + 2Z_{0m} \\ Z_1 &= Z_2 = Z_{0S} - Z_{0m} \end{aligned}$$

where

Z_{0s} = self impedance term of phase characteristic impedance matrix

Z_{0m} = mutual impedance term of phase characteristic impedance matrix

The two aerial modes and the earth mode have different velocities. The earth mode velocity depends on the ground impedance. The aerial mode velocities are almost independent of the ground resistivity, hence frequency, and are close to the speed of light. Mode 3 velocity is usually slightly higher than that of Mode 2.

Appendix C

Signal Processing Techniques

Different signal processing techniques are used in practice to detect required signals from the measured waveforms under noisy conditions. The most commonly used technique in detecting wavefront reflections in travelling wave based protection schemes is the correlation method. The theory behind the correlation function and its applicability to detect faults under noisy conditions are described in this section.

Correlation in Analog Domain

The cross-correlation function of two time invariant signals $x(t)$ and $y(t)$ is given by

$$R_{xy}(\tau) = \lim_{T\to\infty} \frac{1}{T} \int_0^T x(t).y(t+\tau)dt \tag{C.1}$$

The covariance function of two signals $x(t)$ and $y(t)$ is

$$\Phi_{xy}(\tau) = \lim_{T\to\infty} \frac{1}{T} \int_0^T [x(t) - \overline{x}].[y(t+\tau) - \overline{y}]dt \tag{C.2}$$

where the mean values of the signals $x(t)$ and $y(t)$ during the time period T are given by

$$\overline{x} = \frac{1}{T} \int_0^T x(t)dt \quad , \quad \overline{y} = \frac{1}{T} \int_0^T y(t)dt \tag{C.3}$$

and $[x(t)-\overline{x}]$, $[y(t)-\overline{y}]$ give the deviation of the signal from the mean value within the period concerned. Now expanding C.2,

$$\begin{aligned}
\Phi_{xy}(\tau) &= \lim_{T\to\infty}\frac{1}{T}\{\int_0^T x(t).y(t+\tau)dt - \overline{x}.\int_0^T y(t+\tau) - \overline{y}.\int_0^T x(t)dt + \overline{x}.\overline{y}\} \\
&= \lim_{T\to\infty}\frac{1}{T}\int_0^T x(t).y(t+\tau)dt - \overline{x}.\lim_{T\to\infty}\frac{1}{T}\int_0^T y(t+\tau) - \overline{y}.\lim_{T\to\infty}\frac{1}{T}\int_0^T x(t)dt + \overline{x}.\overline{y} \\
&= \lim_{T\to\infty}\frac{1}{T}\int_0^T x(t).y(t+\tau)dt - \overline{x}.\overline{y} - \overline{x}.\overline{y} + \overline{x}.\overline{y} \\
&= \lim_{T\to\infty}\frac{1}{T}\int_0^T x(t).y(t+\tau)dt - \overline{x}.\overline{y} \\
&= R_{xy}(\tau) - \overline{x}.\overline{y} \qquad \text{(C.4)}
\end{aligned}$$

If $y(t)$ is time variant,

$$\begin{aligned}
\Phi_{xy}(\tau) &= \lim_{T\to\infty}\frac{1}{T}\int_0^T \{[x(t)-\overline{x}].[y(t+\tau) - \frac{1}{T}\int_0^T y(t+\tau)dt]\}dt \\
&\qquad \frac{1}{T}\int_0^T x(t)dt.\frac{1}{T}\int_0^T y(t+\tau)dt + \overline{x}.\frac{1}{T^2}\iint_0^T y(t+\tau)dtdt\} \\
&= \lim_{T\to\infty}\frac{1}{T}\int_0^T x(t).y(t+\tau)dt - \overline{x}.\overline{y(\tau)} - \overline{x}.\overline{y(\tau)} + \overline{x}.\overline{y(\tau)} \\
&= \lim_{T\to\infty}\frac{1}{T}\int_0^T x(t).y(t+\tau)dt - \overline{x}.\overline{y(\tau)} \\
&= R_{xy}(\tau) - \overline{x}.\overline{y(\tau)} \qquad \text{(C.5)}
\end{aligned}$$

Correlation in the Digital Domain

In the digital domain the continuous variable t is replaced with the sample number k. The signals are sampled at a frequency at least twice higher than the maximum frequency concerned. The autocorrelation function of a sampled signal $x(k)$ is given by

$$R_x(m\Delta t) = \frac{1}{N}\sum_{k=1}^{N} x(k\Delta t).x(k\Delta t + m\Delta t) \qquad \text{(C.6)}$$

where m is the number of samples the two waveforms are shifted by each other. Here, Δt is the sampling interval and N is the total number of samples in the time interval T.

The cross-correlation function of the two signals $x(k)$ and $y(k)$ is given by

$$R_{xy}(m\Delta t) = \frac{1}{N}\sum_{k=1}^{N} x(k\Delta t).y(k\Delta t + m\Delta t) \tag{C.7}$$

The covariance function of two signals with the mean removal is given by

$$\Phi_{xy}(m\Delta t) = \frac{1}{N}\sum_{k=1}^{N}[x(k\Delta t) - \overline{x}].[y(k\Delta t + m\Delta t) - \overline{y}(m\Delta t)] \tag{C.8}$$

where

$$\overline{x} = \frac{1}{N}\sum_{k=1}^{N} x(k\Delta t) \tag{C.9}$$

$$\overline{y}(m\Delta t) = \frac{1}{N}\sum_{k=1}^{N} y(k\Delta t + m\Delta t) \tag{C.10}$$

Expanding the relationship given by (C.8),

$$\begin{aligned}
\Phi_{xy}(m\Delta t) &= \frac{1}{N}\sum_{k=1}^{N}\{x(k\Delta t).y(k\Delta t + m\Delta t) - \overline{x}.y(k\Delta t + m\Delta t) - \\
&\qquad \overline{y}(m\Delta t).x(k\Delta t) + \overline{x}.\overline{y}(m\Delta t)\} \\
&= \frac{1}{N}\sum_{k=1}^{N} x(k\Delta t).y(k\Delta t + m\Delta t) - \overline{x}.\frac{1}{N}\sum_{k=1}^{N} y(k\Delta t + m\Delta t) \\
&\qquad -\overline{y}(m\Delta t).\frac{1}{N}\sum_{k=1}^{N} x(k\Delta t) + \overline{x}.\overline{y}(m\Delta t)\frac{1}{N}\sum_{k=1}^{N}(1) \\
&= \frac{1}{N}\sum_{k=1}^{N} x(k\Delta t).y(k\Delta t + m\Delta t) - \overline{x}.\overline{y}(m\Delta t) - \overline{y}(m\Delta t).\overline{x} + \overline{x}.\overline{y}(m\Delta t) \\
&= \frac{1}{N}\sum_{k=1}^{N} x(k\Delta t).y(k\Delta t + m\Delta t) - \overline{x}.\overline{y}(m\Delta t) \\
&= R_{xy}(m\Delta t) - \overline{x}.\overline{y}(m\Delta t)
\end{aligned} \tag{C.11}$$

Detection of Signals of Known Shape in Noise

The electrical signals produced by the voltage and current transducers may contain unwanted signals or noise. The noise can be due to thermal effects, defects in the transducers or high frequency "noise" injected due to the occurrence of a fault. The noise component has to be removed in impedance measurement algorithms, before processing the waveforms. This is done through filtering. However, these high frequency signals are essential for the travelling wave algorithms. In a travelling wave relay, the outgoing wavefront is stored and correlated with the reflected waves which contain unwanted noise components. The best filter for detecting the presence of a known signal in white noise is a 'matched filter,' where the received noisy signal is correlated against an uncorrupted version of itself.

In a system using travelling wave techniques, a portion of the forward wave f_2 is stored and correlated with the reflected wave f_1. The signal f_1 is an attenuated, delayed form of the signal f_2. The attenuation can be considered as frequency independent. If the known signal is $x_0(t)$, then the reflected signal $y(t)$ can be assumed to have the shape

$$y(t) = \gamma x_0(t - \Delta T) + \epsilon(t) + n(t) \tag{C.12}$$

where γ is the attenuation of the line, $\epsilon(t) = E\sin(\omega t + \phi)$, the offset due to the signal of the system frequency, ΔT - the delay, and $n(t)$ - the noise signal. ΔT is the required information. If the prefault steady state signal is removed from $x_0(t)$, $\epsilon(t)$ can be assumed as zero. To recover the wanted signal from the noise, this signal is fed to a "filter". Now, the input to this filter is

$$y'(t) = \gamma x_0(t - \Delta T) + n(t) \tag{C.13}$$

The output of the filter $\xi(t)$ contains output due to the wanted signal, $\rho(t)$ and output due to noise, $\sigma(t)$.

$$\xi(t) = \rho(t) + \sigma(t) \tag{C.14}$$

If the delayed signal of $x_0(t)$ is given by $x(t)$,

$$x(t) = \gamma x_0(t - \Delta T) \tag{C.15}$$

Consider the frequency spectrum of $x(t)$.

$$X(\omega) = \gamma X_0(\omega) e^{-j\omega\Delta T} \tag{C.16}$$

where

$$X_0(\omega) = \int_{-\infty}^{\infty} x_0(t) e^{-j\omega t} dt \tag{C.17}$$

If the frequency response of the filter is $H(\omega)$, then the required signal at the output of the filter is given by

$$\rho(t) = \frac{1}{2\pi} \int_{-\infty}^{\infty} H(\omega).X_0(\omega) e^{j\omega t} d\omega \tag{C.18}$$

If the power spectral density of the noise signal $n(t)$ is given by $S_n(\omega)$, then the average power of the noise signal is

$$\begin{aligned} \overline{n^2(t)} &= \frac{1}{T} \int_0^T n^2(t)\ dt \\ &= \frac{1}{2\pi} \int_{-\infty}^{\infty} S_n(\omega) d\omega \end{aligned} \tag{C.19}$$

At the output of the filter, the total power of the noise signal N is given by

$$N = |\sigma(t)|^2 = \frac{1}{2\pi} \int_{-\infty}^{\infty} |H(\omega)|^2 .S_n(\omega) d\omega \tag{C.20}$$

Now, it is required to maximize the signal to noise ratio μ at the output of the filter at some instant in time, say $t = T$. i.e.

$$\mu = \frac{\rho^2(T)}{N} = \frac{\left| \frac{1}{2\pi} \int_{-\infty}^{\infty} H(\omega).X_0(\omega) e^{j\omega t} d\omega \right|^2}{\frac{1}{2\pi} \int_{-\infty}^{\infty} |H(\omega)|^2 .S_n(\omega) d\omega} \tag{C.21}$$

The maximization of the expression can be accomplished by applying the *Schwartz inequality*

$$\left|\frac{1}{2\pi}\int_{-\infty}^{\infty} P(\omega).Q^*(\omega)e^{j\omega t}d\omega\right|^2 \leq \int_{-\infty}^{\infty}|P(\omega)|^2\,d\omega.\int_{-\infty}^{\infty}|Q(\omega)|^2\,d\omega \tag{C.22}$$

where Q^* is the complex conjugate of Q. The equality applies when $P = constant \times Q$. Therefore,

$$\frac{\rho^2(T)}{N} \leq \frac{\int_{-\infty}^{\infty}|H(\omega)|^2\,d\omega.\int_{-\infty}^{\infty}|X_0(\omega)|^2\,d\omega}{\frac{1}{2\pi}\int_{-\infty}^{\infty}|H(\omega)|^2.S_n(\omega)d\omega}$$

The *optimum* filter is a filter that maximizes μ, i.e. the optimum filter is obtained at $t = T$, when

$$H(\omega) = Ke^{-j\omega T}\frac{X_0^*(\omega)}{S_n(\omega)} \tag{C.23}$$

where K is a constant. The frequency response is proportional to $X_0(\omega)$ which emphasizes frequencies which contain large signal components and inversely proportional to $S_n(\omega)$ which de-emphasizes frequencies which contain large noise components. If the noise is considered to be *additive white noise*, I.E.$|S_n(\omega)|^2 = 1$, then the optimum filter is the *matched filter* or *correlator*. The transfer function of the correlator is given by

$$H(\omega) = e^{-j\omega T}X_0^*(\omega) \tag{C.24}$$

Then in the time domain, when $X_0(\omega)$ is real, i.e. when the input signal $x(t)$ is symmetrical,

$$h(t) = Kx(t-T) \tag{C.25}$$

That is, the impulse response of the filter is matched to the delayed replica of the input signal to which the filter is matched. Hence the correlation technique becomes an effective method to extract a known signal in white gaussian noise.

Appendix D

Impedance Measurement of Transmission Lines

Introduction

The basic principle behind impedance relaying is calculating the line impedance seen by the relay at the relay location using the fundamental frequency components of voltage and current signals. The impedance is a function of the voltage and current. Fourier transform based methods can be used to derive the fundamental components of the voltage and current signals. In this section, the basic theory behind the impedance measurement algorithm is introduced.

Impedance Calculation

Fourier analysis can be used to calculate the fundamental frequency component. According to the definition of *Fourier Series*, in the analog domain, a signal $x(t)$ which repeats with period T can be expressed as a sum of cosines and sines as

$$x(t) = a_0 + \sum_{n=1}^{n=\infty} a_n \cos(n\omega_0 t) + \sum_{n=1}^{n=\infty} b_n \sin(n\omega_0 t) \tag{D.1}$$

where

$$\begin{aligned} a_n &= \frac{2}{T}\int_0^T x(t)\ \cos(n\omega_0 t)\ dt \\ b_n &= \frac{2}{T}\int_0^T x(t)\ \sin(n\omega_0 t)\ dt \\ a_0 &= \frac{1}{T}\int_0^T x(t)\ dt \end{aligned} \tag{D.2}$$

and a_0 represents the dc component. Here, $\omega_0 = 2\pi/T$. The Fourier analysis separates the dc, fundamental and harmonic components of $f(t)$. For the n^{th} harmonic, the amplitude is given by

$$|c_n| = \sqrt{(a_n^2 + b_n^2)} \tag{D.3}$$

and the phase angle is given by

$$\theta_n = \tan^{-1}\left(\frac{b_n}{a_n}\right) \tag{D.4}$$

The fundamental frequency components are given by a_1 and b_1.

The Fourier series has certain practical limitations in its use. It assumes that the time function is of infinite duration, whereas practical data in the case of a fault are often a transient having finite duration. Further, it assumes that the data are periodic over an unlimited extent, whereas practical data are usually non-periodic. It is possible to represent non-periodic data by a Fourier Transform (FT). The FT of the time function $x(t)$ is given by

$$X(f) = \int_{-\infty}^{\infty} x(t)\ e^{-j\omega t} dt \tag{D.5}$$

where $\omega = 2\pi/T$. The absolute value of (D.5) yields the frequency amplitude content and the argument gives the phase content.

In digital algorithms, sampled values are used instead of the continuous variables. Hence the continuous integrals given by (D.2) cannot be applied directly to find the fundamental components. Instead the integral is taken over N samples within the time interval T which

immediately precedes the sampling instant in question. The digital domain equivalent of (D.1) is given by,

$$x(k) = A_0 + \sum_{n=0}^{(N-1)/2} A_n \cos\left(\frac{2\pi}{N} nk\right) + \sum_{n=0}^{(N-1)/2} B_n \sin\left(\frac{2\pi}{N} nk\right) \tag{D.6}$$

where $n = 0, 1, 2, ..., (N-1)/2$ and $k = 1, 2, ...(N-1)$. The discrete form of the integrals are given by

$$\begin{aligned} A_n &= \frac{2}{N} \sum_{k=0}^{(N-1)} x(k) \cos\left(\frac{2\pi}{N} nk\right) \\ B_n &= \frac{2}{N} \sum_{k=0}^{(N-1)} x(k) \sin\left(\frac{2\pi}{N} nk\right) \\ A_0 &= \frac{1}{N} \sum_{k=0}^{(N-1)} x(k) \end{aligned} \tag{D.7}$$

where $x(k)$ represents individual samples within the sampling window. This is known as the discrete Fourier series. The amplitude and the phase of the n^{th} harmonic is given by,

$$|C_n| = \sqrt{(A_n^2 + B_n^2)} \tag{D.8}$$

and

$$\theta_n = \tan^{-1}\left(\frac{B_n}{A_n}\right) \tag{D.9}$$

The fundamental frequency components are given by A_1 and B_1.

The discrete form of (D.5) is given by

$$X(n) = \frac{1}{N} \sum_{k=0}^{(N-1)} x(k) e^{-j\left(\frac{2\pi}{N} nk\right)} \tag{D.10}$$

where $k, n = 1, 2, ...N$. The above relationship is known as the DFT. A major use of the DFT is the translation of a time series into an equivalent frequency series. Hence

the DFT can be used effectively to calculate the fundamental components of voltage and current signals. An alternative method of obtaining the DFT, termed as the FFT, can be used to improve the speed of calculation when a number of DFT's are sought (e.g. the fundamental and several harmonics).

Using (D.8) and (D.9), the fundamental components of the voltage and current can be obtained.

$$|C_1| = \sqrt{(A_1^2 + B_1^2)} \tag{D.11}$$

and

$$\theta_1 = \tan^{-1}\left(\frac{B_1}{A_1}\right) \tag{D.12}$$

Using the above equation, the voltage C_V, θ_V and current C_I, θ_I fundamental phasor components can be obtained. The impedance $\overline{Z}$ and phase angle θ_Z can be derived by using

$$|\overline{Z}| = \frac{C_V}{C_I} \tag{D.13}$$

$$\theta_Z = \theta_V - \theta_I \tag{D.14}$$

The above computation is carried out at each sampling interval. This will give an impedance value based on the voltage and current samples of the previous cycle preceding the current sample.

In a three phase system, the mutual coupling between transmission lines affects the sound phases when there is a fault on one phase. If the voltage and current signals from each phase are used to find the impedance according to the above method, the impedance value obtained will not be proportional to the distance to the fault. Transforming phase variables to symmetrical component variables avoids mutual effects between variables except at the fault location.

Symmetrical components

If a fault occurs in a three phase network, the mutual impedance between the phases allows fault induced effects to couple across from the faulted phase to the sound phases.If the impedance is calculated from the line voltages V_a, V_b, V_c and currents I_a, I_b, I_c of the three phases, the calculated values will not have a simple relationship to the distance to the fault. To decouple the phases, the three phase network can be transformed into a new set of phasors known as *symmetrical components.* The new set of components are labelled the 012 set. They are referred to as the zero sequence, positive sequence and negative sequence components [108].

The three phase system can be expressed in a concise form as in (D.15),

$$[V_{abc}] = [Z_{abc}]\,[I_{abc}] \tag{D.15}$$

where V_{abc} is the voltage vector, I_{abc} is the current vector and Z_{abc} is the impedance matrix of the network. The matrix Z_{abc} has mutual elements. This can be transformed into a new set of variables:

$$[V_{012}] = [Z_{012}]\,[I_{012}] \tag{D.16}$$

The elements in (D.16) are related to the values in (D.15) by,

$$\begin{aligned} [V_{abc}] &= [F][V_{012}] \\ [I_{abc}] &= [F][I_{012}] \\ [F]^{-1}[Z_{abc}][F] &= [Z_{012}] \end{aligned} \tag{D.17}$$

where

$$[F] = \begin{bmatrix} 1 & 1 & 1 \\ 1 & a^2 & a \\ 1 & a & a^2 \end{bmatrix}, \quad [F]^{-1} = \frac{1}{3}\begin{bmatrix} 1 & 1 & 1 \\ 1 & a & a^2 \\ 1 & a^2 & a \end{bmatrix} \tag{D.18}$$

Here,

$$a = \left(-\frac{1}{2} + j\frac{\sqrt{3}}{2}\right) = 1\angle 120, \quad a^2 = \left(-\frac{1}{2} - j\frac{\sqrt{3}}{2}\right) = 1\angle 240 \tag{D.19}$$

The matrix Z_{012} in (D.17) is diagonal and the diagonal elements are the eigenvalues of the Z_{abc} matrix if the system is assumed to be perfectly balanced. The diagonal elements Z_0, Z_1, and Z_2 are known as zero, positive, and negative sequence impedance, respectively.

Mho Relay

The mho type distance relay is most suited for protecting long transmission lines. The mho relay has inherent directional discrimination properties. The concept of the mho relay can be explained using the universal relay torque equation [109] given as follows:

$$T = K_1 I^2 + K_2 V^2 + K_3 V I \cos(\theta - \tau) + K \tag{D.20}$$

where θ is the angle between I and V, τ the maximum torque angle, K is the fixed restraining torque and K_1, K_2, K_3 are constants.

In the mho relay, the operating torque is obtained by the V-I element and the restraining torque is due to the voltage element. Hence in D.20, K_1 is set to zero. Neglecting K, the torque equation becomes

$$T = K_3 V I \cos(\theta - \tau) - K_2 V^2 \tag{D.21}$$

For the relay to operate

$$K_3 V I \cos(\theta - \tau) > K_2 V^2 \tag{D.22}$$

or

$$Z < \frac{K_3 V I}{K_2} \cos(\theta - \tau) \tag{D.23}$$

This characteristic when drawn on an impedance plane depicts a circle passing through the origin. The relay operates when the impedance seen by the relay falls within this circle.

Appendix E

Line Configuration and Parameters

The transmission line configuration and parameters of the three phase power network used for simulations in Chapter 4 are given here. The line parameters were generated by the "line constants" program in PSCAD. The transmission line is assumed to have uniform sag and conductor spacing along the total span. The tower configuration is shown in Fig. E.1.

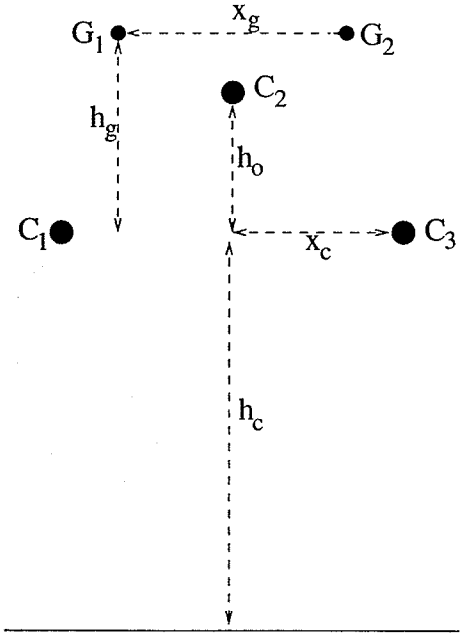

Figure E.1: Tower configuration

Line Configuration Data:

The height of outer conductors, h_c	= 28.956 m
Height of center conductor, $h_c + h_o$	= 38.648 m
Horizontal space between phases, x_c	= 6.7056 m
Conductor radius, r_c	= 1.65354×10^{-2} m
No of conductors in a bundle, n	= 3
Conductor bundle spacing, d_c	= 45.72×10^{-2} m
Sag for all conductors, S_c	= 12.192 m
Height of ground wires, $h_c + h_g$	= 45.659m
Spacing between ground wires, x_g	= 10.11928 m
Ground wire radius, r_g	= 0.54864×10^{-2} m
Sag for ground wires, S_g	= 7.62 m

Line Parameters:

Conductor DC resistance, R_c	= 0.0489 Ω/km
Ground wire DC resistance, R_g	= 2.8651 Ω/km
Ground resistivity, σ_g	= 100 Ωm
Zero sequence resistance, R_0	= 0.3211×10^{-3} Ω/m
Zero sequence reactance, X_0	= 0.1218×10^{-2} Ω/m
Positive sequence resistance, R_1	= 0.1756×10^{-4} Ω/m
Positive sequence reactance, X_1	= 0.3378×10^{-3} Ω/m
Negative sequence resistance, R_2	= 0.1756×10^{-4} Ω/m
Negative sequence reactance, X_2	= 0.3378×10^{-3} Ω/m
Mode 1 surge impedance, Z_1	= $675\angle -6.3$ Ω
Mode 2,Mode 3 surge impedance, Z_2	= $264\angle -0.9$ Ω
Mode 1 surge impedance, v_1	= 204.4 km/ms
Mode 2,Mode 3 surge impedance, v_2	= 294.6 km/ms

Appendix F

Hardware Information

Multichannel Buffered Serial Port

The multichannel buffered serial port (McBSP) consists of a data path and a control path, which connect to external devices. Data is communicated to these external devices via separate pins for transmission and reception. Control information (clocking and frame synchronization) is communicated via four other pins. The device communicates to the McBSP via 32-bit-wide control registers accessible via the internal peripheral bus. The McBSP block diagram is shown in Fig.F.1[1].

The main functional units of the McBSP are described below:

Transmitter The transmitter section is responsible for the serial transmission of data that is written in DXR. The contents of DXR are copied to the transmit shift register XSR. The transfer starts as soon as the transmit frame sync (FSX) is detected. One bit of data is transmitted or shifted out of XSR on every transmit clock CLKX. New data can be written to DXR using either the CPU or the DMA.

Receiver The data received on the DR pin is shifted into the Receive Shift Register (RSR) on every receive clock (CLKR). Again, the actual shifting in of data begins after

[1]Obtained from [78]

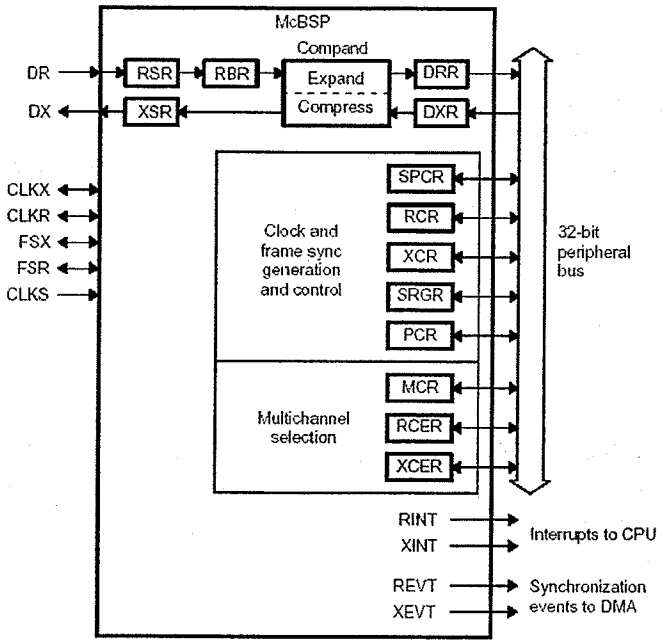

Figure F.1: The McBSP block diagram

detection of a receive frame sync (FSR). The data in RSR is copied to a Receive Buffer Register (RBR) and then to the Data Receive Register (DRR). The DRR can be read by either the CPU or the DMA.

Sample Rate Generator This module generates control signals such as the transmit/receive clocks and frame sync signals necessary for data transfer to and from the McBSP. Clock generation circuitry allows the user to choose either the CPU clock or an external source via CLKS to generate CLKR/X. Frame sync signal properties such as frame period and frame width are also programmable. FSR/X, CLKR/X are bidirectional pins, and therefore can be inputs or outputs.

Events/Interrupt Generation The McBSP generates sync events to the DMA to indicate that data is ready in DRR or that DXR is ready for new data. They are read sync event REVT, and write sync event XEVT. Similarly the CPU can read/write to the McBSP based on interrupts (RINT and XINT) generated by the McBSP.

The TableF.1 gives the McBSP register information. These registers have to be properly initialized in order to use the serial port.

Table F.1: McBSP registers

McBSP0	McBSP1	Abbr.	Description
-	-	RBR	Receive buffer register
-	-	RSR	Receive shift register
-	-	XSR	Transmit shift register
018C0000	01900000	DRR	Data receive register
018C0004	01900004	DXR	Data transmit register
018C0008	01900008	SPCR	Serial port control register
018C000C	0190000C	RCR	Receive control register
018C0010	01900010	XCR	Transmit control register
018C0014	01900014	SRGR	Sample rate generator register
018C0018	01900018	MCR	Multichannel control register
018C001C	0190001C	RCER	Receive channel enable register
018C0020	01900020	XCER	Transmit channel enable register
018C0024	01900024	PCR	Pin control register

The McBSP allows choosing different clocking and framing for both the receiver and transmitter. Fig.F.2[1] is a block diagram of the clock and frame selection circuitry.

The sample rate generator is made of a 3-stage clock divider that provides a programmable data clock (CLKG) and framing signal (FSG), as shown in Fig.F.3[1]. CLKG and FSG are McBSP internal signals that can be programmed to drive receive and/or transmit clocking, CLK(R/X), and framing, FS(R/X). The sample rate generator can be programmed to be driven by an internal clock source or an internal clock derived from an external clock source.

[1]Obtained from [78]

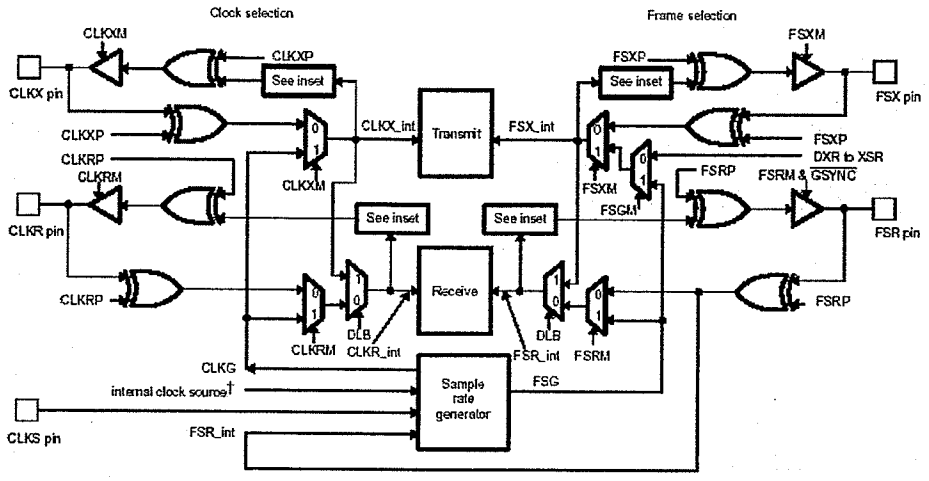

Figure F.2: The McBSP clock and frame generation circuitry

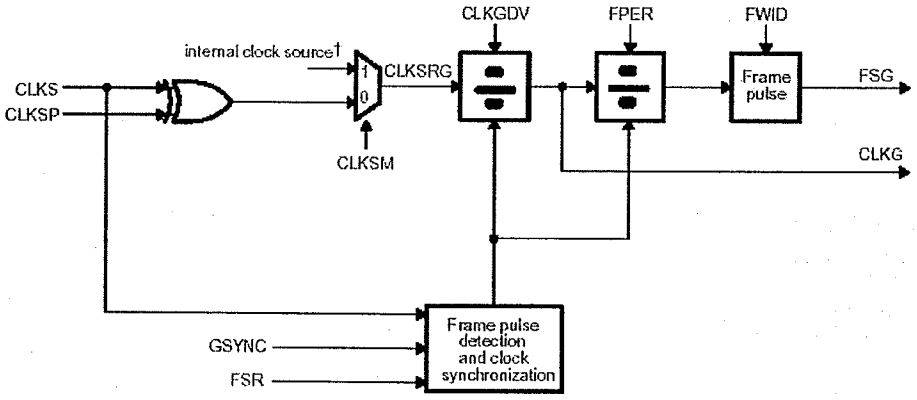

Figure F.3: The McBSP sample rate generator

Timers

The TMS320C6711 has two 32-bit general-purpose timers. The timers have two signaling modes and can be clocked by an internal or an external source. The timers have an input pin and an output pin. The input and output pins, (TINP and TOUT) can function as timer clock input and clock output. Fig.F.4[1] shows a block diagram of the timers.

TableF.2 gives details about the timer registers:

Configuring a timer requires three basic steps:

- If the timer is not currently in the hold state, place the timer in hold (HLD = 0).

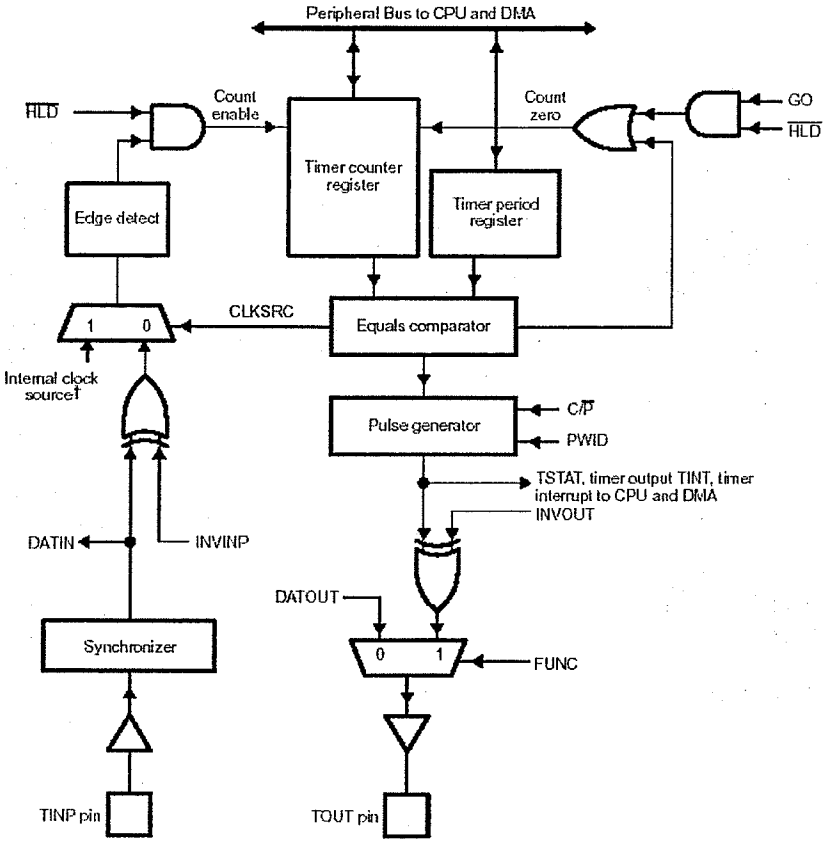

Figure F.4: The C6711 timers

- Write the desired value to the timer period register (PRD).
- Write the desired value to the timer control register (CTL). Do not change the GO and HLD bits of the CTL in this step.
- Start the timer by setting the GO and HLD bits of the CTL to 1.

In pulse mode operation, the output clock frequency is given by;

$$Frequency = \frac{Frequency\ of\ clock\ source}{Timer\ period\ register\ value} \tag{F.1}$$

Table F.2: Timer registers

Timer0	Timer1	Register	Description
01940000	01980000	Timer Control (CTL)	Determines the operating mode of the timer, monitors the timer status, and controls the function of the TOUT pin.
01940004	01980004	Timer Period (PRD)	Contains the number of timer input clock cycles to count. This number controls the TSTAT signal frequency.
01940008	01980008	Timer Counter (CNT)	Current value of the incrementing counter.

In clock mode operation, the output clock frequency is given by;

$$Frequency = \frac{Frequency\ of\ clock\ source}{2 * Timer\ period\ register\ value} \tag{F.2}$$

Acronyms

ADC	Analog to Digital Converter
AI	Artificial Intelligence
ALU	Arithmetic Logic Unit
ANN	Artificial Neural Network
API	Application Programming Interface
ASIC	Application Specific Integrated Circuit
CCVT	Capacitor Coupled Voltage Transformer
CFR	Configuration Register
CLKR	Receive Clock
CLKX	Transmit Clock
COFF	Common Object File Format
CT	Current Transformer
CWT	Continuous Wavelet Transform
DAC	Digital to Analog Converter
DFT	Discrete Fourier Transform
DLL	Dynamic Link Library
DMA	Direct Memory Access
DRR	Data Receive Register
DSK	Digital Signal Processor Starter Kit
DSP	Digital Signal Processor
DWT	Discrete Wavelet Transform
DXR	Data Transmit Register
EDMA	Extended Direct Memory Access
EHV	Extra High Voltage
EMIF	External Memory Interface

EMTDC	Electromagnetic Transient Program for Direct Current
EMTP	Electromagnetic Transient Program
EPI	External Peripheral Interface
EPP	Enhanced Parallel Port
EPROM	Erasable Programmable Read Only Memory
FFT	Fast Fourier Transform
FIFO	First IN First Out
FPGA	Field Programmable Gate Array
FSR	Receive Frame Sync
FSX	Transmit Frame Sync
GPIO	General Purpose Input Output
GUI	Graphical User Interface
HPI	Host Port Interface
HPRC	High-Performance Reconfigurable Computing architecture
IED	Intelligent Electronic Device I/O Input and Output IDE
IRQ	Interrupt Request
ISR	Interrupt Service Routine
IDE	Integrated Development Environment
JTAG	Joint Test Action Group
L1/L2	Level1 / Level2
LSB	Least Significant Bit
McBSP	Multi-Channel Buffered Serial Port
MFLOPS	Million Floating Point Operations Per Second
MIPS	Million Instructions Per Second
MSB	Most Significant Bit
MSPS	Mega Samples Per Second
OVT	Optical Voltage Transformer PC Personal Computer
PCI	Peripheral Component Interconnect
PCR	Pin Control Register

PEROM	Programmable Erasable Read Only Memory
PLL	Phase-Locked-Loop
PnP	Plug and Play Architecture
PPC	Parallel Port Connector
RCR	Receive Control Register
ROM	Read Only Memory
RSL	Runtime Support Library
RTP	Real Time Playback
SCLK	Sample Rate Generator Clock
SDI	Serial Data Input
SDK	Software Development Kit
SDO	Serial Data Output
SDRAM	Synchronous Dynamic Random Access Memory
SPCR	Serial Port Control Register
SPP	Standard Parallel Port
SRG	Sample Rate Generator
SRGR	Sample Rate Generator Register
TIM	Texas Instruments Module
VLIW	Very Long Instruction Word
VT	Voltage Transformer
XCR	Transmit Control Register
XSR	Transmit Shift Register

Reference

[1] D. Novosel, M.M. Begovic, and V. Madani, "Shedding light on blackouts", *IEEE Power and Energy Magazine*, Vol.2, No.1, Jan/Feb 2004, pp.33-43

[2] J.S. Thorp, A.G. Phadke, S.H. Horowitz, and J.E. Beehler, "Limits to impedance relaying", *IEEE Transactions Power Apparatus and Systems*, Vol.98, No.1, Jan/Feb 1979, pp.246-256

[3] S.H. Horowitz, A.G. Phadke, and J.S. Thorp. "Adaptive transmission system relaying", *IEEE Transactions on Power Delivery*, Vol.3, No.4, pp.1436-1445, Oct 1988

[4] L.V. Bewley, "Travelling waves on transmission systems", Dover Publications Inc., New York, Second Edition, 1964

[5] P.A. Crossley, and P.G. McLaren, "Distance protection based on travelling waves", *IEEE Transactions Power Apparatus and Systems*, Vol.102, No.9, Sep 1983, pp.2971-2983

[6] P.A. Crossley, "Distance protection based on travelling waves", Ph.D. Thesis, University of Cambridge, Jan 1983

[7] E.H. Shehab-Eldin, "Travelling wave distance measurement in E.H.V. power systems", Ph.D. Thesis, University of Cambridge, Jan 1988

[8] D.A. Douglass, "Current transformer accuracy with asymmetric and high frequency fault currents", *IEEE Transactions on Power Apparatus and Systems*, Vol.100, No.3, Mar 1981, pp.1006-1012

[9] D.A. Douglass, "Potential transformer accuracy at 60Hz voltage above and below rating and frequencies above 60Hz", *IEEE Transactions on Power Apparatus and Systems*, Vol.100, No.3, Mar 1981, pp.1370-1375

[10] Working Group 05 of Study Committee 36, "Transformers and instruments for measuring harmonics", Electra, No.124, May 1989, pp.92-97

[11] N. Kehtarnavaz, and M. Keramat, "DSP system design using the TMS320C6000", Prentice Hall, 2001

[12] PSCAD/EMTDC Version 3.0 User Manual, Manitoba HVDC Research Centre, 1999

[13] A.R. van C. Warrington, "Protective relays", Vol.1, Chapman & Hall, 1968

[14] A.G. Phadke, and J.S. Thorpe, "Computer relaying for power systems", John Wiley & Sons Inc., 1988

[15] G.D. Rockefeller, "Fault protection with a digital computer", *IEEE Transactions on Power Apparatus and Systems*, Vol.88, No.4, Apr 1969, pp. 438-464

[16] B.J. Mann, and I.F. Morrison, "Digital calculation of impedance for transmission line protection", *IEEE Transactions on Power Apparatus and Systems*, Vol.90, No.1, Jan 1971, pp. 270-279

[17] B.J. Mann, and I.F. Morrison, "Relaying a three phase transmission line with a digital computer", *IEEE Transactions on Power Apparatus and Systems*, Vol.90, No.2, Mar 1971, pp.742-750

[18] G.B. Gilcrest, G.D. Rockefeller, and E.A. Udren, "High-speed distance relaying using a digital computer", *IEEE Transactions on Power Apparatus and Systems*, Vol.91, No.3, May 1972, pp. 1235-1243

[19] A.M. Ranjbar, and B.J. Cory, "An improved method for the digital protection of high voltage transmission lines", *IEEE Transactions on Power Apparatus and Systems*, Vol.94, No.2, Mar 1975, pp.544-550

[20] J.G. Gilbert, and R.J. Shovlin, "High speed transmission line fault impedance calculation using a dedicated mini computer", *IEEE Transactions on Power Apparatus and Systems*, Vol.94, No.3, Jun 1975, pp.872-883

[21] Y. Miki, Y. Sano, and J. Makino, "Study of high-speed distance relay using microcomputer", *IEEE Transactions on Power Apparatus and Systems*, Vol.96, No.2, Mar 1977, pp. 602-613

[22] P.G. McLaren, and M. Redfern, "Fourier series techniques applied to distance protection", IEE Proceedings, Vol.122, No.11, Nov 1975, pp.1301-1305

[23] M.S.Sachdev and M.A.Baribeau, "A new algorithm for digital impedance relays", *IEEE Transactions Power Apparatus and Systems*, Vol.98, 1978, pp.2232-2240

[24] A.A. Girgis and R.G. Brown, "Application of Kalman filtering in computer relaying", *IEEE Transactions Power Apparatus and Systems*, Vol.100, 1981, pp.3387-3397

[25] M. Vitins, "A correlation method for transmission line protection", *IEEE Transactions Power Apparatus and Systems*, Vol.97, No.5, Sep/Oct 1978, pp.1607-1617

[26] M. Chamia, and S. Liberman, "Ultra high speed relay for EHV/UHV transmission lines - development design and application", *IEEE Transactions Power Apparatus and Systems*, Vol.96, No.6, Nov/Dec 1978, pp.2104-2116

[27] M. Vitins, "A fundamental concept for high speed relaying", *IEEE Transactions on Power Apparatus and Systems*, Vol.100, No.1, Jan 1981, pp.163-168

[28] D.W.P. Thomas, M.S. Jones, and C. Cristopoulos, "Phase selection based on superimposed components", *IEE Proceedings on Generation, Transmission and Distribution*, Vol.143, No.3, May 1996, pp.295-299

[29] H.W. Dommel, and J.M. Michels, "High speed relaying using travelling wave transient analysis", *IEEE PES Winter Meeting: N.Y.*, A78, Jan/Feb 1978, pp.214-219

[30] A.T. Johns, "New ultra high speed directional comparison technique for the protection of EHV transmission lines", *IEE Proceedings*, Vol.127 Pt.c, No.4, Jul 1980, pp.228-239

[31] S. Rajendra, and P.G. McLaren, "Travelling-wave techniques applied to the protection of teed circuits: Principle of travelling-wave techniques", *IEEE Transactions on Power Apparatus and Systems*, Vol.104, No.12, Dec 1985, pp.3544-3550

[32] S. Rajendra, and P.G. McLaren, "Travelling-wave techniques applied to the protection of teed circuits: Multi-phase/multi-circuit system", *IEEE Transactions on Power Apparatus and Systems*, Vol.104, No.12, Dec 1985, pp.3551-3557

[33] M.M. Mansour, and G.W. Swift, "A multi-microprocessor based travelling wave relay - theory and realization", *IEEE Transactions on Power Delivery*, Vol.1, No.1, Jan 1986, pp.272-279

[34] E.H. Shehab-Eldin, and P.G. McLaren, "Travelling wave distance protection - problem areas and solutions", *IEEE Transactions on Power Delivery*, Vol.3, No.3, Jul 1988, pp.894-902

[35] C. Christopoulos, D.W.P. Thomas, and A. Wright, "Scheme, based on travelling-waves, for the protection of major transmission lines", *IEE Proceedings, Part C: Generation, Transmission and Distribution*, Vol.135, No.1, Jan 1988, pp.63-73

[36] C. Christopoulos, D.W.P. Thomas, and A. Wright, "Signal processing and discriminating techniques incorporated in a protective scheme based on travelling waves", *IEE Proceedings, Part C: Generation, Transmission and Distribution*, Vol.136, No.5, Sep 1989, pp.279-288

[37] G.B. Ancell, and N.C. Pahalawaththa, "Maximum likelihood estimation of fault location on transmission lines using travelling waves", *IEEE Transactions on Power Delivery*, Vol.9, No.2, Apr 1994, pp.680-689

[38] Z.Q. Bo, M.A. Redfern, and G.C. Weller, "Positional protection of transmission line using fault generated high frequency transient signals", *IEEE Transactions on Power Delivery*, Vol.15, No.3, Jul 2000, pp. 888-894

[39] J. Liang, S. Elangovan, and J.B.X. Devotta, "Pattern recognition technique for travelling wave protection", *Electric Machines and Power Systems, Taylor & Francis Ltd, London, Englnd*, Vol.26, No.10, Dec 1998, pp.1007-1018

[40] J. Liang, S. Elangovan, and J.B.X. Devotta, "Adaptive travelling wave protection algorithm using two correlation functions", *IEEE Transactions on Power Delivery*, Vol.14, No.1, Jan 1999, pp.126-131

[41] A.G. Phadke, and S.H. Horowitz, "Adaptive relaying", *IEEE Computer Applications in Power Magazine*, Vol.3, No.3, Jul 1990, pp.47-51

[42] G.D. Rockefeller, C.L. Wagner, J.R. Linders, K.L. Hicks, and D.T. Rizy, "Adaptive transmission relaying concepts for improved performance", *IEEE Transactions on Power Delivery*, Vol.3, No.4, Oct 1988, pp.1446 - 1458

[43] S.H. Horowitz, A.G. Phadke, and J.S. Thorpe, "Adaptive transmission system relaying", *IEEE Transactions on Power Delivery*, Vol.3, No.4, Oct 1988, pp.1436 - 1445

[44] T.S. Sidhu, H. Singh, and M.S. Sachdev, "Design, implemetation and testing of an artificial neural network based fault direction discriminator for protecting transmission lines", *IEEE Transactions on Power Delivery*, Vol.10, No.2, Apr 1995, pp.697-706

[45] D.V. Coury, and D.C. Jorge, "Artificial neural network approach to distance protection of transmission lines", *IEEE Transactions on Power Delivery*, Vol.13, No.1, Jan 1998, pp.102-108

[46] R. Venkatesan, and B. Balamurugan, "A real-time hardware fault detector using an artificial neural network for distance protection", *IEEE Transactions on Power Delivery*, Vol.16, No.1, Jan 2001, pp.75-82

[47] O. Rioul, and M. Vetterli, "Wavelets and signal processing", *IEEE Signal Processing Magazine*, Vol.8, No.4, Oct 1991, pp.14-38

[48] L.G. Weiss, "Wavelets and wideband correlation processing", *IEEE Signal Processing Magazine*, Vol.11, No.1, Jan 1994, pp.13-32

[49] C.H. Lee, Y. Wang, and W.L. Huang, "A literature survey of wavelets in power engineering applications", *Proceedings of the National Scince Council, Republic of China*, Vol.14, No.4, 2000, pp.249-257

[50] D.C. Robertson, O.I. Camps, J.S. Mayer, and W.B. Gish, "Wavelets and electromagnetic power system transients", *IEEE Transactions on Power Delivery*, Vol.11, No.2, Apr 1996, pp.1050-1058

[51] F.H. Magnago and A. Abur, "Fault location using wavelets", *IEEE Transactions on Power Delivery*, Vol.13, No.4, Oct 1998, pp.1475-1480

[52] L. Shang, G. Herold, and J. Jaeger, "A new approach to high-speed protection for transmission line based on transient signal analysis using wavelets", *Developments in Power System Protection*, 2001, pp.173-176

[53] X. Yibin, D.C. Wai, and W.W.L.A Keerthipala, "A new technique using wavelet analysis for fault location", *Sixth International Conference on Developments in Power System Protection*, Conf. Publ. No.434, Mar 1997, pp.231-234

[54] D.C. Wai, and X. Yibin, "A novel technique for high impedance fault identification", *IEEE Transactions on Power Delivery*, Vol.13, No.3, Jul 1998, pp.738-744

[55] "The protective relay IED in the automation world", IEEE Power Engineering Society Tutorial, 03TP162

[56] Y. Serizawa, M. Myoujin, K. Kitamura, N. Sugaya, M. Hori, A. Takeuchi, I. Shuto, and M. Inukai, "Wide-area current differential backup protection employing broadband communications and time transfer systems", *IEEE Transactions on Power Delivery*, Vol.13, No.4, Oct 1998, pp.1046-1052

[57] J.C. Tan, P.A. Crossley, P.G. McLaren, P.F. Gale, I. Hall, and J. Farrell, "Application of a wide area backup protection expert system to prevent cascading outages", *IEEE Transactions on Power Delivery*, Vol.17, No.2, Apr 2002, pp.375-380

[58] G.W. Swift, "The spectra of fault-induced transients", *IEEE Transactions on Power Apparatus and Systems*, Vol.98, No.3, May/Jun, 1979, pp.940-947

[59] G.B. Ancell, and N.C. Pahalawaththa, "Effects of frequency dependence and line parameters on single ended travelling wave based fault location schemes", *IEE Proceedings-C*, Vol.139, No.4, Jul 1992, pp.332-342

[60] L.M. Wedepohl, "Application of matrix methods to the solution of travelling-wave phenomena in polyphase systems", *Proceedings of IEE*, Vol.110, No.12, Dec 1963, pp.2200-2212

[61] P.C. Magnusson, "Travelling waves on multi-conductor open-wire line - A numerical survey of the effects of frequency dependence of modal composition", *IEEE Transactions Power Apparatus and Systems*, Vol.92, No.3, May/Jun 1973, pp.999-1005

[62] K.G. Beauchamp, and C.K. Yuen, "Digital methods for signal analysis", George Allen and Unwin Ltd, 1979

[63] G.L. Richard, "Understanding Digital Signal Processing", Addisson Wesley, 1997

[64] W.H. Press, S.A. Teukolsky, W.T. Vetterling, B.P. Flannery, "Numerical Recipes in Fortran 90", Cambridge University Press, Second Edition, 1996

[65] L.H. Christensen, "Design, construction, and test of a passive optical prototype high voltage instrument transformer", IEEE Transactions on Power Delivery, Vol.10, No.3, Jul 1995, pp.1332-1337

[66] Real Time Playback User's Guide, Revision 1.1, Manitoba HVDC Research Center, June 2001

[67] Dakar F5 Carrier Board Technical Reference, Spectrum Signal Processing Inc., Document Number 500-00353, Revision 1.10, May 1998

[68] TMS320C4x User's Guide, SPRU063, Texas Instruments Incorporated, May 1998

[69] Dakar F5 Carrier Board User's Guide, Spectrum Signal Processing Inc., Document Number 500-00354, Revision 2.11, October 1998

[70] Toolbox Configuration Utilities User Guide, Spectrum Signal Processing Inc., Document Number 500-00409, Revision 1.00, June 1998

[71] Code Composer Studio v3.0 User's Guide, GO DSP Corporation, 1998

[72] TMS320C4x C Source Debugger User's Guide, SPRU054, Texas Instruments Incorporated, May 1992

[73] DL3-A1 DL3ADA100 Analog Module User Guide, Spectrum Signal Processing Inc., Document Number 500-00352, Revision 1.03, December 1998

[74] DSP-LINK3 Memory Mapped Expansion Bus Interface Specifications, Spectrum Signal Processing Inc., Revision 1.02, Nov 1998

[75] C6211/C6711 DSK Hardware Installation Quick Start, SPRU436A, Texas Instuments Incorporated, 2001

[76] C6211/C6711 DSP Starter Kit (DSK) Quick Start, SPRU437A, Texas Instuments Incorporated, 2001

[77] TMS320C6000 Technical Brief, SPRU197D, Texas Instuments Incorporated, Feb 1999

[78] TMS320C6000 Peripherals Reference Guide, SPRU190D, Texas Instruments Incorporated, 2001

[79] Code Composer Studio Getting Started Guide, SPRU509, Texas Instruments Incorporated, 2001

[80] Code Composer Studio Users Guide, SPRU328B, Texas Instruments Incorporated, 2000

[81] TMS320C6000 Code Composer Studio Tutorial, SPRU301C, Texas Instruments Incorporated, 2000

[82] TMS320C6000 Optimizing C Compiler User's Guide, SPRU187I, Texas Instruments Incorporated, 2001

[83] TMS320C6000 Assembly Language Tools User's Guide, SPRU186I, Texas Instruments Incorporated, 2001

[84] TMS320C6000 Chip Support Library API Reference Guide, SPRU401B, Texas Instruments Incorporated, 2001

[85] TMS320C62x DSP Library Programmer's Reference, SPRU402, Texas Instuments Incorporated, 2000

[86] The C++ Programming Language, Third Edition, Bjarne Stroustrup, Addison-Wesley, 1999

[87] RIDE User's Manual, v4.2, Hyperception Inc., Jan 2001

[88] RIDE Function Reference, v4.1,Hyperception Inc., Feb 1998

[89] Visual C++ User's Guide, Version 6.0, Microsoft Corporation, 1999

[90] Data Converter Selection Guide, Texas Instruments Incorporated, 2001

[91] 12-bit, 4 Analog Input, 6 MSPS, Simultaneous Sampling Analog- to-Digital Converters, SLAS217H, Texas Instruments Incorporated, May 1999

[92] THS1206EVM User's Guide, SLAU042B, Texas Instruments Incorporated, January 2001

[93] Designing with the THS1206 High-Speed Data Converter, SLAA094, Texas Instruments Incorporated, April 2000

[94] TLV2548EVM 12-bit ADC EVM User's Guide, SLAU029A, Texas Instruments Incorporated, May 1999

[95] TLV2548, 12-bit, 200KSPS, 8-channel, Low Power Serial Analog-to-Digital Converters with Auto Power Down, SLAS198E, Texas Instruments Incorporated, February 1999

[96] Interfacing the TLV2544/TLV2548 ADC to the TMS320C5402 DSP, SLAA093A, Texas Instruments Incorporated, October 2000

[97] TMS320C6000 EVM Daughterboard Interface, SPRA478, Texas Instruments Incorporated, December 1998

[98] TMS320 Cross-Platform Daughtercard Specification Revision 1.0, SPRA711, Texas Instruments Incorporated, 2000

[99] TMS320 Cross-Platform Daughtercard Adapter, SLAU074, Texas Instruments Incorporated, May 2001

[100] TMS320C6000 Programmer's Guide, SPRU198F, Texas Instruments Incorporated, 2001

[101] TMS320C6000 McBSP Initialization, SPRA488, Texas Instruments Incorporated, 1998

[102] TMS320C6000 CPU and Instruction Set Reference Guide, SPRU189F, Texas Instruments Incorporated, 2000

[103] Using the TMS320C5402 DMA Channels to Read From the TLV2548, SLAA095, Texas Instruments Incorporated, 2000

[104] Interfacing the TLV2544/TLV2548 ADC to the TMS320C31 DSP, SLAA101, Texas Instruments Incorporated, 2000

[105] ADS8364EVM User's Guide, SLAU084, Texas Instruments Incorporated, April 2002

[106] ADS8364, 250kHz, 16-Bit, 6-Channel Simultaneous Sampling Analog-to-digital Converters, SBAS219A, Texas Instruments Incorporated, June 2002

[107] Software Control of the ADS8364, SLAA155, Texas Instruments Incorporated, August 2002

[108] A.G. Phadke, M. Ibrahim, and T. Hlibka, "Fundamental basis for distance relaying with symmetrical components", *IEEE Transactions on Power Apparatus and Systems*, Vol.96, No.2, Mar 1977, pp.635-646

[109] C.L. Wadhwa, "Electrical power systems", New Age Publications, Second Edition, September 1991